AD NUMBER

AD430301

LIMITATION CHANGES

TO:

Approved for public release; distribution is unlimited.

FROM:

**Distribution authorized to U.S. Gov't. agencies and their contractors;
Administrative/Operational Use; JUL 1963. Other requests shall be referred to Defense Atomic Support Agency, Washington, DC.**

AUTHORITY

DNA ltr 29 Jun 1973

POR-1815
(WT-1815)

DEPARTMENT OF DEFENSE
U.S. ATOMIC ENERGY COMMISSION

Project DANNY BOY

NEVADA TEST SITE
5 MARCH 1962

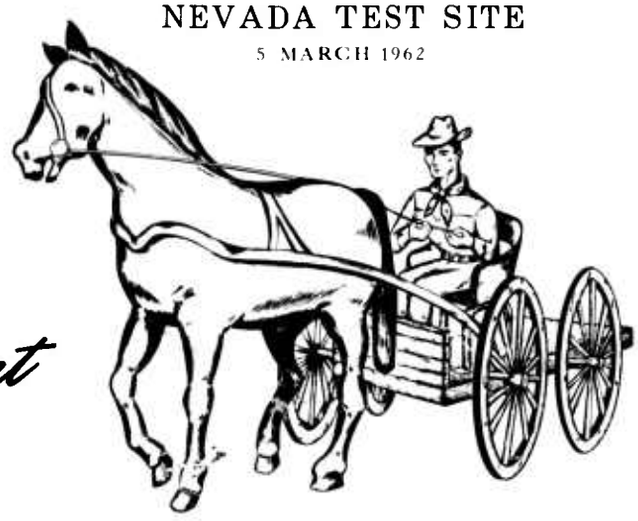

Final Report

Project 1.6

MASS DISTRIBUTION MEASUREMENTS OF CRATER EJECTA AND DUST

A. D. Rooke, Jr., Project Officer
L. K. Davis

WATERWAYS EXPERIMENT STATION

ISSUED 13 FEBRUARY 1964

Inquiries relative to this report may be made to

Chief, Defense Atomic Support Agency
Washington 25, D. C.

When no longer required, this document may be destroyed in accordance with applicable security regulations.

DO NOT RETURN THIS DOCUMENT

USAEC Division of Technical Information Extension, Oak Ridge, Tennessee

[redacted]

OPERATION NOUGAT

DANNY BOY EVENT

POR (WT) 1815

PROJECT 1.6

MASS DISTRIBUTION MEASUREMENTS OF CRATER EJECTA AND DUST

A. D. Rooke, Jr., Project Officer
L. K. Davis

U. S. Army Corps of Engineers
Waterways Experiment Station
Vicksburg, Mississippi

July 1963

[redacted]

ABSTRACT

An array of tarpaulins was placed in a concentric circular pattern about the ground zero (GZ) of a nuclear device with an intended yield of 470 tons (4.26×10^5 kg). The device was detonated at a depth of 33.5 meters (110 feet) in a basalt medium. After the shot, when the residual radioactivity permitted, samples of ejecta and dust thrown from the crater and deposited on the tarpaulins were recovered, weighed, and analyzed for particle size. The nearest samples to GZ were recovered at a radial distance of 94 meters (≈ 310 feet) and the most remote at 268 meters (≈ 880 feet). From a total of 158 collector stations, 27 samples were recovered. Mass distribution per unit area and size distribution were tabulated and shown graphically as functions of radial distance from GZ. The amount of deposition was found to decrease sharply with distance; most of the deposition was from within 150 meters (≈ 490 feet) of GZ. Particle size similarly decreased with distance from GZ, the percentage of fines increasing rapidly beyond the 94-meter collector ring. Results of similar experiments are summarized and compared with Danny Boy data by means of dimensionless plots.

NOTATIONS

C_s = charge shape factor, dimensionless

d_a = apparent crater depth, meters

f = a function of

g = acceleration due to gravity, m/sec^2

k = a constant

L = dimensional notation for length

m = an exponential value. On a logarithmic graph, it denotes slope (y/x)

M = dimensional notation for mass

n = algebraic expression denoting any number

o = any point on a logarithmic graph

r = common ratio of a geometric progression

r_a = apparent crater radius, meters

R = radial distance from GZ, meters

R/r_a = units of crater radii, dimensionless

T = dimensional notation for time

v = surface wind velocity, mph

V_d = velocity of detonation, m/sec

W = charge weight, kg (metric), ton or KT (English)

x = algebraic expression for an unknown; the abscissa of a graphical representation

y = algebraic expression for an unknown; the ordinate of a graphical representation

Z = depth or height of burst, meters

δ = mass distribution, kg/m^2 (gm/m^2 in equation 7 only)

θ = relative thermal properties of explosive, dimensionless

λ = scaled charge depth (height) of burst, $m/W^{1/3}$

ρ = density of cratered medium, kg/m^3

CONTENTS

TABLES

FIGURES

CHAPTER 1

INTRODUCTION

1.1 OBJECTIVE

The objective of Project 1.6 was to determine the distribution of crater ejecta and dust occurring as a result of the detonation of a nominal 0.5-KT device buried 33.5 meters (110 feet) deep in a basalt medium (Shot Danny Boy).

1.2 BACKGROUND INFORMATION

In the study of explosive cratering phenomena, relatively little information has been obtained regarding the distribution of spoil resulting from the explosion, especially insofar as nuclear detonations are concerned. Engineering Research Associates, Inc., (ERA) sampled debris from underground TNT explosions in 1951 and 1952. Similar studies were conducted at the Suffield Experimental Station (SES) in Canada; one study was of deposition patterns for a 5-ton high-explosive (HE) shot in 1959, and the second study was of deposition patterns for a 100-ton HE shot in 1961. The Boeing Airplane Company also conducted mass distribution, or throwout, experiments in 1960-61 on the surface and underground HE events Scooter, White Tribe, and Stagecoach, followed by a similar, although more extensive study on the nuclear event Sedan (1962), all at the Atomic Energy Commission's Nevada Test Site (NTS). In 1962, the Sandia Corp. published the results of its findings on the Stagecoach and Buckboard throwout experiments, the latter being a series of HE detonations in basalt, conducted in 1960. References 1 through 9 describe these studies, the results of which

are summarized in Tables A.1 and A.2 of Appendix A. Also contained in Table A.1 are references to two additional experiments--Jangle HE-2 and Teapot Ess--for which Boeing gathered enough data to make limited observations on throwout.

The foregoing studies have permitted the tentative establishment of certain empirical relations between charge yield and position and the size and distribution of the ejected material under the experimental and environmental conditions of the tests. These relations are of interest in evaluating the hazards from throwout resulting from large explosions and in determining the military significance of this phenomenon in the case of near-misses on hardened targets under nuclear attack. In view of the scarcity of information on this subject and the limitations inherent in explosion modeling (References 1 and 10), it was considered desirable to include such an experiment in the Danny Boy event, which was scheduled as a low-yield (470 tons, or 4.26×10^5 kg) nuclear device to be detonated near optimum depth in basalt.

1.3 THEORY

Due to the many variables associated with explosively formed craters, no completely general prediction method has been formulated to quantitatively describe ejecta throwout and distribution. However, several important contributions have been made in this direction. The University of California Lawrence Radiation Laboratory (LRL) has developed an empirical equation which describes throwout in terms of mass per unit area (Reference 11). Aimed chiefly at prediction of this phenomenon for deep explosions, the formula places rather heavy dependence upon surface wind. As will be seen in Chapter 4, its correlation with Danny Boy ejecta

distribution at certain radial distances is very good. Interesting observations on the relation of ejecta mass and crater volume are made in References 8 and 9, which have been expanded upon and from which a prediction technique has been developed by Boeing (Reference 2).

For the Danny Boy event, it was anticipated that the cratering mechanism would include ejection of spoil by spalling at the rock-air interface as well as by the venting of the gas bubble. No formal prediction of throwout distribution was attempted, but the collector array (discussed in paragraph 2.2) was arranged to insure complete coverage for the experiment.

Correlation with previous studies (Chapter 4) is based on relations derived from dimensional analysis, coupled with experimentally obtained knowledge of cratering phenomena.

CHAPTER 2

THE EXPERIMENT

2.1 TEST CONDITIONS

The Danny Boy shot was detonated at 1015 hours 5 March 1962 in Area 18 of NTS (Figure 2.1). Actual yield was 420 tons $\pm$ 40 tons ($3.82 \times 10^5 \pm 3.62 \times 10^4$ kg), as determined by radiochemistry (Reference 12). Shot geometry and crater dimensions are shown in Figure 2.2.

2.1.1 Environmental Conditions. The test area was a large mesa extending generally northwest to southeast; it is basically a formation resulting from basaltic lava flow. Ground zero (GZ), at elevation 5474 feet above mean sea level, and the area immediately surrounding are shown in Figure 2.3. Loose, weathered basaltic rocks of small boulder size are numerous on the surface, and the thin overburden consists of an unconsolidated, very fine-grained material resembling silt. The basalt is largely vesicular, becoming more consolidated with depth. Vegetation on the mesa consists mostly of varieties of sagebrush.

2.1.2 Weather Conditions. Weather on D-day was partly cloudy and cold, the surface temperature and relative humidity being 42 degrees F and 27 percent, respectively. Surface winds were recorded at 12 knots from the south southeast (168 degrees), and did not vary significantly up to a height of 200 feet.

2.2 EXPERIMENTAL ARRAY

2.2.1 Pattern of Array. One hundred fifty-eight (158) waterproof tarpaulins, each 16.0 ft^2 (1.49 m^2) in area, were placed in a surveyed

pattern around GZ at radial distances from GZ of 220, 310, 440, 625, 880, 1250, 1770, 2500, 3540, 5000, and 7080 feet. The array was symmetrical and circular except for that portion described by the 7080-foot radius, which was a circular sector centered on north, the approximate direction in which it was anticipated that the prevailing wind would transport dust thrown from the crater. The tarpaulins were located on rays emanating from GZ and spaced on 22.5-degree intervals. The circular rings each contained 16 tarpaulins; each arc within the sector contained 7. Figure 2.4 shows a layout of the experimental array.

2.2.2 Selection of Radial Distances. LRL, sponsoring agency for the project, prescribed the tarpaulin layout and arranged for the necessary survey. It was assumed that the decrease in density of ejecta deposition with increasing distance from GZ would be manifested as a geometric progression of common ratio, r . Therefore, beginning with a distance from GZ calculated to lie near the outer edge of the crater lip (220 feet), and choosing 7000 feet (roughly 70 crater radii) as an approximate maximum distance for sampling,

$$r^{n-1} = \frac{7000}{220}$$

which, for an arbitrarily selected number of radial distances (n = 11), yields

$$r^{10} = 32 \text{ ; or}$$

$r = \sqrt{2}$, the multiplier used to determine the radial distances of the sampling rings and sectors.

2.2.3 Placement and Numbering of Stations. Each station consisted of one 4-foot-square tarpaulin spread on the ground, roughly leveled and

oriented, and secured in place by spikes driven into the earth (Figures 2.5, 2.6). Stations were designated by letters for rings and sectors, and by arabic numerals for radials, as shown in Figure 2.4. Thus, the station located due north of GZ on the 220-foot ring was A-1. To facilitate cleaning of the tarpaulins prior to the shot, those which were expected to accumulate debris in the interim (i.e. stations near roads, GZ, etc.) were covered with sheets of polyethylene plastic.

2.3 RECOVERY AND WEIGHING OF SPECIMENS

2.3.1 Early Recovery Efforts. It was vital to the objectives of the experiment that particulate deposition on the tarpaulins be measured at the earliest possible time following the shot in order to minimize redistribution of the fine materials by winds. Accordingly, recovery was begun at H+4 hours, but was initially limited to those stations lying off the mesa because of objectionable radiation levels. There was no evidence of dust or ejecta on any of the stations examined on D-day (I-, J- and K-4, K-3, and K-2). This supported earlier observations which indicated that throwout did not travel far in any direction from GZ. Recovery was resumed on D+1, the field party beginning at the southernmost stations and working in a semicircular sector toward GZ. Work was severely hampered by snow, mud, and occasional high winds, but continued until D+5, at which time 63 stations had been examined. South of GZ, the party had progressed inward to the F ring (1250 feet, 381 meters, from GZ), while inspection of all stations from the outermost ring into and including the H ring (2500 feet, 762 meters, from GZ) had been accomplished to the north. No deposition was found on these collectors. Due to the relatively high level of radioactivity closer to GZ, it was decided to postpone the remaining fieldwork.

2.3.2 Later Recovery. Recovery was resumed on D+30 when it was determined that radiation levels permitted further work. By D+36, all stations had been examined, and 27 samples had been collected and weighed. Recovery was accomplished by carefully brushing the contents of the tarpaulins into 5-gallon paint cans, after which the lids were sealed and the cans marked. Some small samples were later transferred to 1-gallon syrup cans. Figure 2.7 shows recovery and marking of a typical throwout specimen.

2.4 WEIGHING AND SIEVE ANALYSES

2.4.1 Weight Determination. Weighing of the samples was accomplished by means of two scales--one of 35-pound capacity with 0.01-pound graduations and one of 300-pound capacity with 1/4-pound graduations. With the exception of the largest sample recovered (B-16), which contained boulders too large for handling, all samples were transported to Frenchman Flat for weighing and sieve analyses. B-16 was weighed at the test site. To avoid excessive handling of the specimens and to reduce the radiation exposure of members of the field party, average tare weights of the containers were determined and deducted from the gross sample weights. For small samples, however, the contents were removed from the containers and weighed in a scoop. These operations were accomplished with due regard to radiation safety measures; protective clothing, markings, etc., were employed.

2.4.2 Sieve Analyses. In view of the small number of recovered samples (27), it was decided to analyze all of them for particle-size distribution. This was done by personnel of the Waterways Experiment Station (WES) Soils Division who were working in the Frenchman Flat area, NTS, at the time. Sieves of the 1-1/2- and 3/4-inch and numbers 4, 10, and 200

sizes, together with a mechanical shaker, were used in the analyses, which were conducted in a small shelter to eliminate effects of wind.

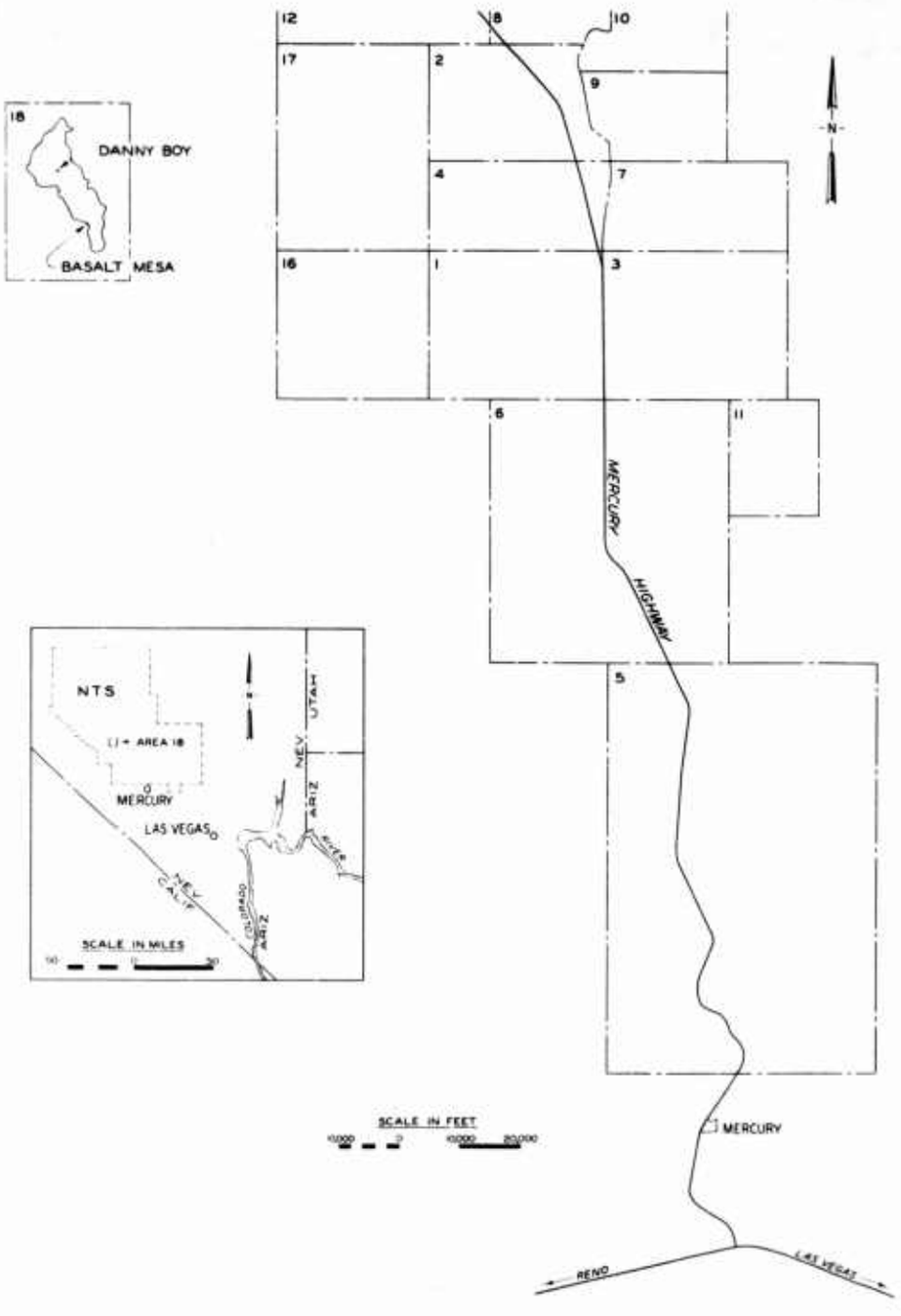

Figure 2.1 Vicinity map of Nevada Test Site, showing location of Shot Danny Boy.

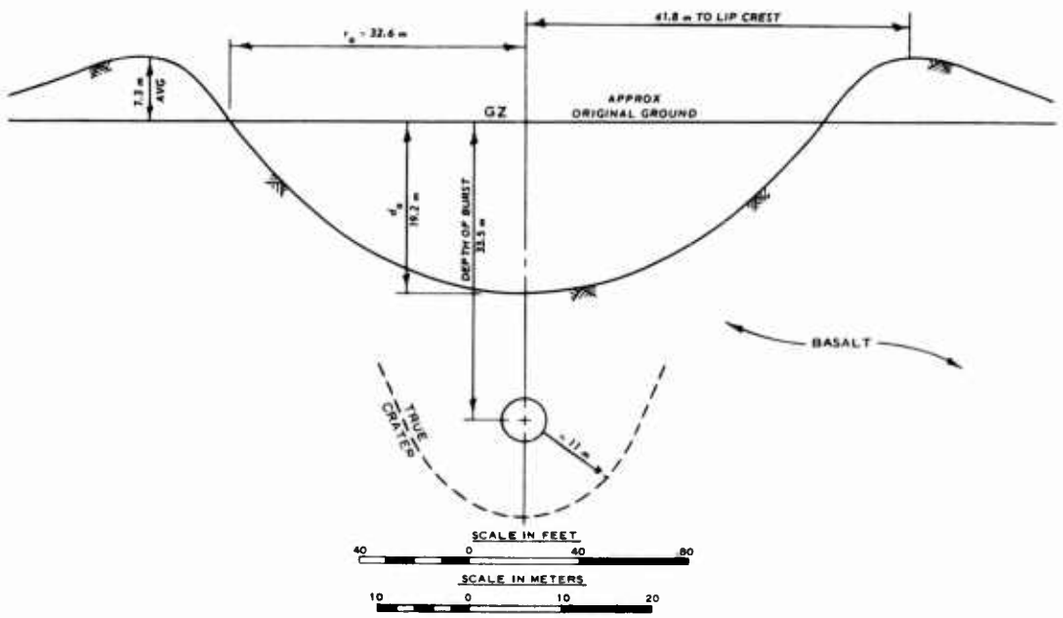

Figure 2.2 Shot geometry and crater dimensions, Danny Boy.

Figure 2.3 Oblique aerial view of Danny Boy test site, looking east. Construction activity is at GZ.

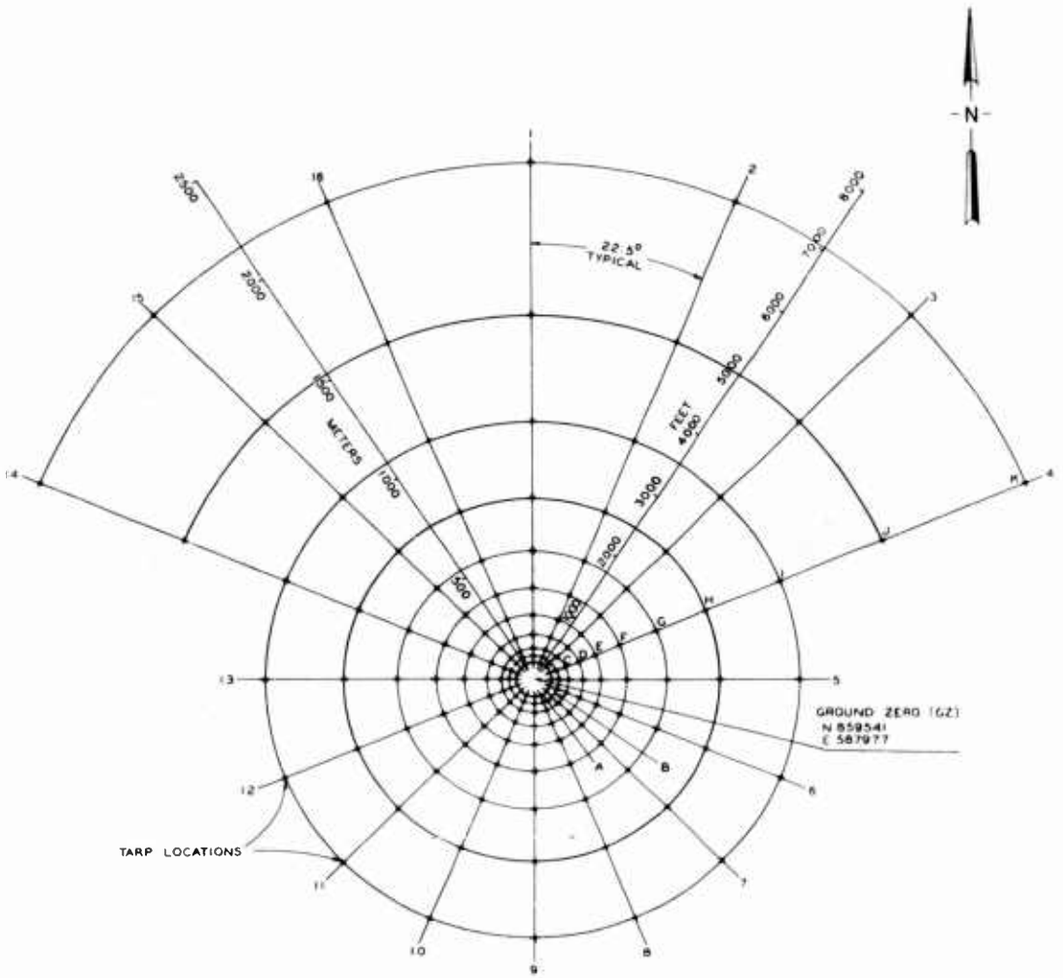

Figure 2.4 Tarpaulin array. Radial distances of rings from GZ are 220, 310, 440, 625, 880, 1250, 1770, 2500, 3540, 5000, and 7080 feet. Angular interval between radii equals 22.5 degrees.

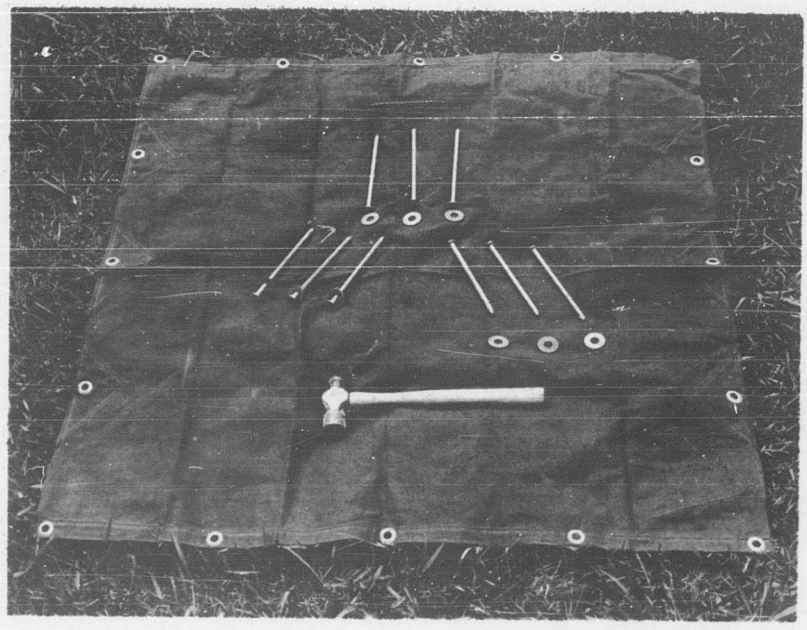

Figure 2.5 Tarpaulin, 4 by 4 feet, used as throwout collector, with materials used for emplacement. Ten- and twelve-ounce tarpaulins were used. Spike sizes varied with the depth of overburden.

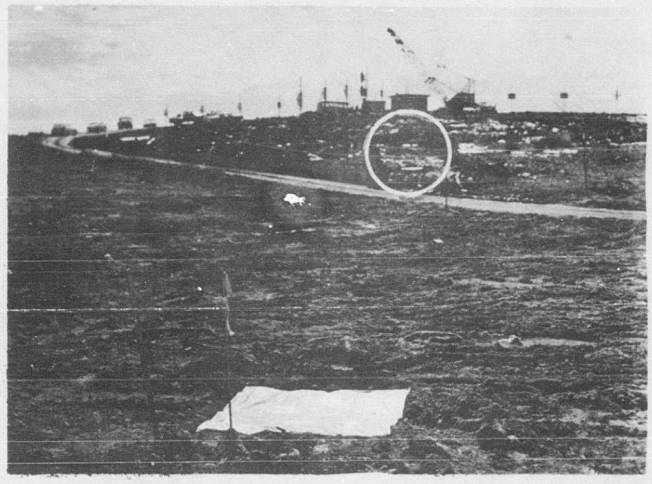

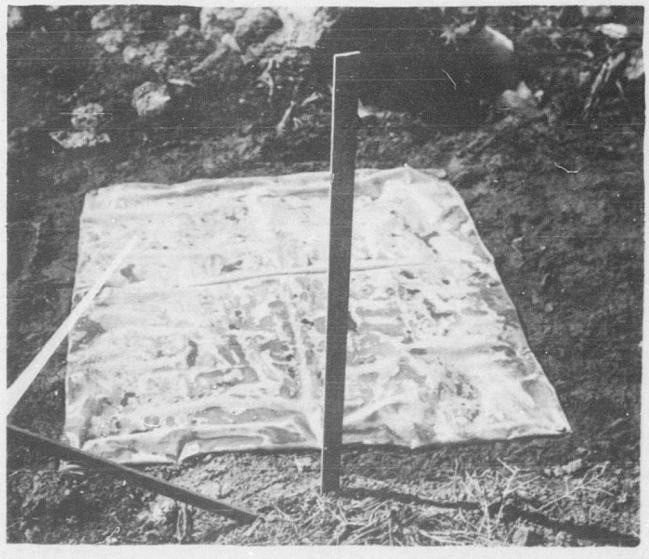

Figure 2.6 Preshot views of typical polyethylene-covered tarpaulin stations (C-2 and A-9). In top photograph, note circled stations on A and B rings of radial 2. Activity in background is in vicinity of GZ.

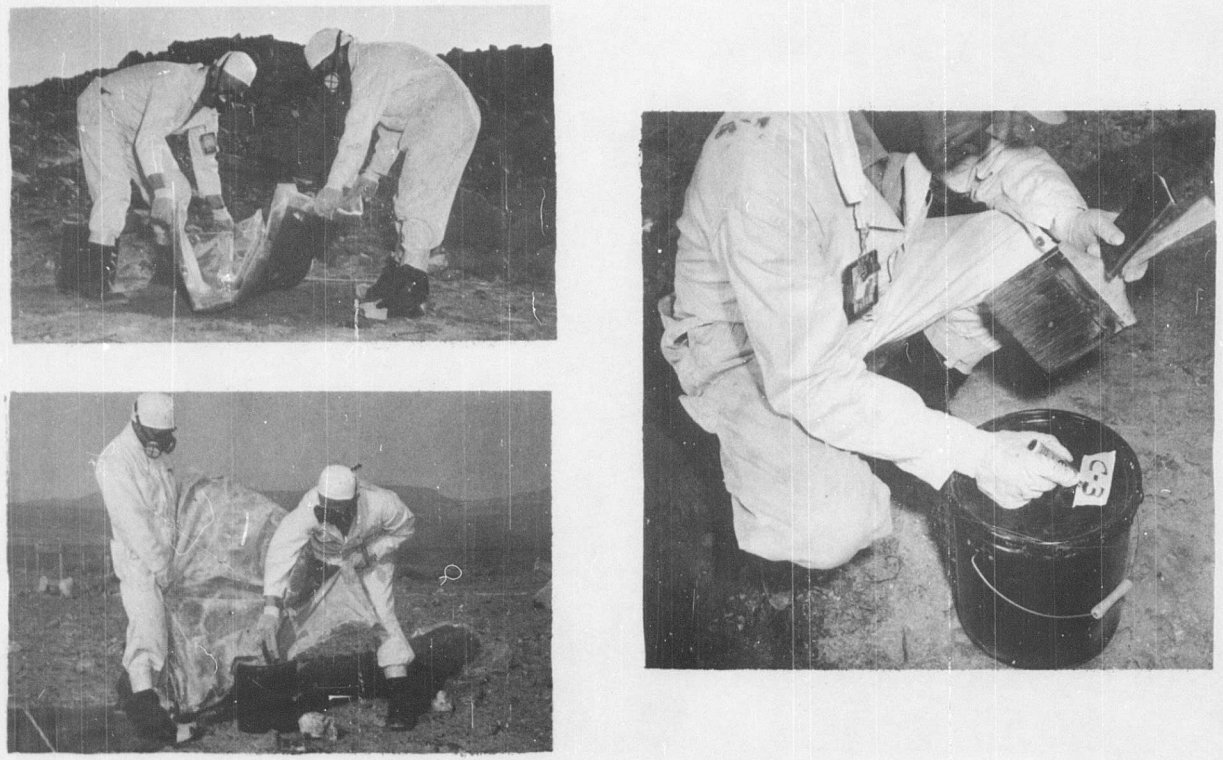

Figure 2.7 Steps in recovery of typical throwout sample. Crater lip is in background of top photograph.

CHAPTER 3

RESULTS

3.1 MASS DISTRIBUTION

Figure 3.1 is an aerial view of the Danny Boy crater taken on D+2, showing the lip and general pattern of ejecta distribution. Table 3.1 shows the results of weight determinations for all recovered specimens. Figure 3.2 is a plot of all data points, showing computed mass distribution at each collector station and distances from GZ at which recoveries were made. Figures 3.3 and 3.4 show similar data for various radials, plotted on a logarithmic scale; only those radials for which two or more data points are available are included in these plots. The large circumferential variation of ejecta distribution is apparent from these plots. A straight-line fit for mass distribution averages on all collector rings versus radial distances from GZ is presented in Figure 3.5. The ring averages are based on arithmetic means in which all recoverable stations are included. Each of the logarithmic plots (Figures 3.3-3.5) is an electronically computed best fit derived by means of the method of least squares. Contours of mass distribution are included in Figure 3.6. Recovery of tarpaulins at stations beneath the lip was not feasible; however, profiles of the lip have been prepared from a topographic map of the crater, and the average lip profile is presented in Figure 3.7. Ring locations are shown in Figure 3.7 to illustrate the approximate thicknesses of deposition on nonrecoverable collectors. No attempt is made to show upthrust under the lip, the extent of which is unknown at this time. However, ejecta deposition in the region of the crater lip will be

described in an addendum to this report following completion of an investigation by the WES Soils Division.

3.2 PARTICLE-SIZE DISTRIBUTION

A summary of the results of all sieve analyses is presented in Table 3.2. Particle-size distribution as a function of distance from GZ for individual radials is plotted semilogarithmically in Figures 3.8 through 3.12. Figure 3.13 compares grain-size distribution around the C ring, the only ring on which samples were obtained on practically the entire circumferential array.

TABLE 3.1 MASS DISTRIBUTION OF EJECTA AND DUST

Station	Radial Distance from GZ	Field Weight of Specimen	Metric Weight of Specimen	Mass Distribution per Unit Area[a]	Remarks
	m	lb	kg	kg/m^2	
B-1	94	85.75	38.93	$2{,}613 \times 10^{-2}$	Stations not recovered on B ring were under crater lip.
B-8		32.50	14.76	991×10^{-2}	
B-13		59.14	26.85	$1{,}802 \times 10^{-2}$	
B-14		26.20	11.90	799×10^{-2}	
B-15		14.84	6.75	453×10^{-2}	
B-16		416.25	188.98	$12{,}683 \times 10^{-2}$	Large tear in tarpaulin caused some loss of specimen.
C-1	134	0.40	0.18	12×10^{-2}	C ring was completely recovered except for C-10, which was destroyed by postshot operations of another organization.
C-2		17.96	8.15	547×10^{-2}	
C-3		19.90	9.04	607×10^{-2}	
C-4		53.77	24.41	$1{,}638 \times 10^{-2}$	
C-5		2.27	1.03	69×10^{-2}	
C-6		3.78	1.72	115×10^{-2}	
C-7		1.58	0.72	48×10^{-2}	
C-8		4.33	1.97	132×10^{-2}	
C-9		2.12	0.96	64×10^{-2}	
C-11		0.22	0.10	7×10^{-2}	
C-12		1.62	0.74	50×10^{-2}	
C-13		1.58	0.72	48×10^{-2}	
C-14		2.04	0.93	62×10^{-2}	
C-15		0.06	0.03	2×10^{-2}	
C-16		2.27	1.03	69×10^{-2}	
D-2	191	0.04	0.02	1×10^{-2}	Stations not listed on D and E rings contained no identifiable specimens.
D-8		2.23	1.01	68×10^{-2}	
D-13		0.51	0.23	15×10^{-2}	
D-14		0.56	0.25	17×10^{-2}	
D-16		0.04	0.02	1×10^{-2}	
E-2	268	0.26	0.12	8×10^{-2}	

[a] To determine g/m^2, substitute multiplier of 10; to determine g/cm^2, substitute multiplier of 10^{-3}.

TABLE 3.2 SIZE DISTRIBUTION OF EJECTA AND DUST

Station[a]	Total Weight of Analyzed Specimen	Percent Retained on Sieve					Percent Passing Sieve
	kg	1-1/2 inch	3/4 inch	No. 4	No. 10	No. 200	No. 200
B-1	38.93	65	3	4	4	20	4
B-8	14.76	12	1	5	10	60	12
B-13	26.85	28	6	8	11	42	5
B-14	11.90	33	3	5	6	48	5
B-15	6.75	19	7	6	7	53	8
B-16	198.98[b]	85	3	2	2	7	1
C-1	0.18	93	0	0	1	5	1
C-2	8.15	28	2	5	8	49	8
C-3	9.04	66	5	6	3	14	6
C-4	24.41	43	2	9	8	32	6
C-5	1.03	75	0	2	2	18	3
C-6	1.72	0	1	3	3	76	17
C-7	0.72	56	0	2	1	30	11
C-8	1.97	0	0	1 (-)	1	73	25 (+)
C-9	0.96	0	0	0	1	47	52
C-11	0.10	0	77	9	5	9	0
C-12	0.74	61	3	3	1	23	9
C-13	0.72	0	0	2	1	72	25
C-14	0.93	20	8	7	1	40	24
C-15	0.03	0	0	25	8	59	8
C-16	1.03	0	0	17	18	50	15
D-2	0.02	0	0	12	12	51	25
D-8	1.01	0	0	1	1 (-)	58 (+)	40
D-13	0.23	0	0	0	3	62	35
D-14	0.25	0	0	0	1	36	63
D-16	0.02	0	0	0	25	63	12
E-2	0.12	0	0	0	1	34	65

[a] Stations omitted were not recoverable or contained no specimens.

[b] Large boulders were not included in sieve analysis.

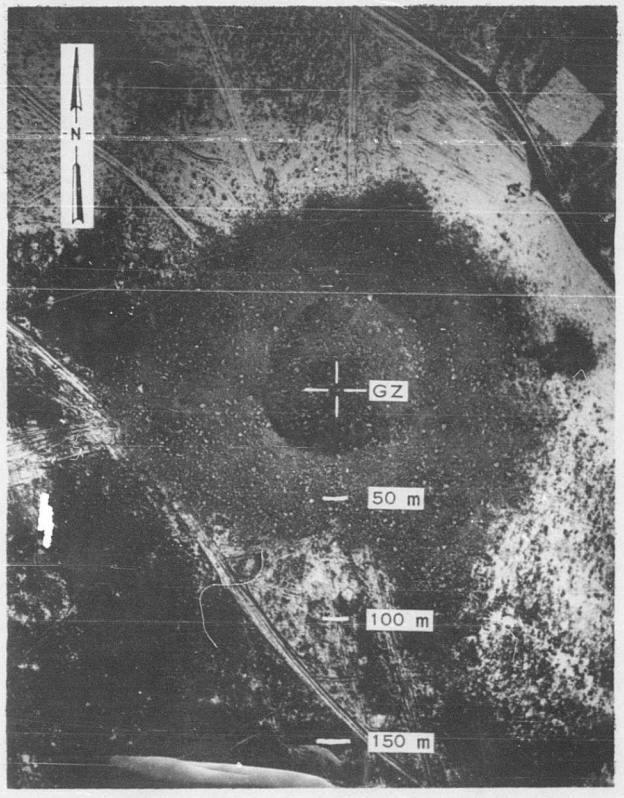

Figure 3.1 Aerial view of Danny Boy crater and lip, showing distribution of ejecta. Photograph scale is approximately 1:3,000.

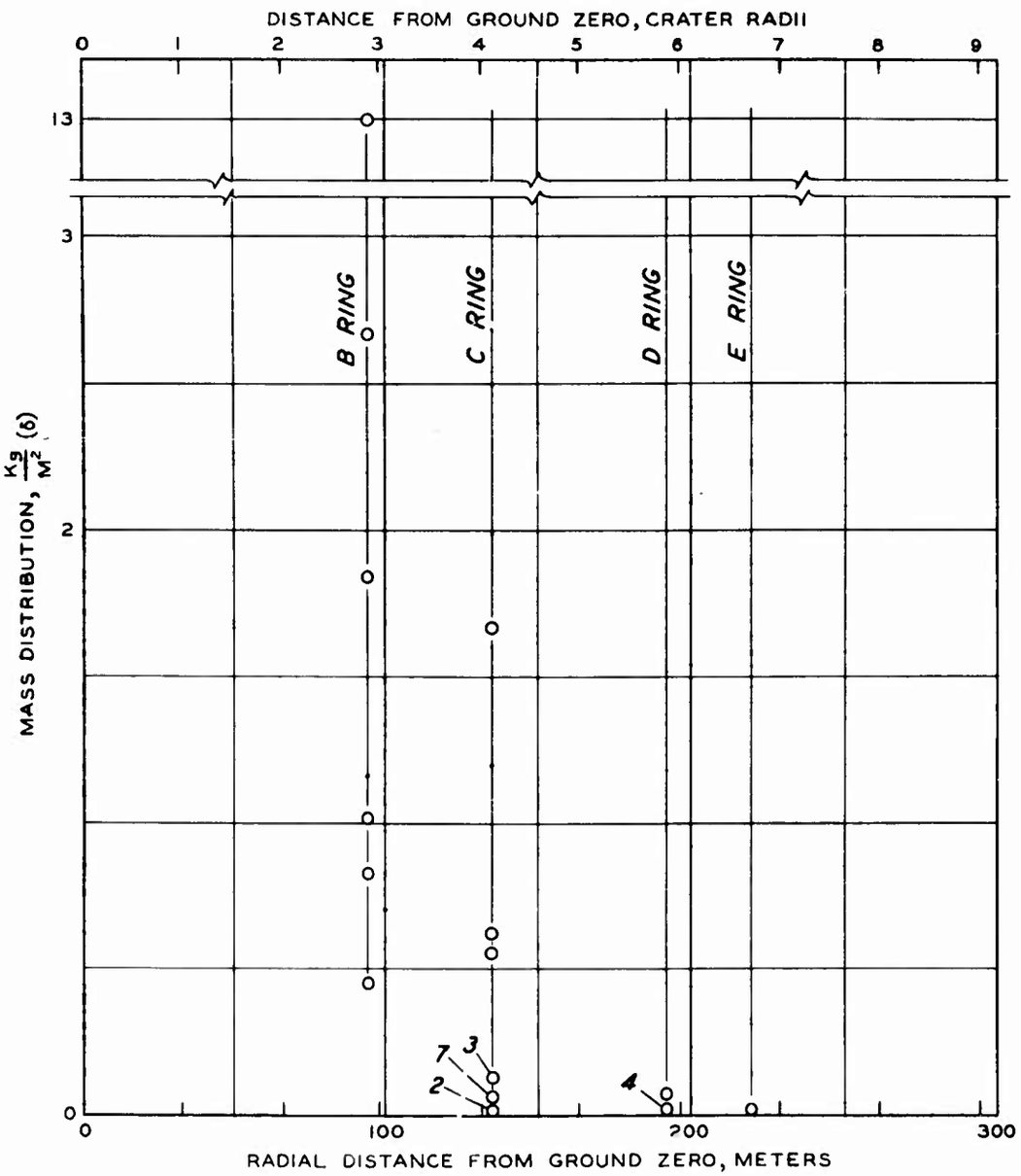

Figure 3.2 Data points, mass distribution versus radial distances from GZ.

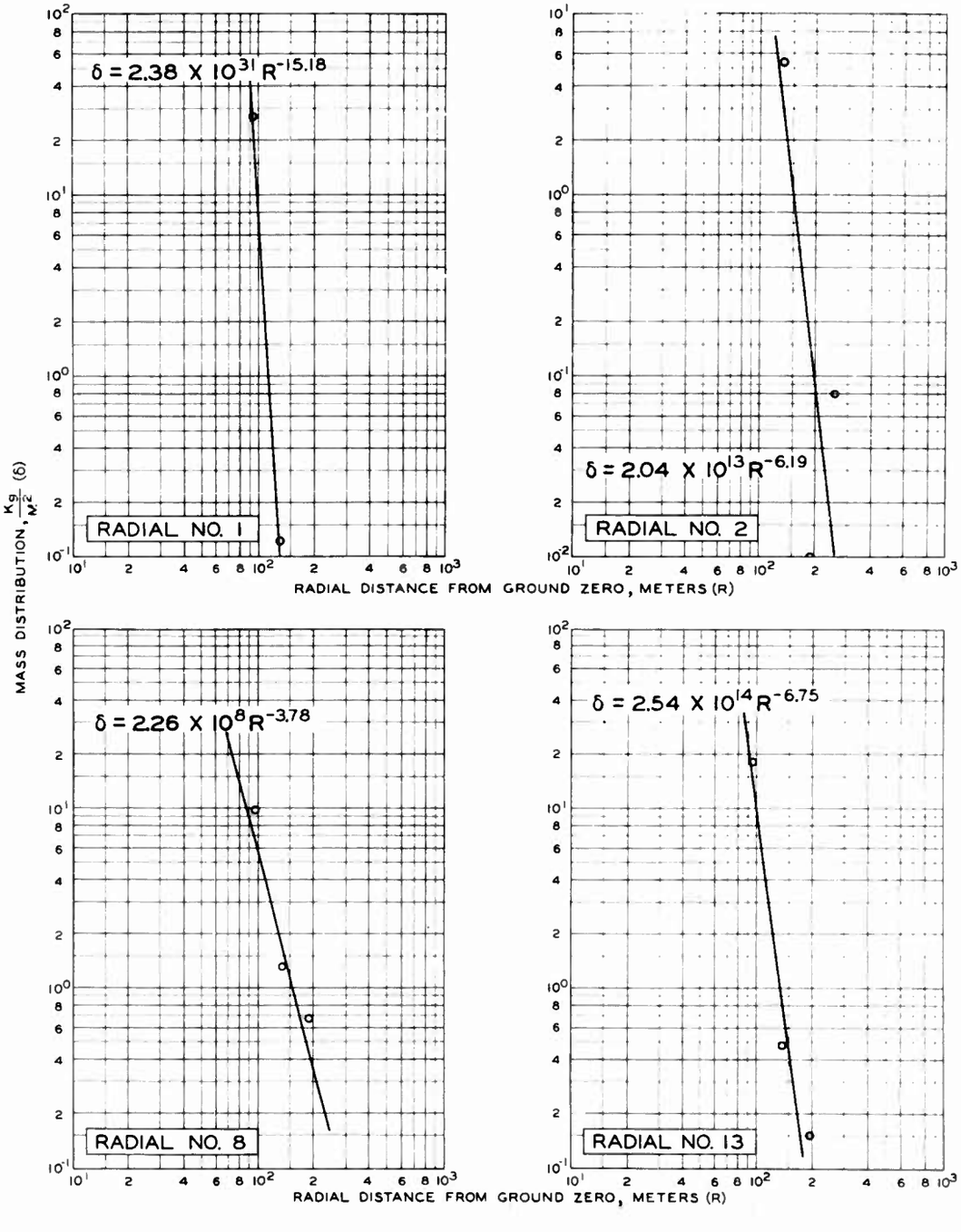

Figure 3.3 Logarithmic graphs of mass distribution versus radial distances from GZ for radials 1, 2, 8, and 13.

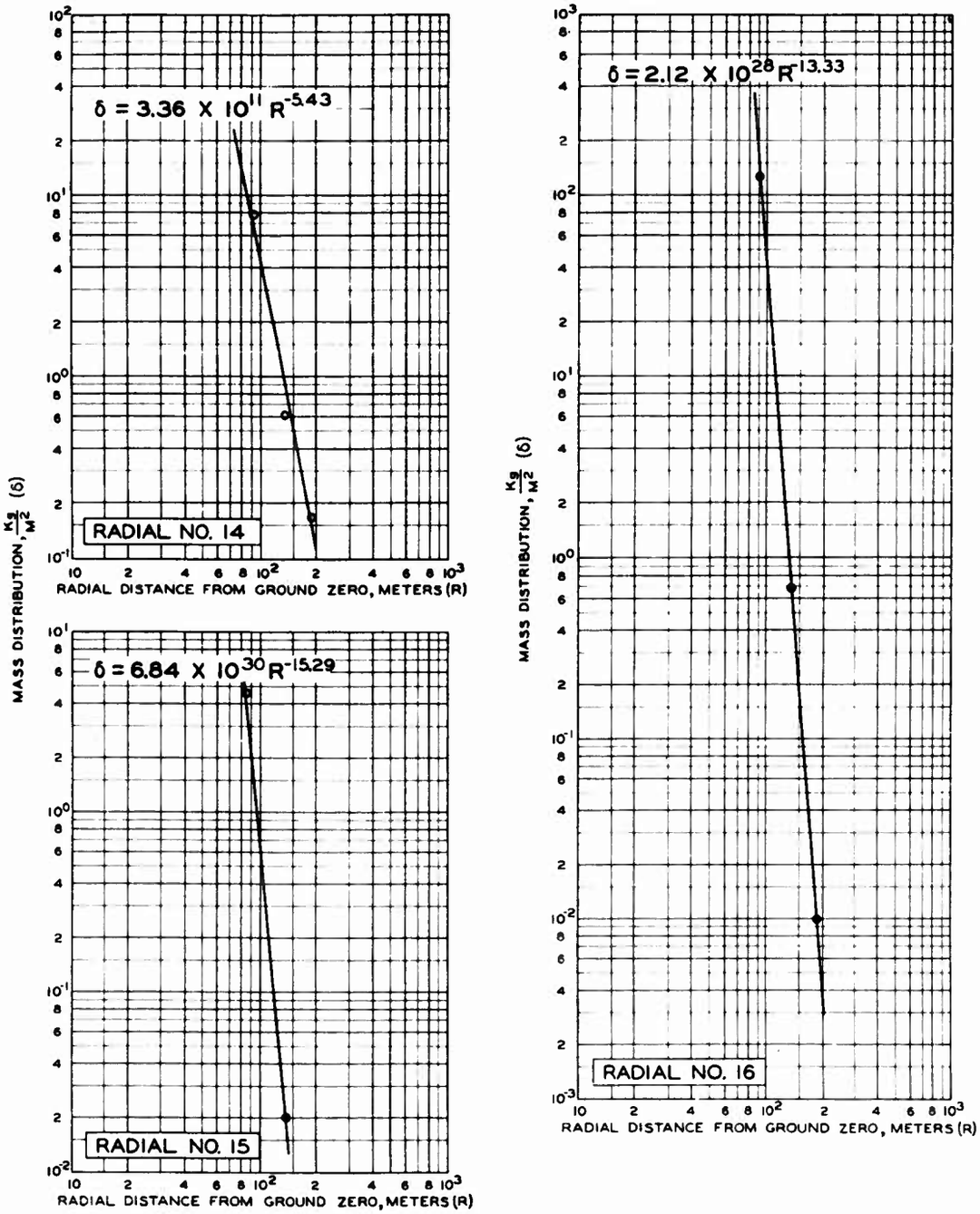

Figure 3.4 Logarithmic graphs of mass distribution versus radial distances from GZ for radials 14, 15, and 16.

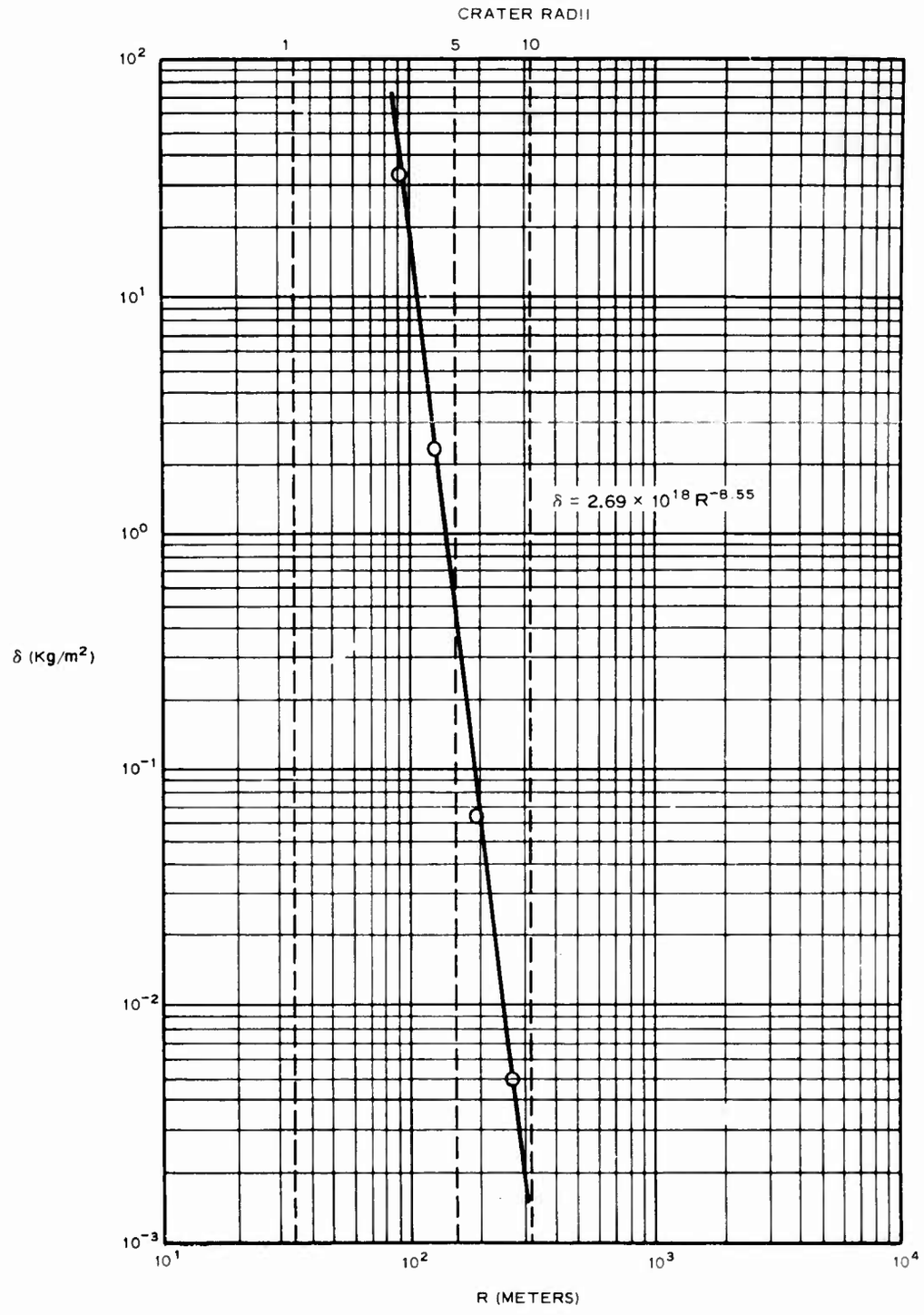

Figure 3.5 Average mass distribution (δ) versus radial distance from GZ (R) for Danny Boy.

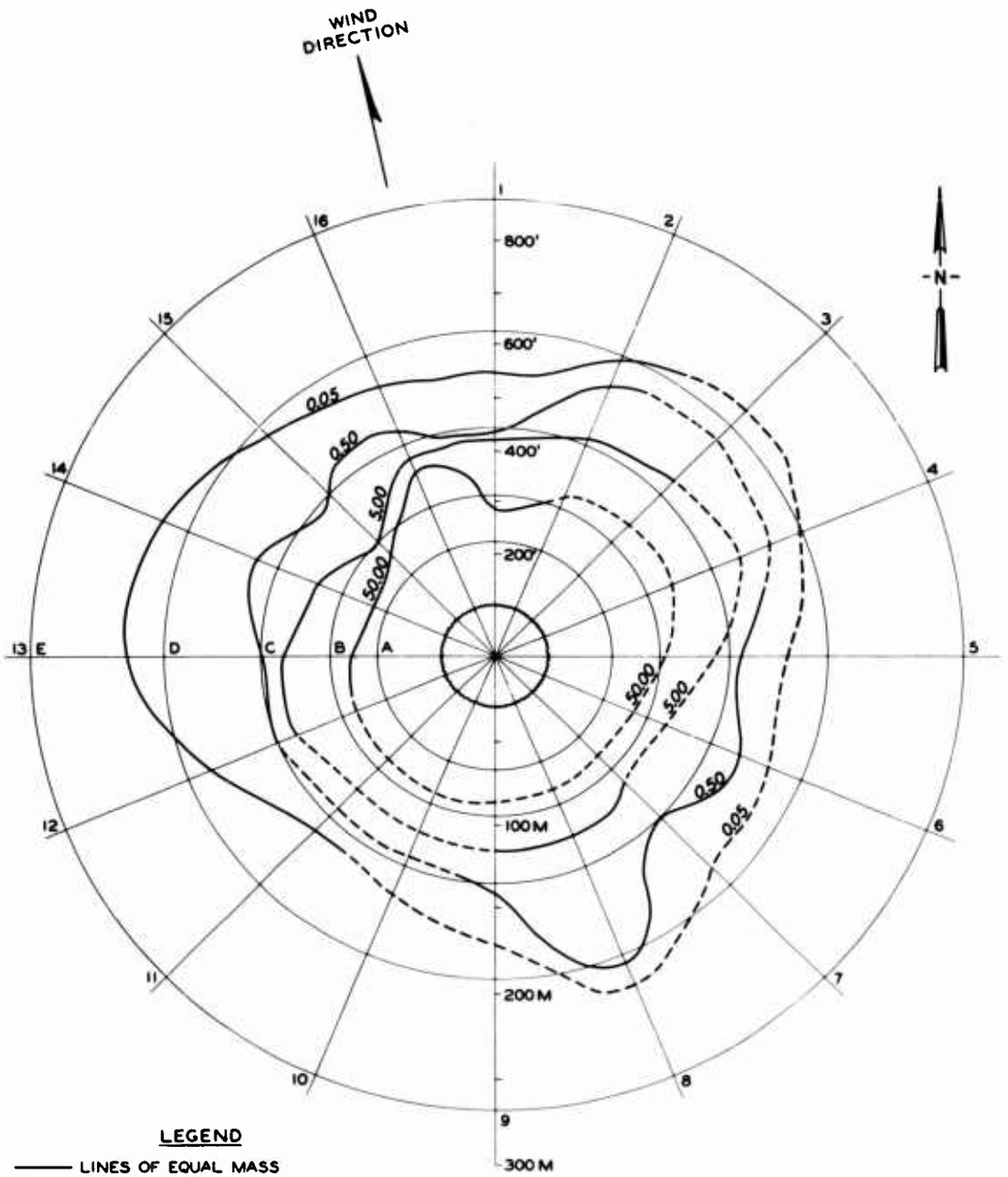

LEGEND

——— LINES OF EQUAL MASS DISTRIBUTION (K_g/m^2)

- - - - - ESTIMATED LINES OF EQUAL MASS DISTRIBUTION (K_g/m^2)

~~~~~ LIMIT OF APPARENT CRATER

NOTE: SURFACE WIND VELOCITY WAS 12 KNOTS FROM SOUTH-SOUTHEAST (168°) UP TO 200' ABOVE GROUND SURFACE.

Figure 3.6 Mass distribution contours in kg/m^2, Danny Boy.
~~~~~

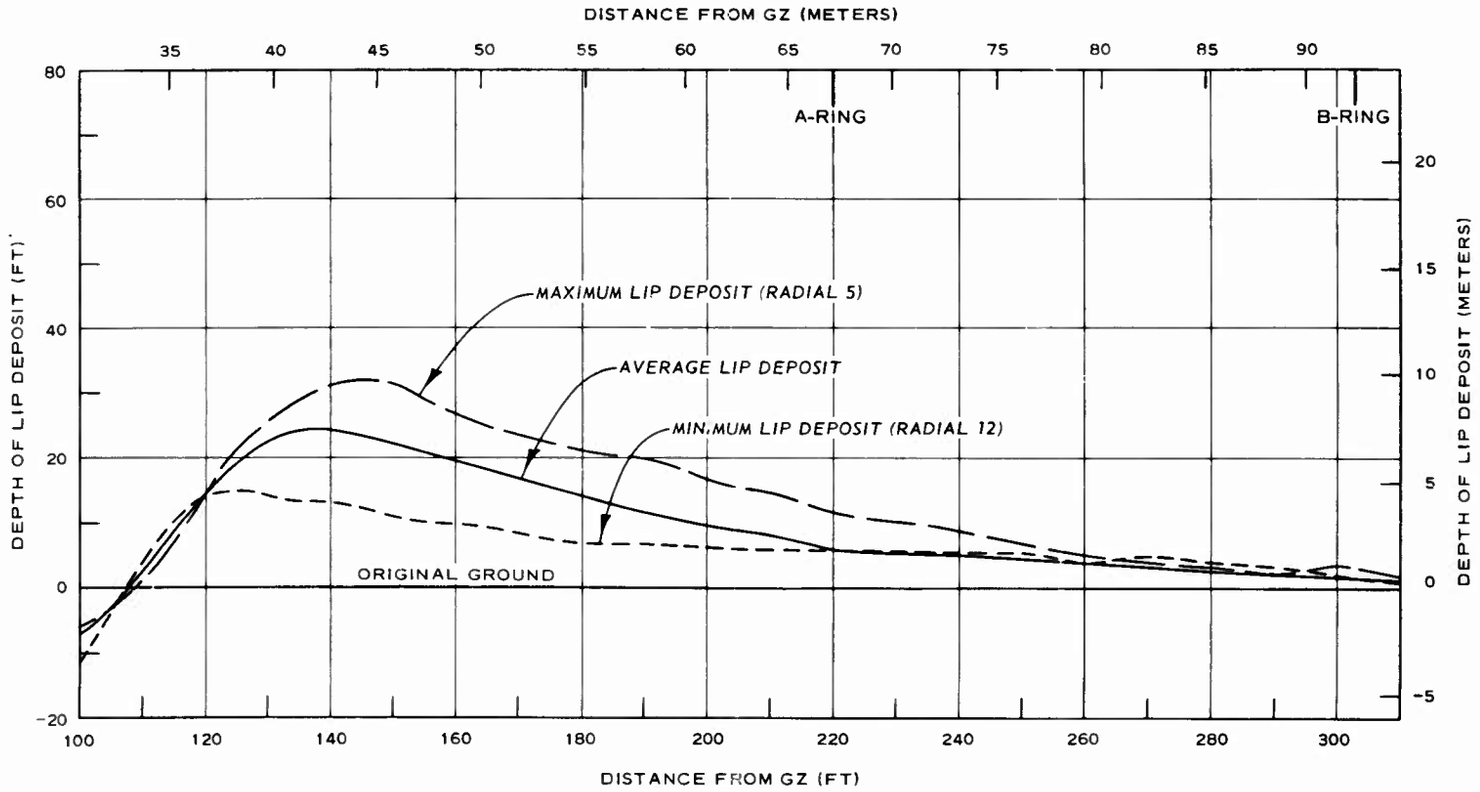

Figure 3.7 Ejecta deposition in the region of the lip, Danny Boy.

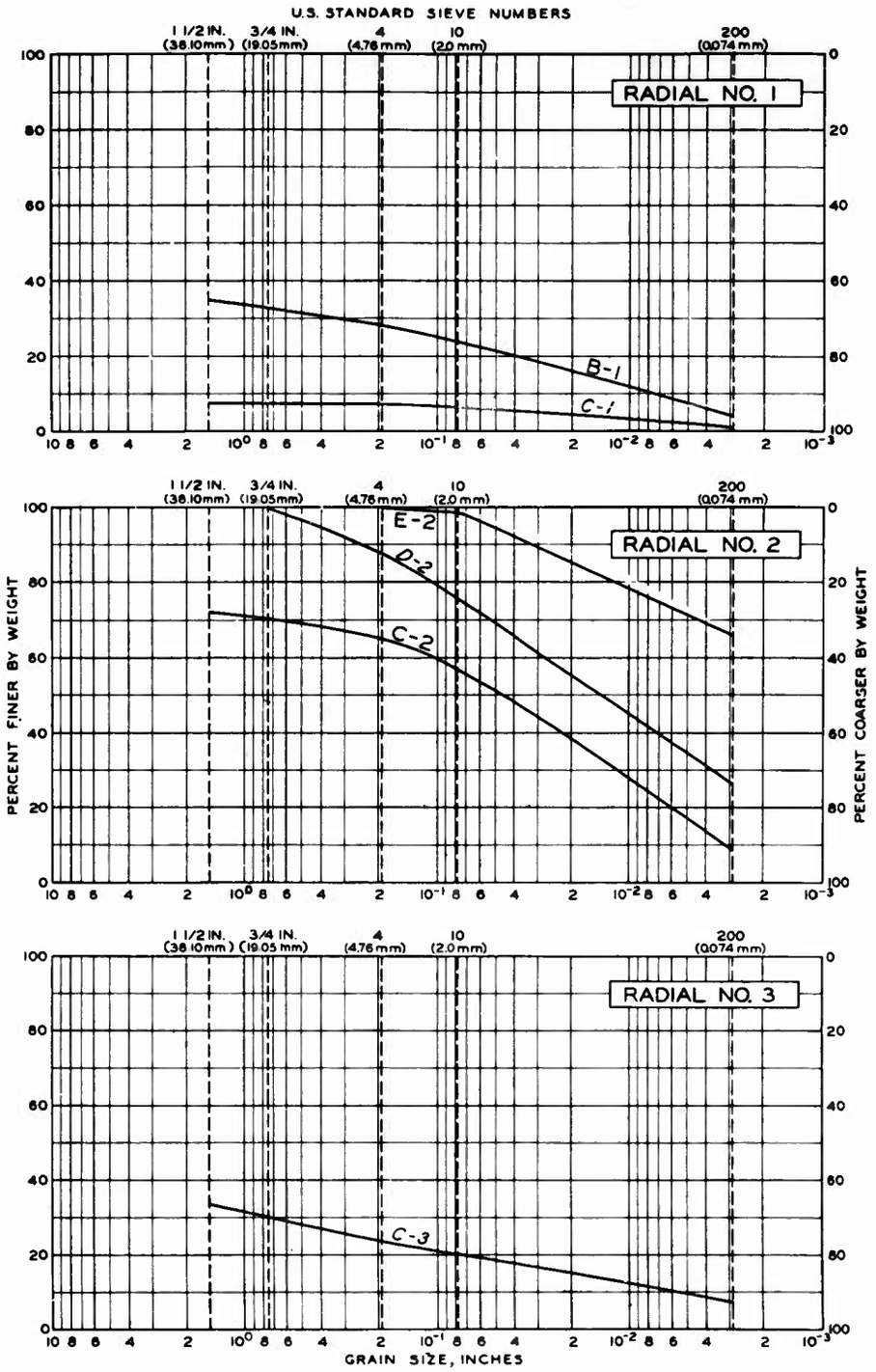

Figure 3.8 Grain-size distribution on radials 1, 2, and 3, Danny Boy.

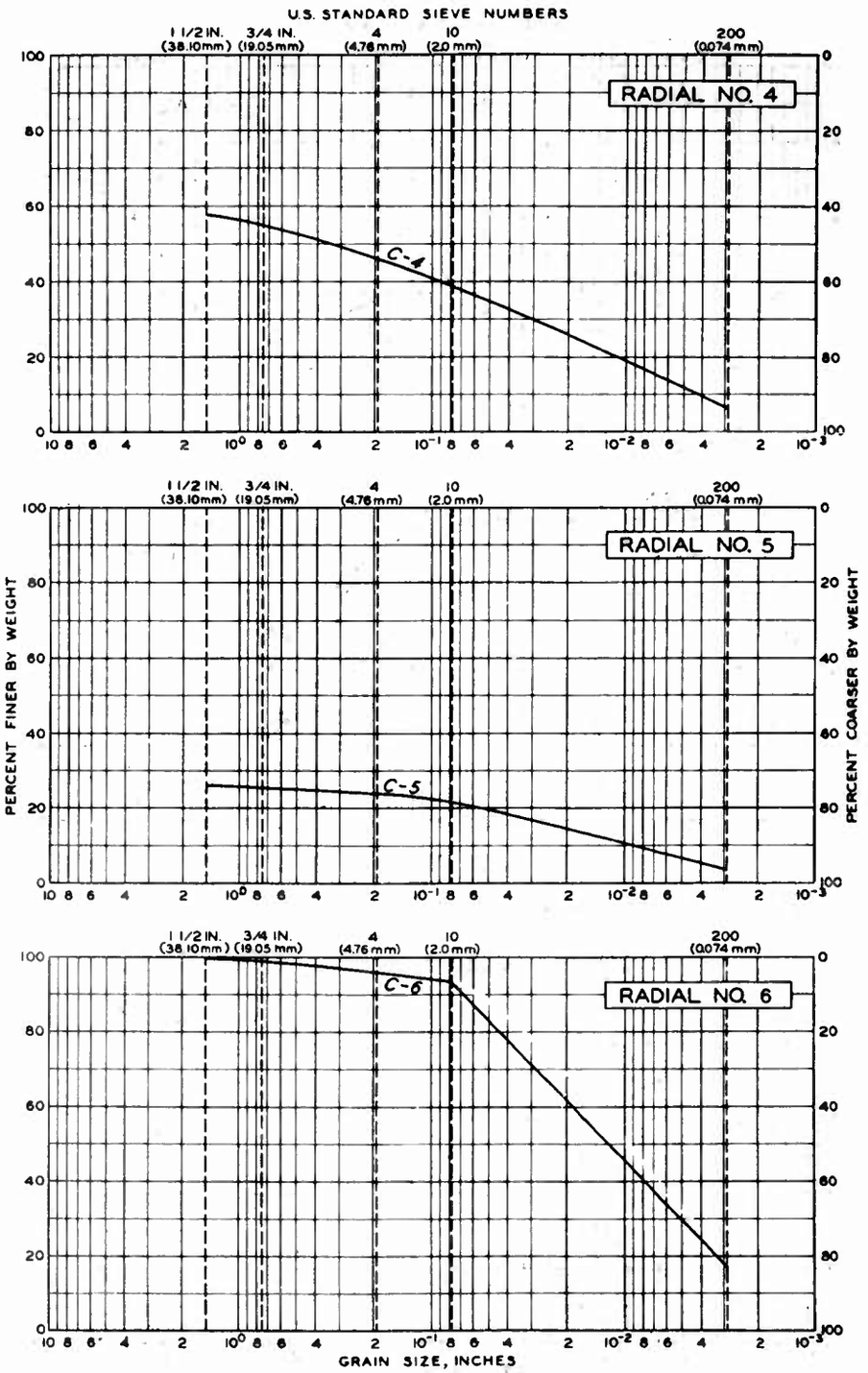

Figure 3.9 Grain-size distribution on radials 4, 5, and 6, Danny Boy.

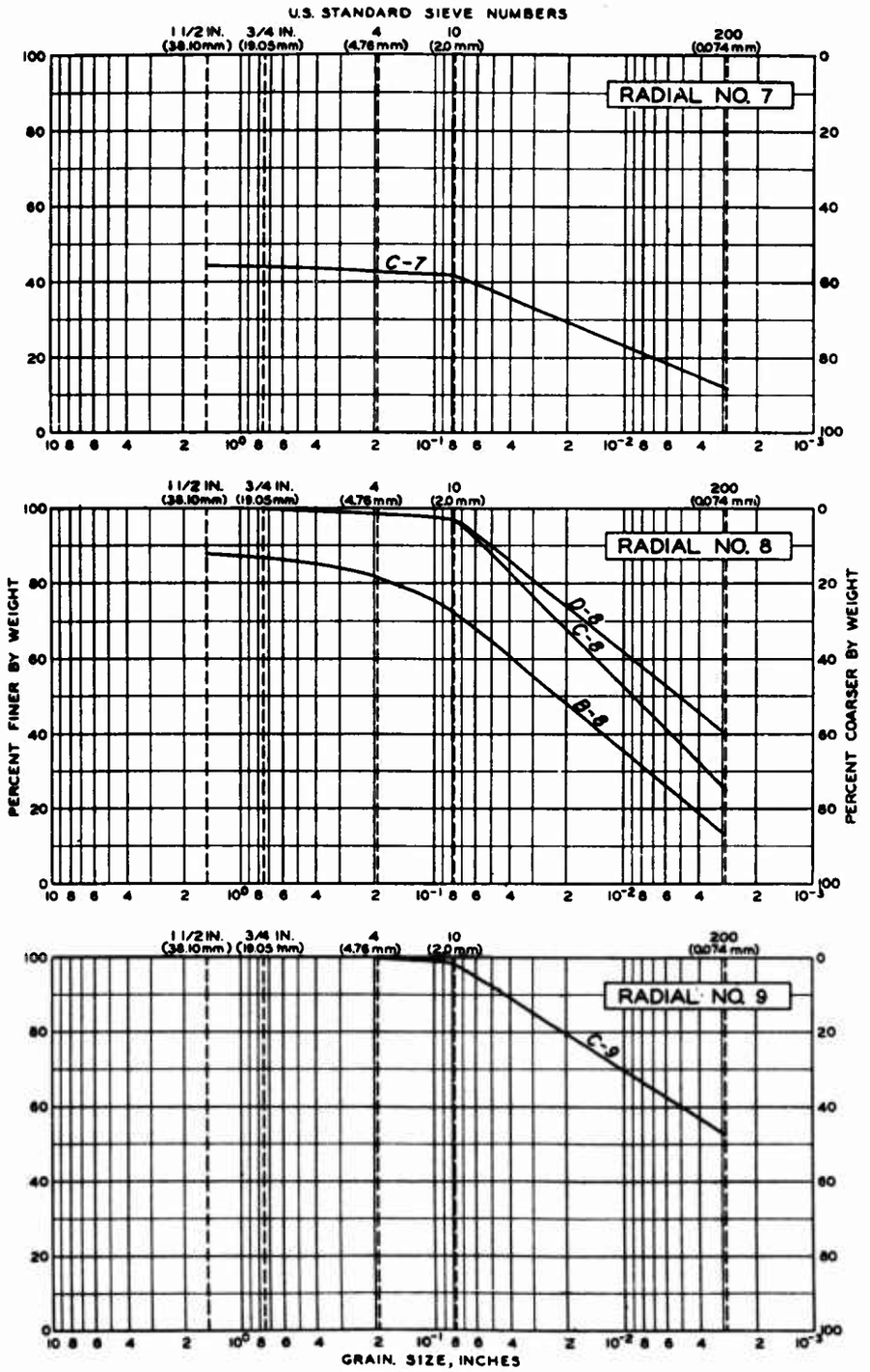

Figure 3.10 Grain-size distribution on radials 7, 8, and 9, Danny Boy.

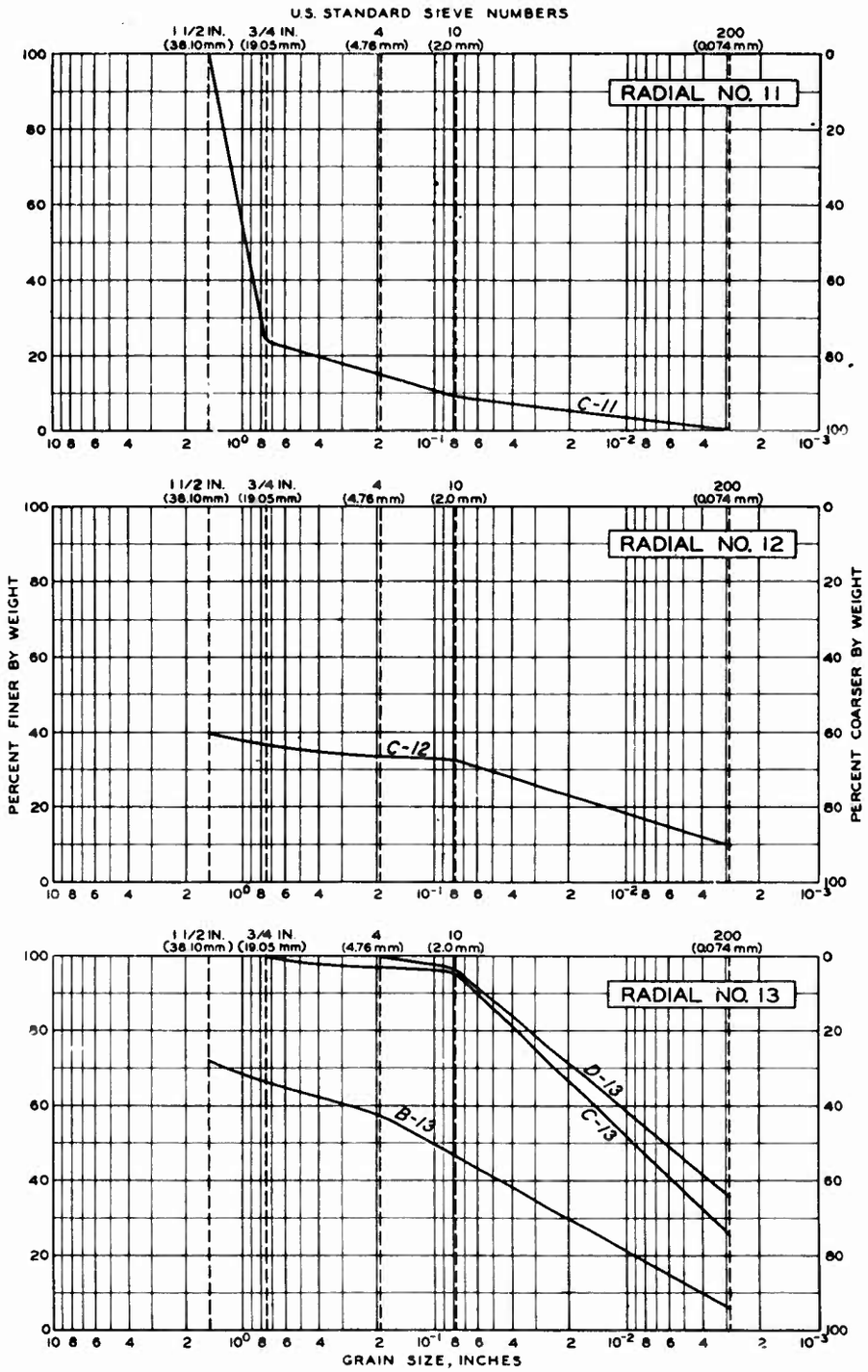

Figure 3.11 Grain-size distribution on radials 11, 12, and 13, Danny Boy.

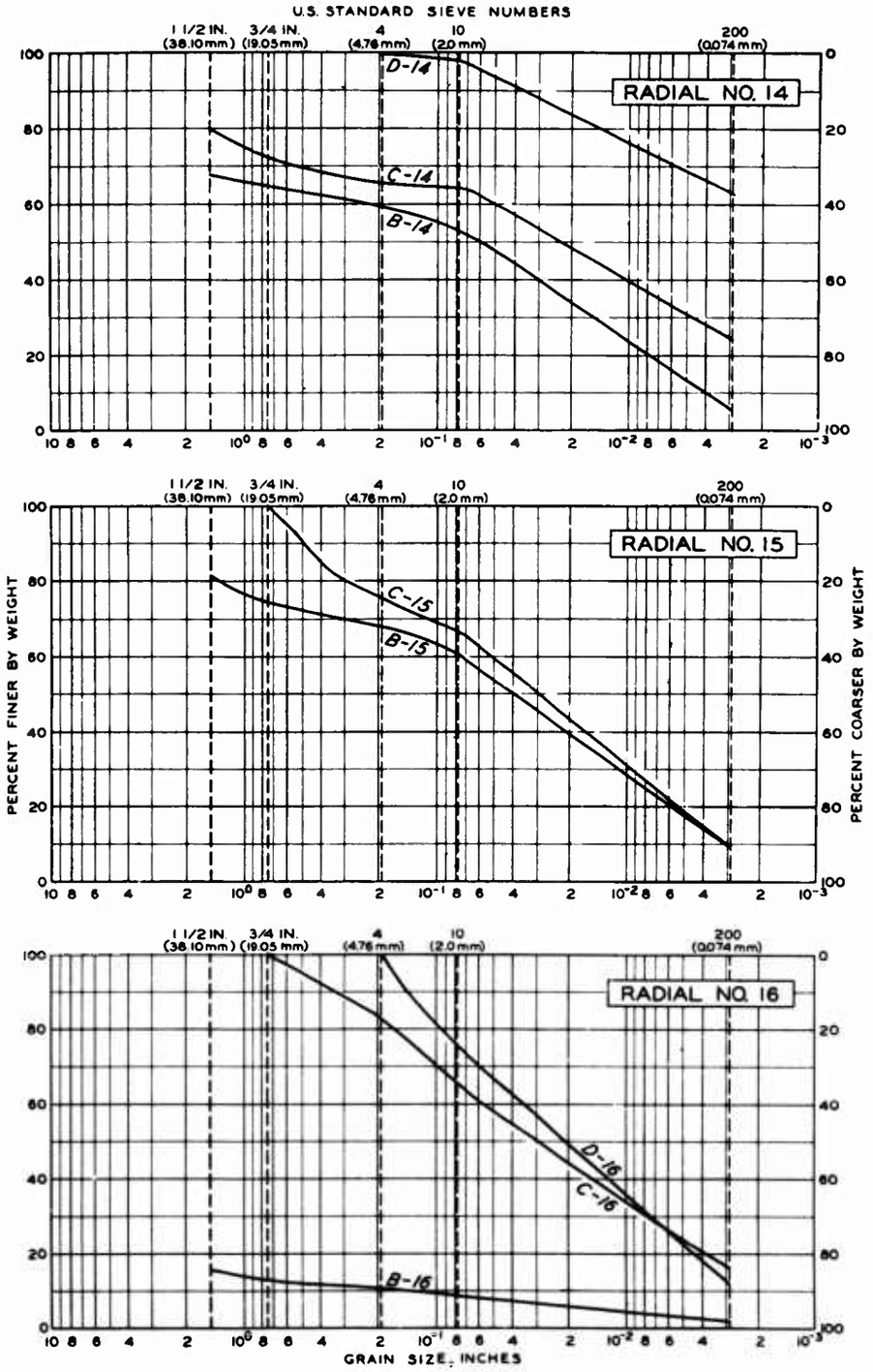

Figure 3.12 Grain-size distribution on radials 14, 15, and 16, Danny Boy.

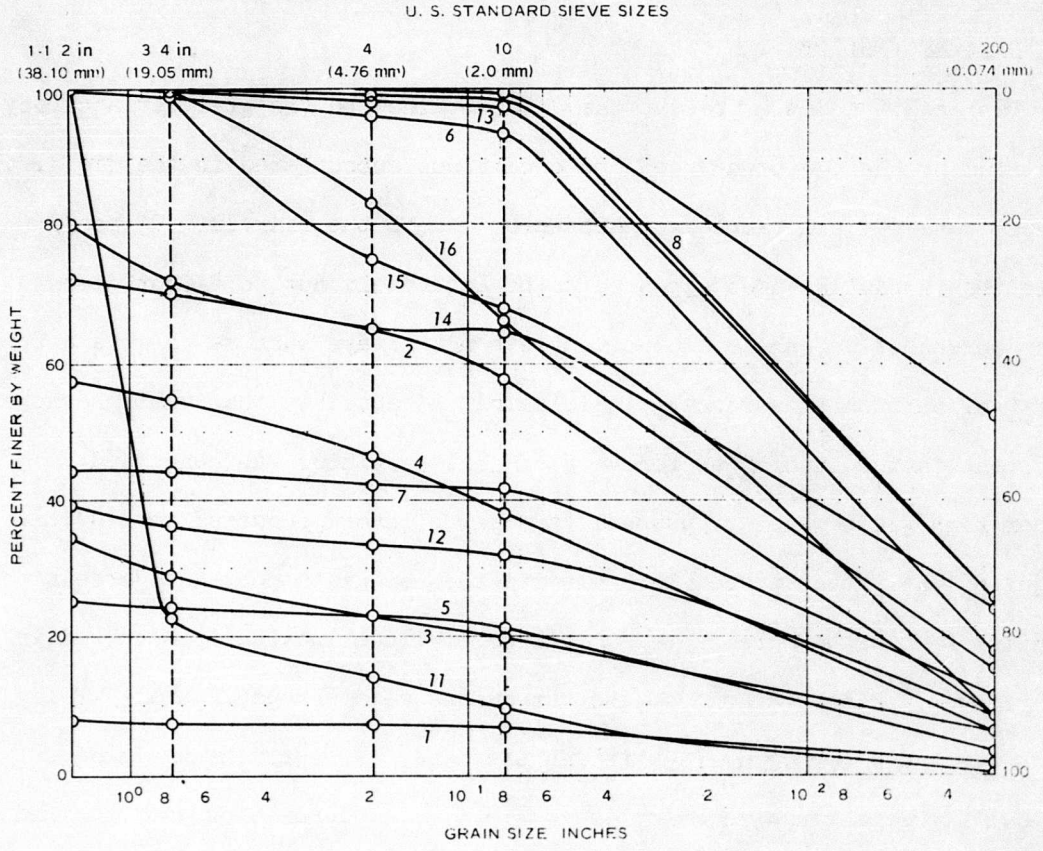

Figure 3.13 Comparison of grain-size distribution around C ring.

CHAPTER 4

DISCUSSION

4.1 DATA RELIABILITY

Tables 3.1 and 3.2 present the data obtained to the greatest accuracy justified by the equipment used and conditions encountered in the field. In most cases, final sample weights were read to the nearest 0.01 pound. While the tarpaulins used appeared to be accurately cut to 4-foot dimensions on each side, their emplacement was not always such as to give a true 16 ft^2 of horizontal surface. It is almost a certainty that weather was an important factor insofar as recovery of fine particles was concerned. Rather high winds were not unusual (a small blizzard occurred on D+4); it is quite likely that these winds altered the immediate postshot deposition quantities. Furthermore, some small loss of fines inevitably occurred in the recovery process. Some of the tarpaulins were damaged, notably B-16, which was badly torn. Where this was the case, every effort was made to achieve as realistic a recovery as possible, i.e. deposition was obtained from fragments of the tarpaulin which remained in place. The matter of moisture content is another unknown. The mass distribution measurements presented herein are for the samples as found, and do not take into consideration any weight changes which may have occurred as a result of changes in moisture content from the time of detonation to the time of recovery. In view of the arid climate of Nevada, and since all specimens were recovered in an apparently dry condition, these differences are probably minor. The A ring (67 meters from GZ) was completely covered by the crater lip, and 10 of the 16 stations on the B ring (94 meters from GZ)

were similarly lost under the outer edge of the lip. Aside from this and the loss of one other station (C-10) as a result of postshot operations by another party, all stations were found in place, and where identifiable samples were present, recovery and processing were accomplished successfully. The most remote recovery was from station E-2 (268 meters), the only sample found on the E ring.

4.2 ANALYSIS OF DATA

4.2.1 Factors Contributing to the Throwout Problem. The rather bewildering array of variables (Reference 12) and environmental conditions accompanying cratering experiments make isolation of those effects most significant with respect to throwout very difficult. The following selection of variables is offered:

1. Charge yield. This is the source of energy which provides the initial impetus for dissociation of the individual earth (or other medium) particles, as well as their ejection into a ballistic path. The velocity with which this energy is propagated varies with the explosive, slow-detonating charges being, as a rule, more efficient in cratering. In high explosives, yield is directly related to charge weight. It is common practice to relate all explosives, including nuclear, to their equivalent weights (energy release) of TNT. Additionally, nuclear explosions are characterized by much higher pressures and temperatures than are HE detonations. The only apparent effect of this characteristic on throwout is the loss of some unknown quantity of ejecta through vaporization.

2. Charge shape. The HE charge shape ordinarily used for cratering experimentation is the sphere. This most closely duplicates the behavior of the point energy source which nuclear detonations resemble. As brought

out in Appendix A (SES tests), charge shape may affect the dimensions of the crater, and may therefore alter throwout deposition. It appears, however, that this effect is noticeable only in large detonations, such as the SES 100-ton shot. Comparison of the plots of mass distribution versus radial distance from GZ for the White Tribe and SES events with those for spherical charges does not reveal any outstanding differences.

3. Depth (height) of burst (DOB or HOB) in relation to the earth-air interface. A depth (height) of burst sufficiently distant from the earth-air interface for the yield involved will cause no crater, hence no throwout. It follows that the charge position must greatly affect both crater shape (References 13, 14) and the resulting ejecta distribution.

4. Medium cratered. The composition of the cratered medium determines the degree of containment of and resistance to the explosive force of the charge. Undoubtedly a competent rock, such as the medium of the Danny Boy shot, will be affected differently than a dry, sandy soil. There are probably many properties of the medium which should be taken into account in any complete consideration of this problem--tensile, compressive, and shear strengths, void ratio, moisture content, and elastic properties, to name a few. Density is sometimes referred to as an overall indicator of the behavior to be expected of the cratered medium.

5. Gravity. An obvious consideration in any crater-formation and throwout problem is acceleration due to the force of gravity. Particularly is this true in the case of the apparent crater. Gravity is the dominant factor shaping the trajectory of large ejecta after the initial velocity provided by the explosion. In scaling explosions, differences in crater size and ejecta distribution due to gravitational effects become

increasingly pronounced as the model size becomes smaller in comparison to the prototype. Although these effects are recognized, current knowledge does not permit their explicit evaluation, and they do not appear in the empirical expression developed in this chapter.

6. Weather. The atmosphere, especially the wind, is the second factor shaping the ballistic trajectory of particles after ejection; it may be dominant in the case of small particles. Very minute particles, commonly called fallout, are essentially windborne. In this report, however, no attempt is made to include measurements of this type of deposition.

4.2.2 Mathematical Expression of Mass Distribution. In most throwout studies the deposition of ejecta and dust is expressed in terms of mass per unit area (δ). As shown in Chapter 3. this report makes use of this notation, employing the metric system (kg/m^2). It becomes immediately apparent that, in such an expression, the deposition or mass distribution must decrease with radial distance (R) from GZ.

Considering the foregoing discussion, it may be said that

$$\delta = f\,(W,\ \theta,\ C_s,\ V_d,\ Z,\ \rho,\ R,\ g). \qquad (1)$$

Certain assumptions are inherent in this expression; namely, that the density of the medium is a valid indicator of its several properties which are significant with respect to cratering and that the effects of weather are negligible.

While Equation 1 may imply a pseudocomplete solution to the throwout problem, the current state of knowledge in this field does not permit such detailed treatment. A simplified empirical expression is used in this report, wherein mass (weight) distribution is equated to some constant

multiplied by the radial distance from GZ raised to some negative exponential value. As used in Chapter 3, its general form is

$$\delta = k\, R^{-m} . \qquad (2)$$

For Danny Boy, least squares fits have been calculated for several of the individual radials, as well as for the arithmetic averages of all recoverable stations on each ring (Figures 3.3-3.5). This latter equation is

$$\delta = 2.69 \times 10^{18}\, R^{-8.85}\ (kg/m^2). \qquad (3)$$

This averaging of data is simply a means for distributing the asymmetric deposition into a symmetric pattern. As may be seen in Table 3.1, this variation for Danny Boy amounted to a factor of 819 (station C-4/station C-5). However, as in the case of the B ring where more than half of the collector array was buried beneath the crater lip, such treatment may tend to bias the data. In this case, exclusion of these stations tends to flatten the slope of the equation. On the other hand, a more complete collection of fine particles and dust, which might have been accomplished under more controlled conditions, would probably have had the opposite effect. The results of sieve analyses show that fines have a definite tendency to travel farther than heavier material.

4.3 CORRELATION WITH PREVIOUS TEST DATA

4.3.1 Examination of Previous Throwout Studies. The attempt to evaluate Danny Boy Project 1.6 was necessarily preceded by a search for and examination of previous, similar experiments. Appendix A, wherein results of studies by Boeing, Sandia Corp., SES, and ERA are presented, represents the results of this effort. In general, the Boeing studies

(References 2, 4-7) present throwout information obtained under a rather wide variety of experimental and environmental conditions. Observations by Sandia, SES, and Bell Telephone Co. are incorporated in Boeing's findings. The ERA dust studies (Reference 1), which were actually studies of both ejecta and dust, provide a wealth of meticulously recorded data, mostly for small charges. Three HE shots for which mass distribution measurements were made and which provide the only comparative information for a basalt medium are reported by Sandia (Reference 9). Certain limitations applying to the foregoing studies are discussed in the appendix.

4.3.2 Correlation by the Method of Dimensions. As will be seen from examination of Tables A.1-A.3, the wide fluctuation of the coefficient k (Equation 2) practically precludes direct comparison of the empirical expressions for mass distribution. Correlation by means of dimensional analysis (References 1, 15) is attempted herein. Making use of Equations 1 and 2, the following selection of variables has been made:

Variable	Notation	Dimensional Representation
Mass distribution	δ*	$ML^{-1}T^{-2}$
Charge weight	W	MLT^{-2}
Radial distance from GZ	R	L
Apparent crater depth	d_a	L
Apparent crater radius	r_a	L

where dimensional representation is in terms of mass-length-time (MLT). It will be noted that most of the significant factors developed in Equation 1

* Here δ is defined as weight per unit area rather than mass per unit area.

are apparently missing. Some have been eliminated as being of secondary importance. In place of others, certain crater parameters have been selected as being more readily predicted or measured. These parameters are chosen as indicators of the terms in Equation 1. Thus, apparent crater depth, a relatively sensitive parameter, is an indicator of the efficiency of the charge, its position, and the resistance of the medium. This term probably indicates better than any other the amount of energy which actually contributed to throwout. In this respect, it is more reliable than the true crater depth, which may have been formed with little or no resulting throwout, as in the case of a camouflet or near-camouflet. The apparent radius, although less sensitive, provides a further description of the crater and also a convenient "measuring stick" when combined with radial distance to give crater radii (R/r_a).

Mathematically, the variables discussed above may be shown as follows:

$$\delta = f\,(W,\ d_a,\ r_a,\ R), \tag{4}$$

which, in dimensional form, becomes

$$ML^{-1}\,T^{-2} = f\,(MLT^{-2},\ L,\ L,\ L). \tag{5}$$

Balancing the equation dimensionally, we obtain

$$\frac{\delta\, d_a\, r_a}{W} = f\,(R/r_a). \tag{6}$$

A number of similar relations can be established. The expression in Equation 6 has been found to provide good correlation between throwout studies while utilizing terms which, except for δ, are readily obtainable or predictable.

The dimensionless graphs shown in Figures 4.1-4.3 were developed by means of Equation 6. (Note that δ in Equation 6 is defined as weight per unit area and not as mass per unit area.) For each shot, the term δ has been evaluated by the use of Equation 2 and then combined with known values of the other terms, i.e. r_a, d_a, R, and W, to provide comparisons between the mass distribution study of Danny Boy and those of Boeing (Figure 4.2), and ERA and Sandia (Figure 4.3). The events selected for comparison represent what is considered the most applicable data and are restricted to yields $\geq$ 5 tons ($\approx$ 4500 kg). Although good comparisons may be obtained using other events enumerated in Appendix A, it is felt that, in view of the difficulties inherent in explosion modeling (Reference 10), the larger yields are most indicative of the results which will be obtained in large-scale testing.

The positions of the curves in these figures do not readily suggest any clear divisions due to differences in yield, medium, of other variables. However, a general trend toward an absolute increase in the exponent m (Equation 3), with a correspondingly steeper slope, may be noted with increasing yield, as it may with significant increases in DOB within a given medium (see Tables A.1-A.3). It appears that the Danny Boy curve may approach the lower limit of the dimensionless plot.

4.3.3 Other Correlative Efforts. The following equation for determining throwout has been proposed by LRL (Reference 11),

$$\delta\ (gm/m^2) = \frac{5 \times 10^6}{1 + 0.02v^3} \left(\frac{R}{W^{1/3}}\right)^{-(3.85 \pm 0.1v)} . \qquad (7)$$

The equation form has been slightly altered to agree with the system of units adopted in this report. In Equation 7, v represents surface wind

velocity in miles per hour, R is in units of 100 yards, and W is in kilotons. The various instructions and limitations relating to the formula are fully discussed in Reference 11. Ignoring the differences imposed by wind direction (compensated for by the $\pm$ 0.1v in the exponent), the following values of δ are indicated for Danny Boy:

Distance, R (m)	δ by Equation 7 (kg/m^2)	Actual average δ (kg/m^2)
94 (B ring)	5.4×10^{-1}	32.2
134 (C ring)	1.4×10^{-1}	2.3
191 (D ring)	3.6×10^{-2}	6.4×10^{-2}
268 (E ring)	9.7×10^{-3}	5.0×10^{-3}

As can be seen, these values agree fairly well for the larger values of R despite the fact that wind manifested no appreciable effect on the sampled Danny Boy ejecta (Figure 3.6).

Sandia Corp. has graphically correlated apparent crater volume with throwout (References 8, 9), and Boeing has expanded somewhat upon this technique, presenting a method of predicting throwout in alluvium and sand-clay media (Reference 2). Preliminary calculations indicate that the total mass of ejecta in the Danny Boy shot was significantly larger than would be anticipated from these references, a possibility which was foreseen in the analysis of the Buckboard data. However, to properly correlate the Danny Boy data with these references, more information is needed than is now available concerning the degree of upthrust of the original ground surface and its contribution to the apparent crater lip. This information should be available in the near future (see paragraph 3.1).

4.4 PREDICTION BY DIMENSIONLESS GRAPHS

A simple prediction technique involving dimensionless plots of the data from Danny Boy and previous studies appears feasible. This technique involves one unknown, δ, which may be desired in the form of a straight-line equation such as Equation 2, or as some value in the dimensions $ML^{-1}T^{-2}$ at a given distance from GZ. Also involved is the value W, which must be known at least approximately, and two predictable parameters, r_a and d_a. As discussed in paragraph 4.3.2, these terms can be combined with R to form dimensionless graphs on which a range of experimental observations can be shown. Figure 4.4 illustrates the envelope of plots presented in Figures 4.1-4.3. Using Figure 4.4, a straight-line representation of δ can be constructed by inspection, or a value of $\delta r_a d_a/W$ can be obtained by entering the argument for crater radii and selecting a specific point in the envelope of data (and implied data curves). If the former technique is used, the equation of δ may be determined by the following steps:

1. Read the value of the ordinate where the constructed line (Figure 4.5) intersects 10° on the abscissa. This becomes the term k in the general equation $y = k\,x^m$.

2. Measure the negative slope, $-m$, of the constructed line.

3. Substitute values in Equation 6 and solve for δ. The solution may be in terms of crater radii,

$$\delta = \left(\frac{k\,W}{r_a d_a}\right)\left(\frac{R}{r_a}\right)^{-m} \tag{8}$$

or in terms of R,

$$\delta = \left(\frac{k\,W}{d_a}\right)(r_a)^{m-1}\,R^{-m}. \tag{9}$$

The coefficient k may also be found after m has been determined by choosing any point o on the predicted curve and solving

$$k = \frac{y_o}{x_o^{-m}} . \tag{10}$$

If the alternate technique is employed in the solution of δ, enter the abscissa argument with the appropriate value for crater radii and select from an inspected point o on the graph the corresponding value of $\delta\, r_a d_a / W$ on the ordinate and solve for δ. The foregoing prediction techniques, illustrated in Figure 4.5, should provide a rough approximation of the average throwout which may be expected from large-yield shots in various materials. The upper and lower limits of data (dashed curves, Figure 4.5) may also be used to predict the possible extremes of the deposition pattern.

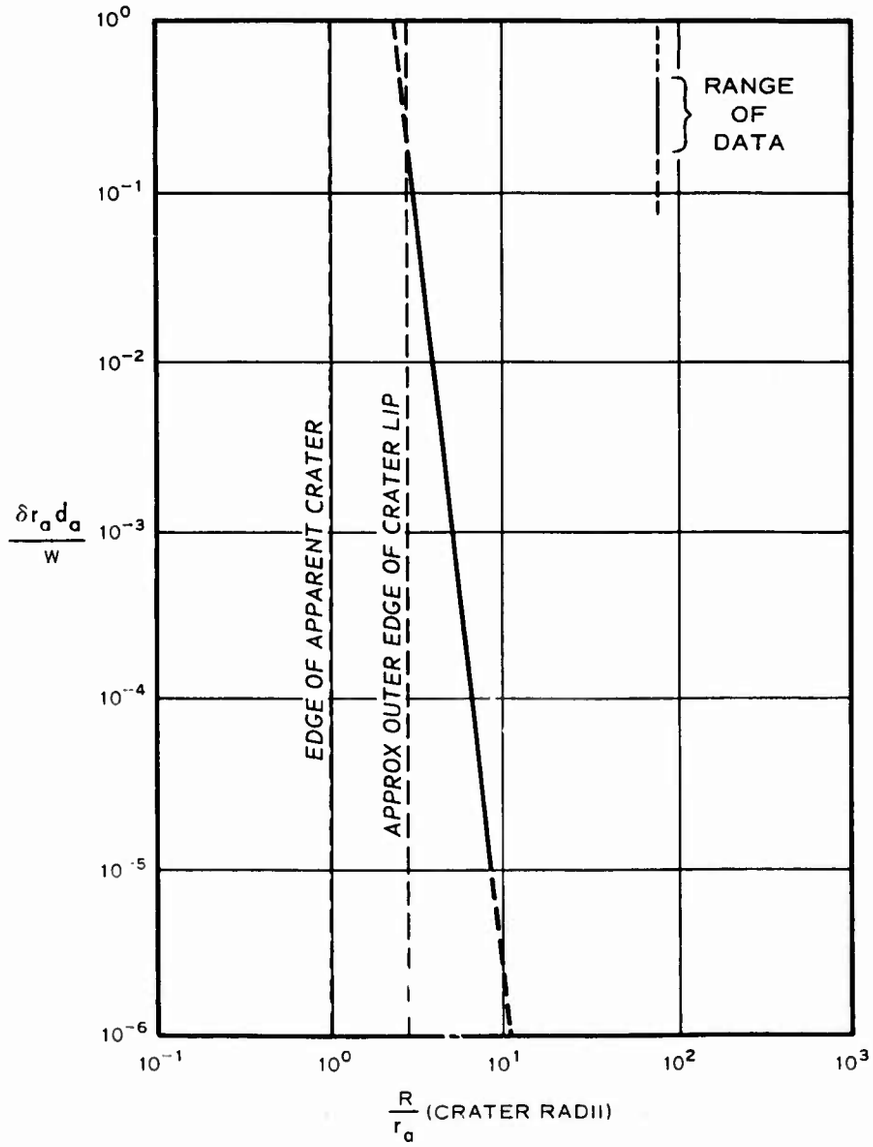

Figure 4.1 Dimensionless mass distribution plot for Danny Boy mass distribution.

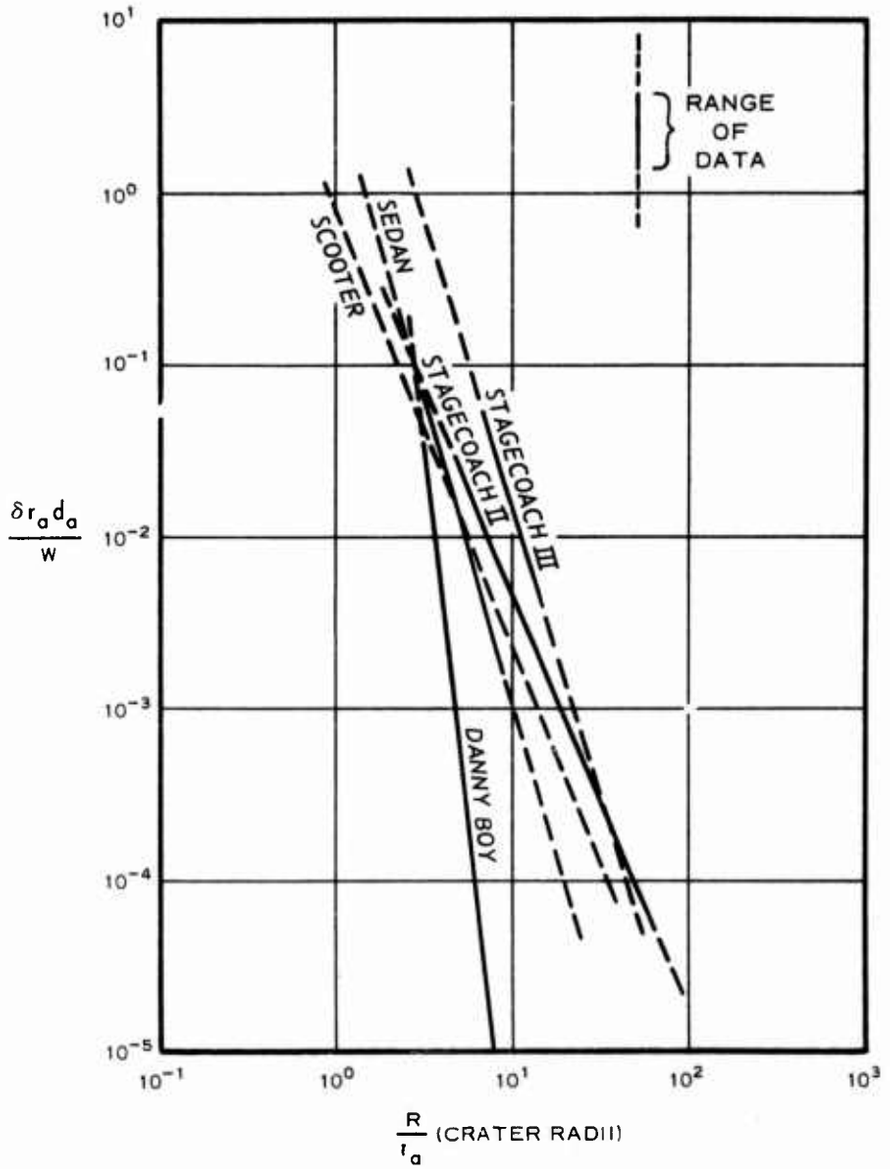

Figure 4.2 Dimensionless mass distribution plot comparing Danny Boy with Boeing studies.

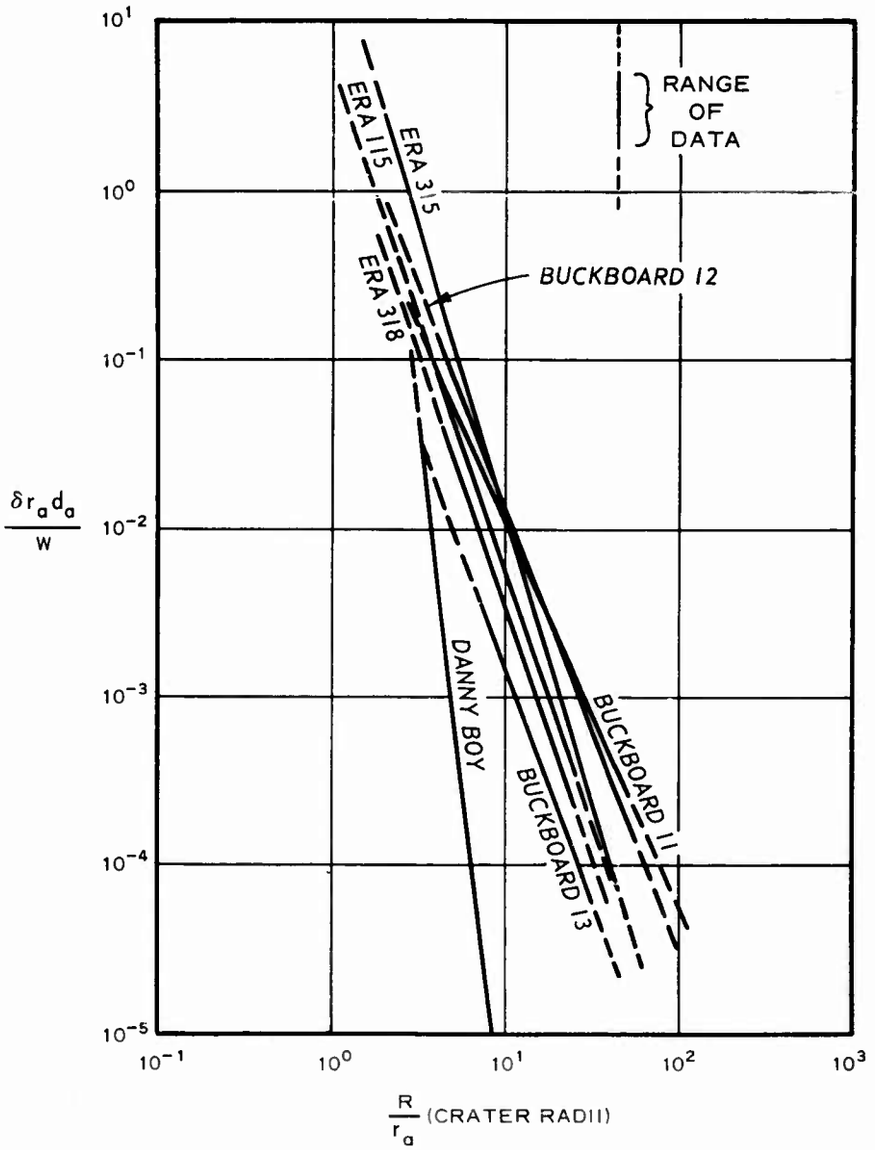

Figure 4.3 Dimensionless mass distribution plot comparing Danny Boy with ERA and Sandia studies.

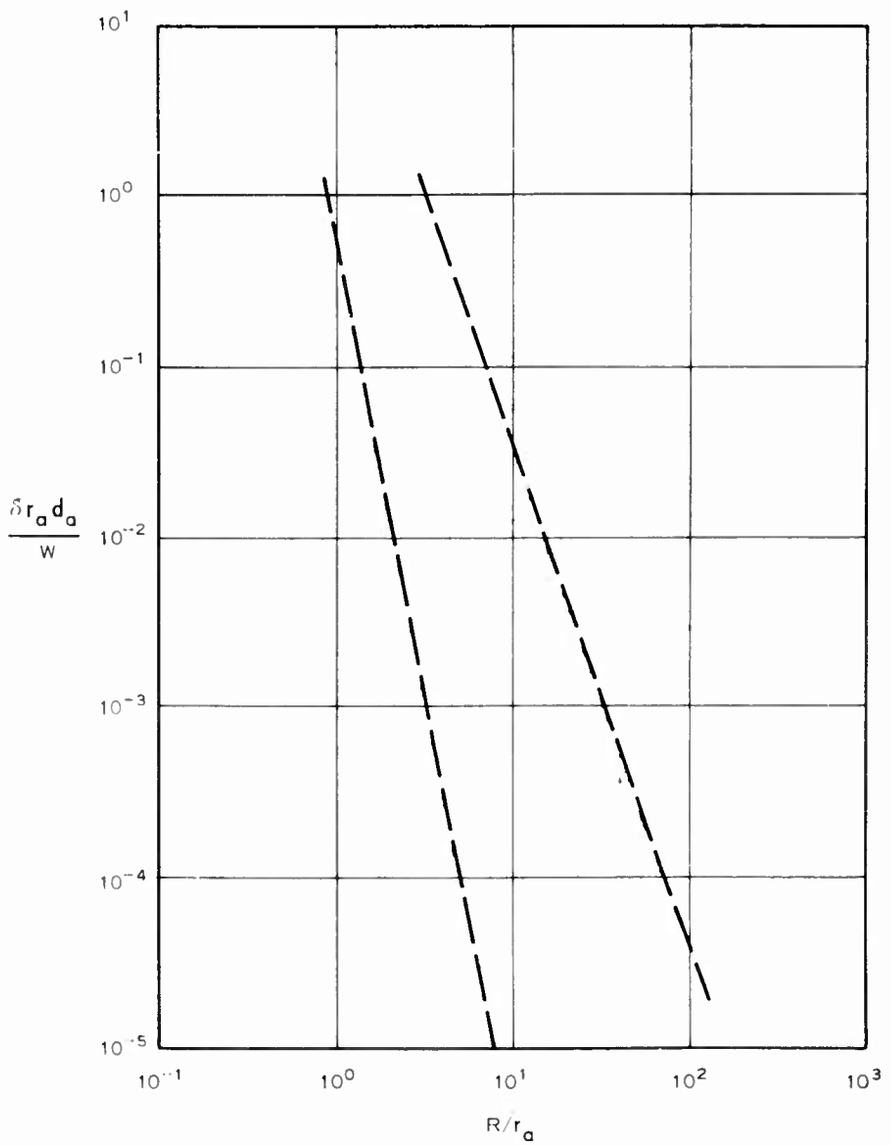

Figure 4.4 Envelope of dimensionless mass distribution curves.

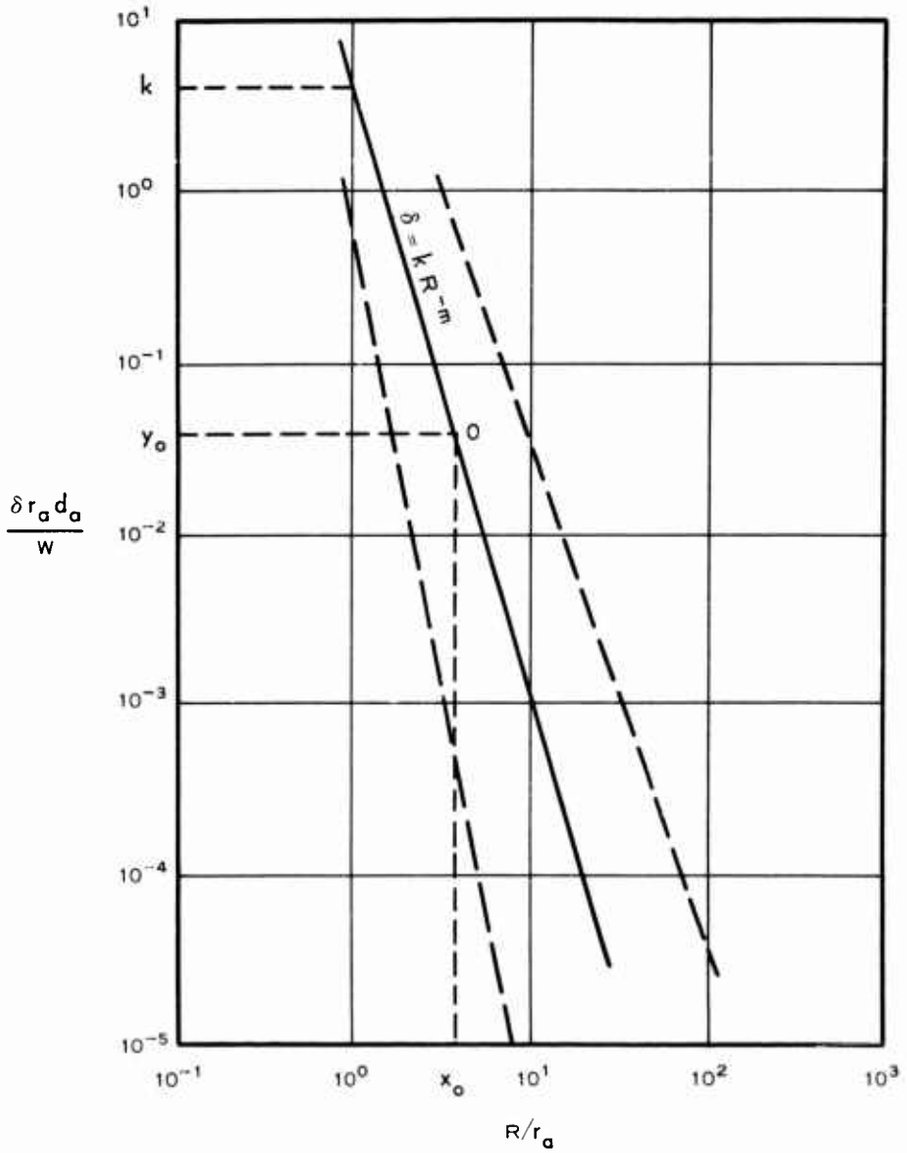

Figure 4.5 Illustration of prediction techniques (see paragraph 4.4).

CHAPTER 5

CONCLUSIONS AND RECOMMENDATIONS

5.1 CONCLUSIONS

A relatively simple experiment in connection with the Danny Boy event made it possible to obtain valuable information on the distribution of ejecta from a nuclear cratering experiment in hard rock. Although safety restrictions, unavoidable in nuclear tests, and unfavorable weather conditions limited the success of sample recovery, the data obtained well justified the experiment.

All of the observed and measured ejecta were deposited close to GZ (within ≈ 8 crater radii), showing negligible effects from wind. The close-in deposition resulted in the formation of a crater lip extending outward to a distance just less than 3 crater radii.

Shot Danny Boy is unique insofar as mass distribution studies are concerned, since it is, by a considerable margin, the largest charge ever fired in very dense rock and permitted to vent. The resulting mass distribution curve represents one of the extremes when correlated with similar studies.

Correlation and prediction of throwout, neglecting the effect of wind, appear feasible by means of dimensionless plots. In conjunction with other techniques discussed in Chapter 4, this method should provide as satisfactory an appreciation of mass distribution as the current state of the art permits.

5.2 RECOMMENDATIONS

In view of the scarcity of data on the subject of mass distribution, as well as its questionable correlation between similar experiments in some instances, and in view of the need for this information, it is recommended that additional experiments of this nature be conducted in connection with full-scale tests, if possible involving a variety of charge positions and media. It seems probable that only with the careful collection of a large amount of data under many different conditions will the physical law(s) governing this phenomenon be understood.

The unevenness of ejecta deposition, as well as the question of wind effects, makes a circumferential sampling array almost mandatory for valid results. The optimum collector layout would, of course, provide samples from the crater edge to the greatest distance at which specimens could be distinguished. In this connection, it seems that some standardization of terminology might be beneficial, as, for instance, in the terms "throwout" (ejecta) and "fallout." Experimental results of the two should complement one another, but they are essentially different problems and are usually the subject of different studies. It is suggested that the former is primarily a missile and an overburden problem and the latter primarily a radiation problem, and that the delineation be on this basis.

Since recovery of collectors within the crater lip region is usually not practicable, future experiments of this nature should include plans for sufficient postshot trenching to enable determination of the ejecta-ground interface and subsequent expression of the magnitude of throwout in the lip. Some such observations have been made in the past, but not, as far as is known, as part of throwout studies. Perhaps a planned exchange

of information would be helpful in this respect. In the case of the Danny Boy experiment, publication of an addendum to this report is contemplated (probably by the end of CY 63) to include this type of information; it will be prepared after completion of a study of the properties of nuclear craters now being conducted by the Soils Division, WES.

APPENDIX A

PREVIOUS MASS DISTRIBUTION STUDIES

A.1 SUMMARIES OF DATA

Tables A.1 and A.2 summarize previous mass distribution studies for which a relation in the form of Equation 2 has been established. Table A.3 compares data from ERA and Sandia's Buckboard studies, combining into single equations those events in which experimental and environmental conditions were (with the exception of weather) identical.

Figures A.1-A.7 represent δ versus R plots of mass distribution studies summarized in Table A.1, and Figures A.8-A.40 similarly represent events summarized in Table A.2. Sources of these data are References 1, 2, 4-7, 8, 9, 16, and 17.

All throwout studies known to the author have been credited in this report. Most are presented in this appendix, the only intentional omissions being Danny Boy, which is discussed in the main body of the report, and certain ERA shots for which fewer than three usable (average $\delta \geq 5$ gm/m^2) data points were available.

A.2 DATA LIMITATIONS

Certain limitations of the data contained in this appendix are discussed in the following paragraphs.

A.2.1 Suffield (SES). These data were obtained principally from two narrow sectors in the case of the 100-ton shot and from a 45-degree sector in the case of the 5-ton shot, the latter being a missile survey. Circumferential variation of ejecta may have affected the results of both shots.

Further, the 5-ton shot was made on soil which had previously been disturbed. Both of these shots employed hemispheres of HE, thus departing from the simulated point energy sources usually used in cratering experiments. Although the explosive was in contact with (resting upon) the ground surface, its center of gravity was somewhat above the earth. The result, especially in the case of the larger shot, appears to have been a crater of larger diameter/depth ratio than is normally experienced. It seems likely that these factors may have influenced the equation for mass distribution.

A.2.2 White Tribe. This was an experiment involving three triple bursts (nine charges), in which each charge was geometrically similar to the SES charges. One collector radial extended outward from each charge. Although the array was designed for minimum interference between charges, it is probable that some overlap of deposition occurred on all radials. Also, the question of circumferential variation should be considered.

A.2.3 ERA Underground Explosion Tests. These experiments were conducted under relatively controlled conditions, and, particularly when combined with Sandia's Buckboard series, provide very interesting throwout information for a wide range of yields, media, and DOB. It should be borne in mind, however, that most of the charges were small, and the applicability of the results to full-scale (i.e. nuclear) tests cannot be assured.

A.2.4 Scooter. Boeing's mass distribution curve for this event was derived from a total of six observations on two diametrically opposed radials. Data points for Sandia's curve have not been published.

TABLE A.1 SUMMARY OF MASS DISTRIBUTION STUDIES BY BOEING AIRPLANE CO.[a]

Event	Yield	Type of Explosive	Depth of Burst	λ	Apparent Depth and Radius	Medium	Mass Distribution Formula	
	kg KT or tons		m	$\frac{m}{kg^{1/3}}$	m			
Scooter	4.5×10^5 0.5-KT	HE	38	0.50	22.8 46.6	Desert alluvium	$8.9 \times 10^6 R^{-2.60}$	
Sedan	9.1×10^7 100-KT	NE	193	0.43	97 195	Desert alluvium	$5.77 \times 10^{12} R^{-3.64}$	
Stagecoach II	1.8×10^4 20-ton	HE	5.2	0.20	7.2 15.4	Desert alluvium	$1.95 \times 10^5 R^{-2.46}$	b
Stagecoach III	1.8×10^4 20-ton	HE	10.4	0.40	8.6 17.8	Desert alluvium	$7.32 \times 10^7 R^{-3.39}$	b
Suffield[c]	4.5×10^3 5-ton	HE	Contact[d]	0.00	3.8 6.1	Silt and clay	$4.5 \times 10^4 R^{-2.93}$	
Suffield	9.1×10^4 100-ton	HE	Contact[d]	0.00	6.2 23.5	Silt and clay	$2.56 \times 10^8 R^{-3.65}$	
White Tribe[e] (I-III)	5.2×10^3 6-ton approx.	HE	Contact[d]	0.00	2.5 5.3	Caliche	$8.9 \times 10^4 R^{-2.73}$	
Teapot Ess	1.1×10^6 1.2-KT	NE	20.3	0.20	27.4 44.4	Desert alluvium	--	f
Jangle HE-2	1.8×10^4 20-ton	HE	1.6	0.05	4.5 12.1	Desert alluvium	--	f

[a] See References 2, 4-7.

[b] Equation computed by WES. Includes fit of Sandia Corp. data, excepting samples < 5 gm/m^2.

[c] Original mass distribution study conducted by Bell Telephone.

[d] Hemispherical charge with center of gravity slightly above ground surface.

[e] Data is average of nine shots.

[f] Mass distribution equations vary with distance from GZ (see Reference 2).

TABLE A.2 SUMMARY OF SHOT DATA, ERA AND SANDIA (BUCKBOARD)[a]

Medium	W	DOB	Crater Dimensions r_a	Crater Dimensions d_a	δ[b]	Round Number	Remarks
	kg	m	m	m	kg/m^2		
Engineering Research Associates:							
Dry sand	145	1.1	4.0	2.3	$3.83 \times 10^2 R^{-1.98}$	110	
	1,161	0.8	5.5	3.0	$3.64 \times 10^4 R^{-2.71}$	108	
	1,161	2.1	9.1	3.7	$9.46 \times 10^6 R^{-3.75}$	112	
	18,144	5.4	22.9	7.0	$2.05 \times 10^7 R^{-3.17}$	115	
Dry clay	50	0.7	2.7	1.8	$4.98 \times 10^2 R^{-2.18}$	316	
	145	1.1	3.2	1.8	$7.45 \times 10^4 R^{-3.36}$	304	
	145	1.1	3.4	2.1	$1.10 \times 10^5 R^{-3.37}$	310	
	145	1.1	3.9	2.4	$2.40 \times 10^3 R^{-2.27}$	313	
	145	2.1	3.6	2.1	$4.35 \times 10^5 R^{-3.69}$	305	
	145	2.1	3.8	2.1	$4.02 \times 10^4 R^{-3.00}$	Symmetry	
	1,161	0.8	6.1	3.7	$1.22 \times 10^4 R^{-2.56}$	308	
	1,161	2.1	6.6	4.7	$1.12 \times 10^6 R^{-3.51}$	309	
	1,161	2.1	7.9	4.6	$1.12 \times 10^4 R^{-2.14}$	312	
	18,144	5.3	19.5	12.8	$1.62 \times 10^8 R^{-3.59}$	315	
	145,150	10.7	36.6	18.3	$9.91 \times 10^7 R^{-3.03}$	318	
Wet clay	145	0.8	5.7	3.0	$5.51 \times 10^2 R^{-1.84}$	402	
	145	0.8	5.3	3.5	$1.12 \times 10^4 R^{-2.32}$	404	
	1,161	1.5	12.7	3.9	$7.15 \times 10^6 R^{-3.40}$	403	
Sandstone	145	0.8	--	--	$2.21 \times 10^2 R^{-2.01}$	803	Apparent crater data not available for sandstone shots
	145	0.8	--	--	$6.23 \times 10^1 R^{-1.43}$	807	
	145	0.8	--	--	$7.02 \times 10^3 R^{-2.74}$	808	
	145	0.8	--	--	$2.60 \times 10^3 R^{-2.39}$	819	Cemented in place with hydrostone, possibly affecting energy partition
	145	1.5	--	--	$1.51 \times 10^2 R^{-1.65}$	804	
	145	3.8	--	--	$3.20 \times 10^3 R^{-2.45}$	805	
	1,161	1.5	--	--	$8.83 \times 10^7 R^{-3.99}$	810	
	1,161	1.5	--	--	$2.71 \times 10^5 R^{-2.98}$	811	
	18,144	3.8	--	--	$3.59 \times 10^6 R^{-2.88}$	814	
	18,144	3.8	--	--	$6.10 \times 10^5 R^{-2.56}$	815	
	145,150	7.6	--	--	$1.51 \times 10^9 R^{-3.35}$	817	
Limestone	145	2.0	--	--	$5.94 \times 10^2 R^{-1.84}$	501	Apparent crater dimensions not available
Project Buckboard:							
Basalt	18,144	7.8	13.6	7.6	$2.43 \times 10^5 R^{-2.36}$	11	
	18,144	13.0	17.4	10.6	$1.35 \times 10^6 R^{-2.68}$	12	
	18,144	17.9	11.2	4.9	$3.88 \times 10^5 R^{-2.86}$	13	

[a] Excludes shots with fewer than three usable data points.

[b] Based on averages at given radial distances. Excludes data points where ejecta and dust weight < 5 gm/m^2.

TABLE A.3 COMPARISON OF SHOT DATA, ERA AND SANDIA (BUCKBOARD)

Medium	W	$W^{1/3}$	λ	δ	Round Number
	kg	kg	$m/kg^{1/3}$	kg/m^2	
Engineering Research Associates:					
Dry sand	145	5.3	0.2	$3.83 \times 10^2 R^{-1.98}$	110
↓	1,161	11	0.1	$3.64 \times 10^4 R^{-2.71}$	108
	1,161	11	0.2	$9.46 \times 10^6 R^{-3.75}$	112
	18,144	26	0.2	$2.05 \times 10^7 R^{-3.17}$	115
Dry clay	50	3.7	0.2	$4.98 \times 10^2 R^{-2.18}$	316
↓	145	5.3	0.2	$6.21 \times 10^3 R^{-2.63}$	304, 310, 313
	145	5.3	0.4	$5.89 \times 10^4 R^{-3.14}$	305, Symmetry
	1,161	11	0.1	$1.22 \times 10^4 R^{-2.56}$	308
	1,161	11	0.2	$3.49 \times 10^4 R^{-2.55}$	309, 312
	18,144	26	0.2	$1.62 \times 10^8 R^{-3.59}$	315
	145,150	53	0.2	$9.91 \times 10^7 R^{-3.03}$	318
Wet clay	145	5.3	0.2	$3.50 \times 10^3 R^{-2.16}$	402, 404
↓	1,161	11	0.1	$7.15 \times 10^6 R^{-3.40}$	403
Sandstone	145	5.3	0.2	$1.74 \times 10^2 R^{-1.78}$	803, 807, 808, 819
↓	145	5.3	0.3	$1.51 \times 10^2 R^{-1.65}$	804
	145	5.3	0.7	$3.20 \times 10^3 R^{-2.45}$	805
	1,161	11	0.1	$1.22 \times 10^6 R^{-3.22}$	810, 811
	18,144	26	0.1	$2.45 \times 10^6 R^{-2.81}$	814, 815
	145,150	53	0.1	$1.51 \times 10^9 R^{-3.35}$	817
Limestone	145	5.3	0.4	$5.94 \times 10^2 R^{-1.84}$	501
Sandia (Buckboard):					
Basalt	18,144	26	0.3	$2.42 \times 10^5 R^{-2.36}$	11
↓	18,144	26	0.5	$1.35 \times 10^6 R^{-2.68}$	12
	18,144	26	0.7	$3.88 \times 10^5 R^{-2.86}$	13

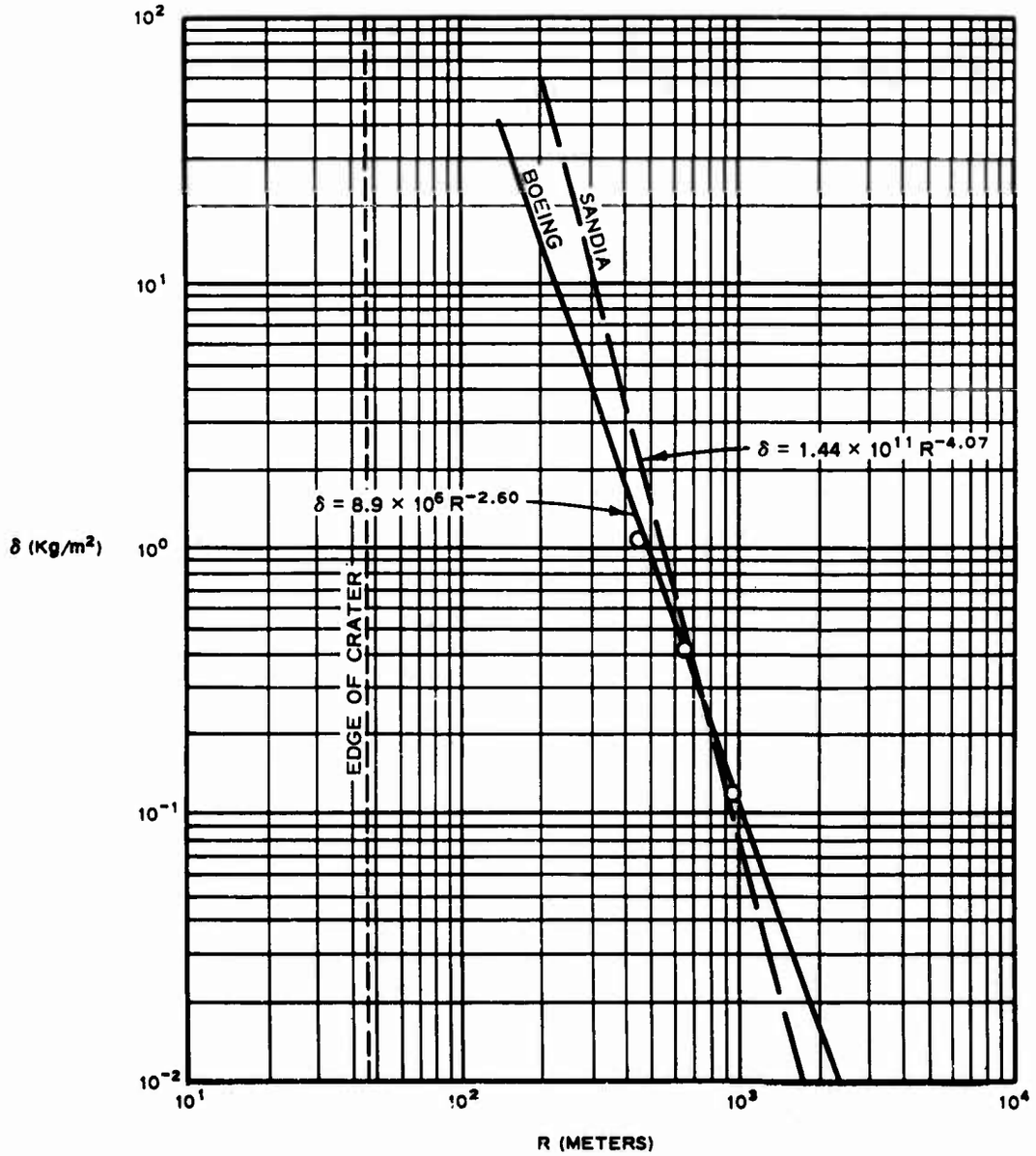

Figure A.1 Mass distribution (δ) versus radial distance from GZ (R) for Scooter.

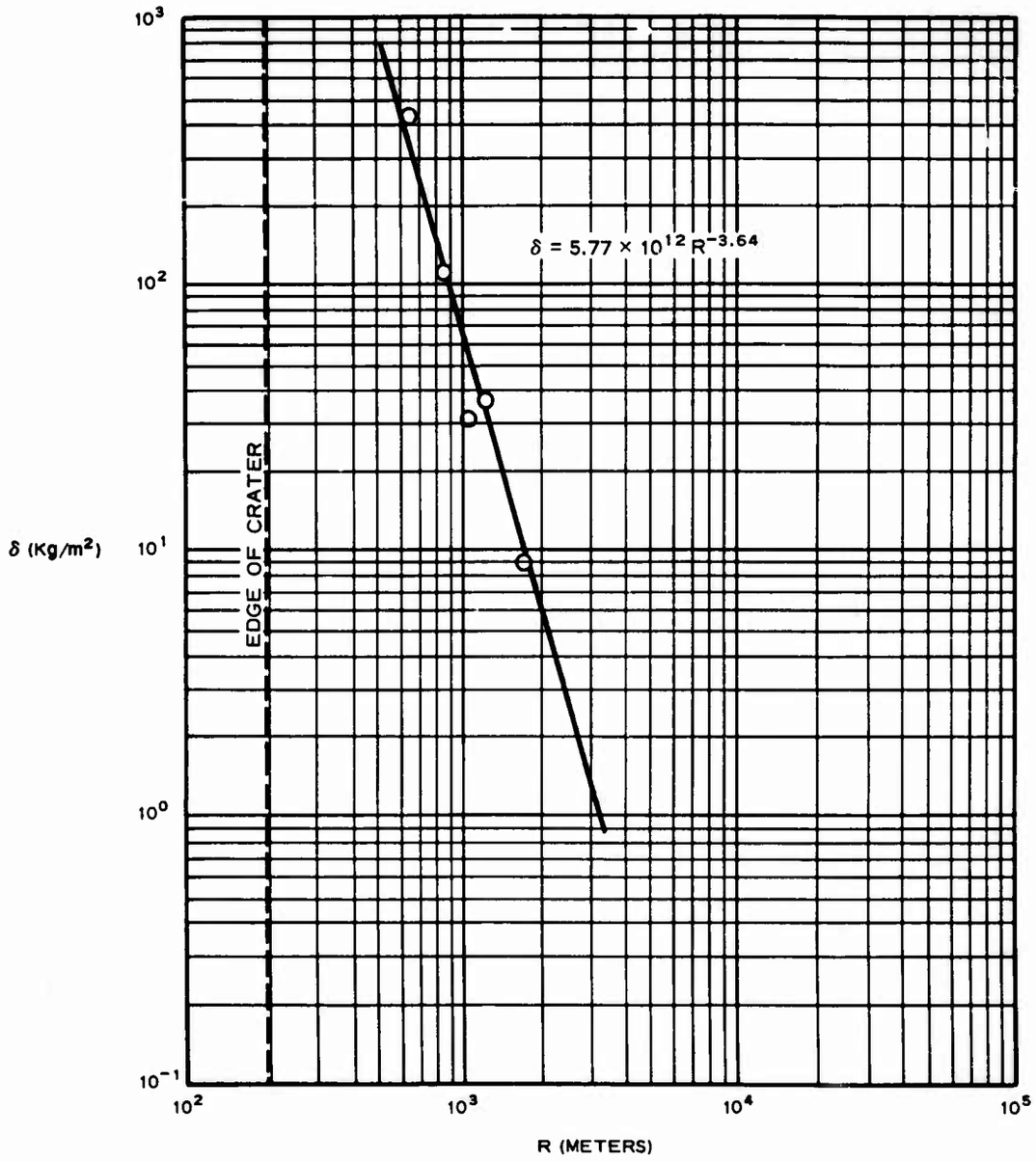

Figure A.2 Mass distribution (δ) versus radial distance from GZ (R) for Sedan.

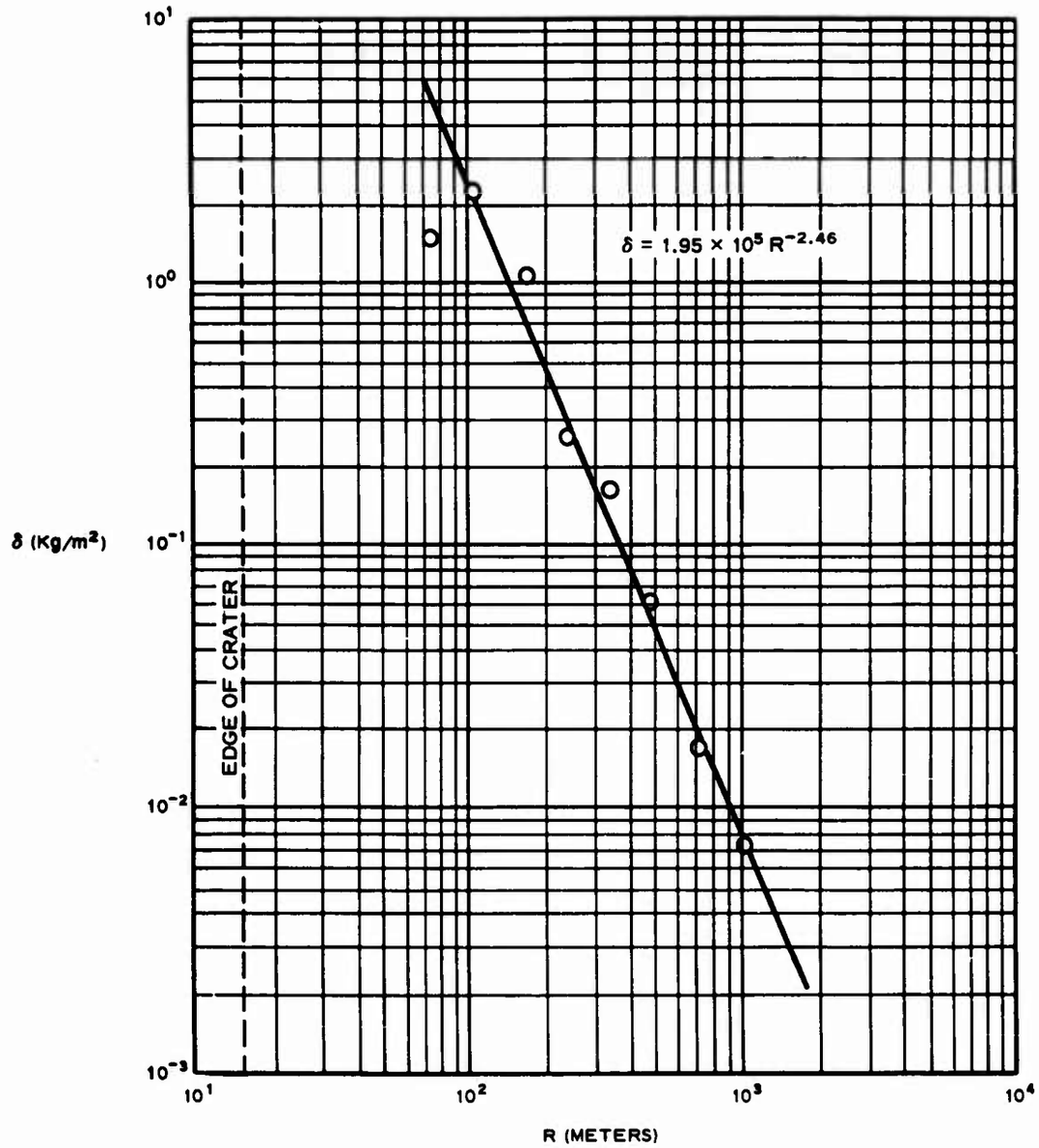

Figure A.3 Mass distribution (δ) versus radial distance from GZ (R) for Stagecoach II.

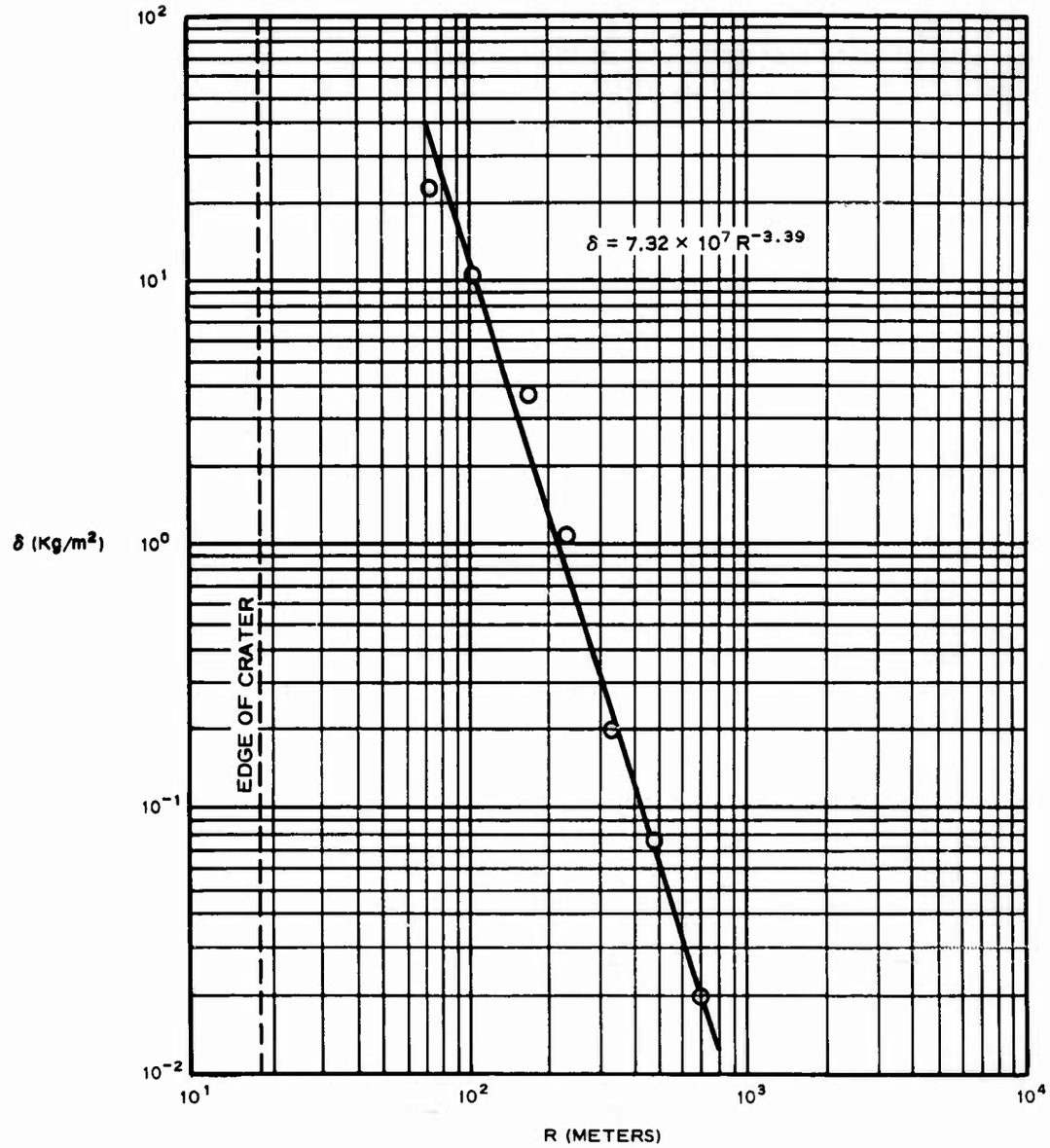

Figure A.4 Mass distribution (δ) versus radial distance from GZ (R) for Stagecoach III.

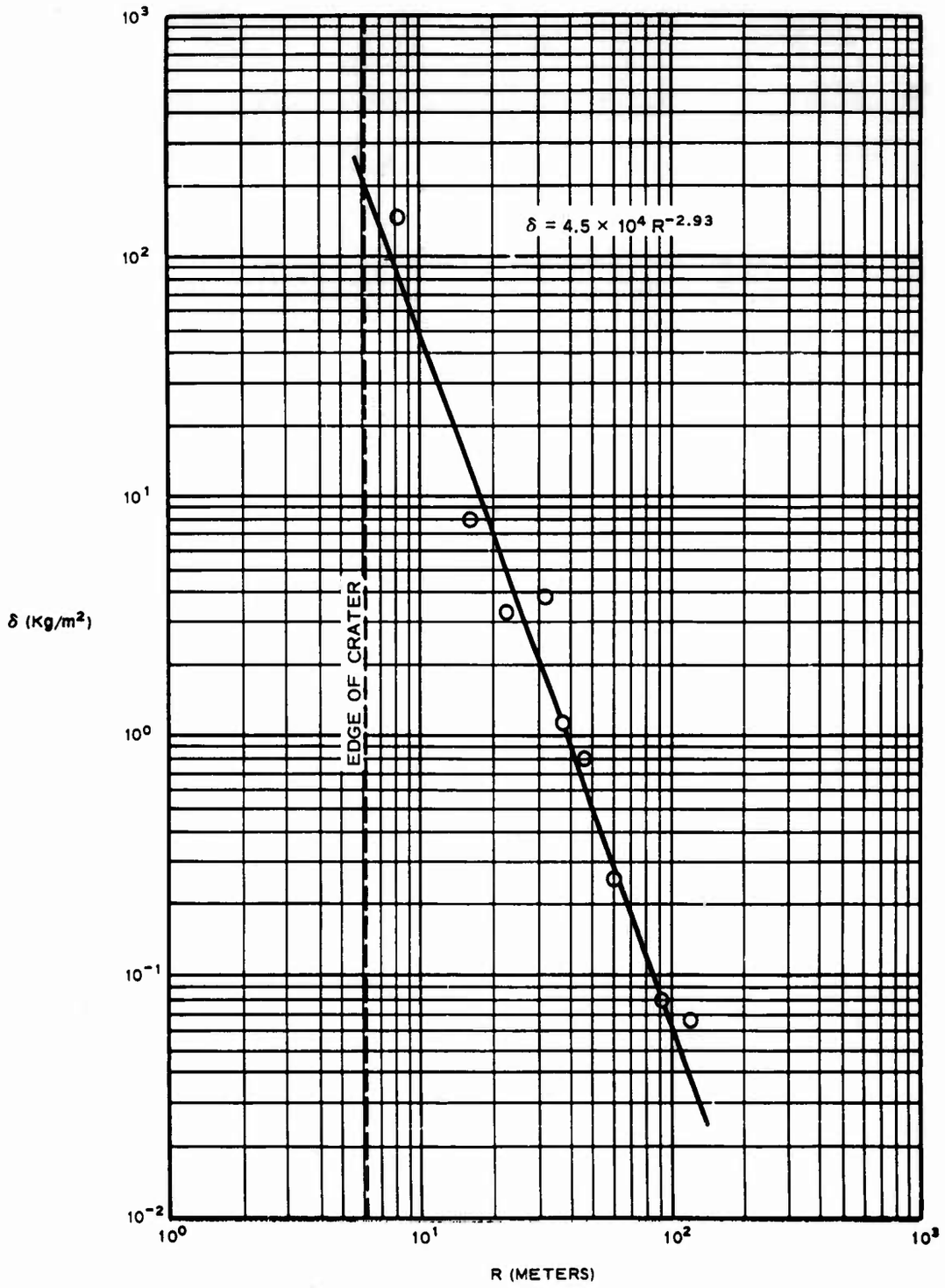

Figure A.5 Mass distribution (δ) versus radial distance from GZ (R) for Suffield 5-ton event.

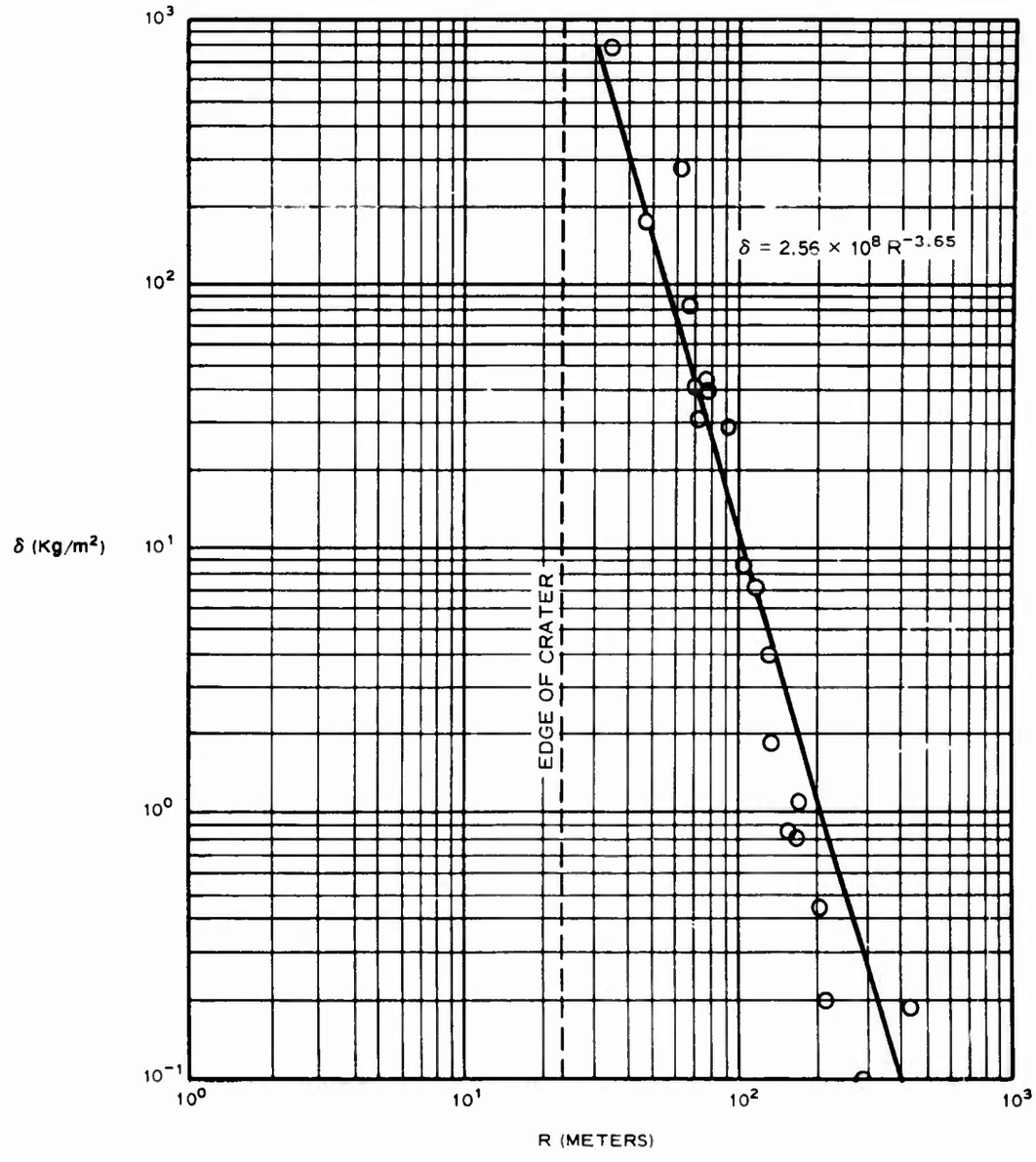

Figure A.6 Mass distribution (δ) versus radial distance from GZ (R) for Suffield 100-ton event.

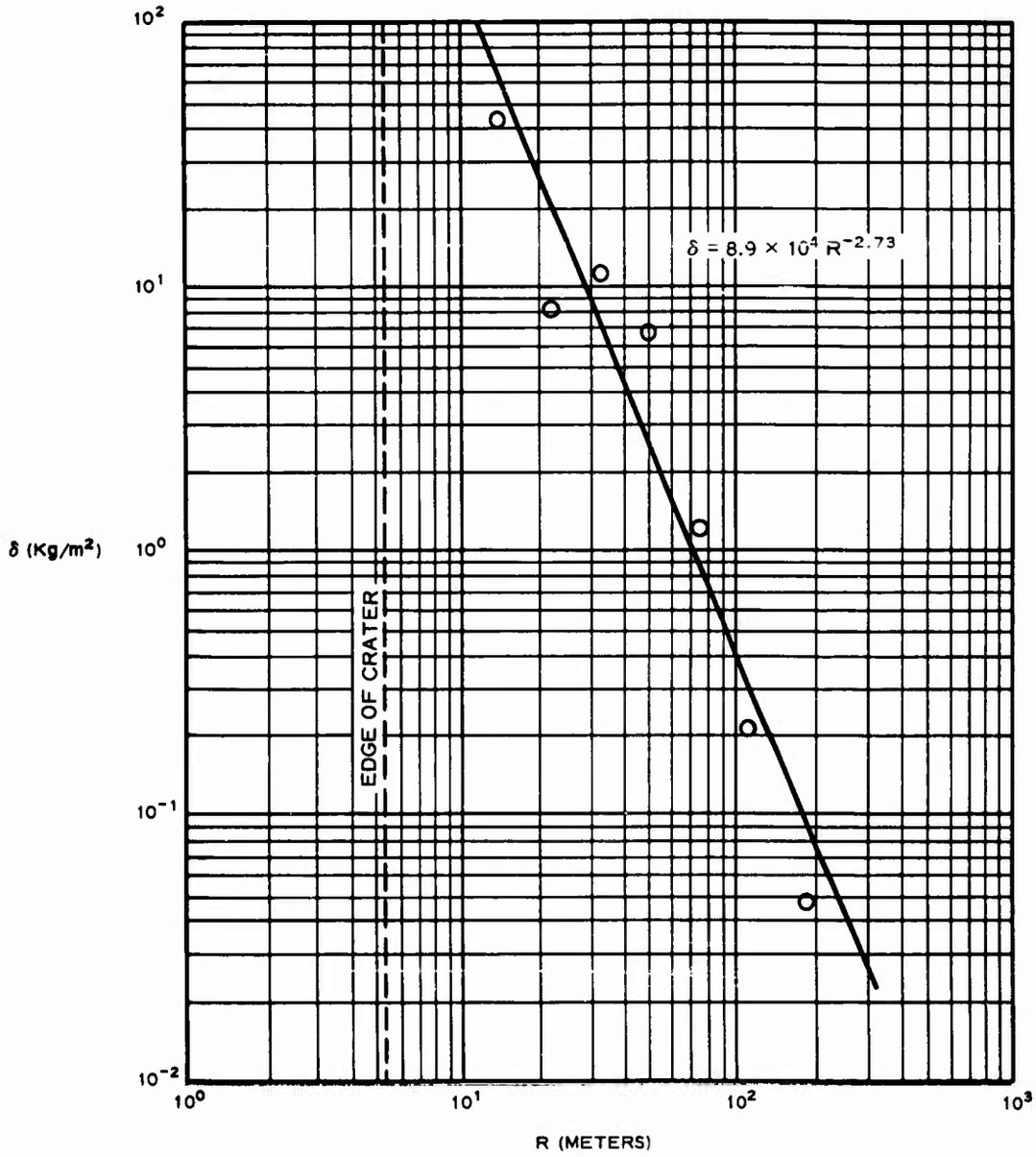

Figure A.7 Mass distribution (δ) versus radial distance from GZ (R) for the averages of White Tribe data.

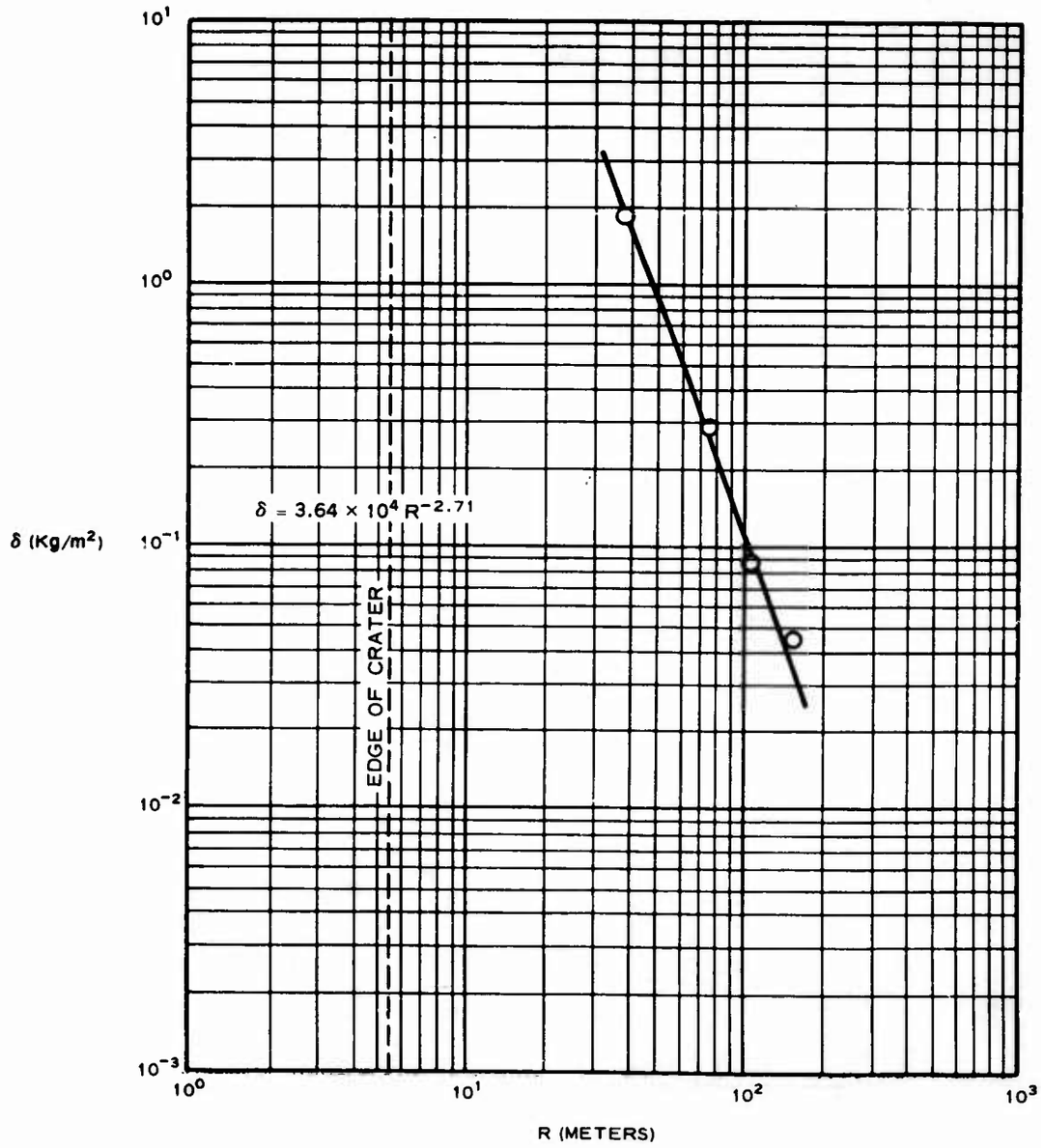

Figure A.8 Mass distribution (δ) versus radial distance from GZ (R) for ERA Round 108.

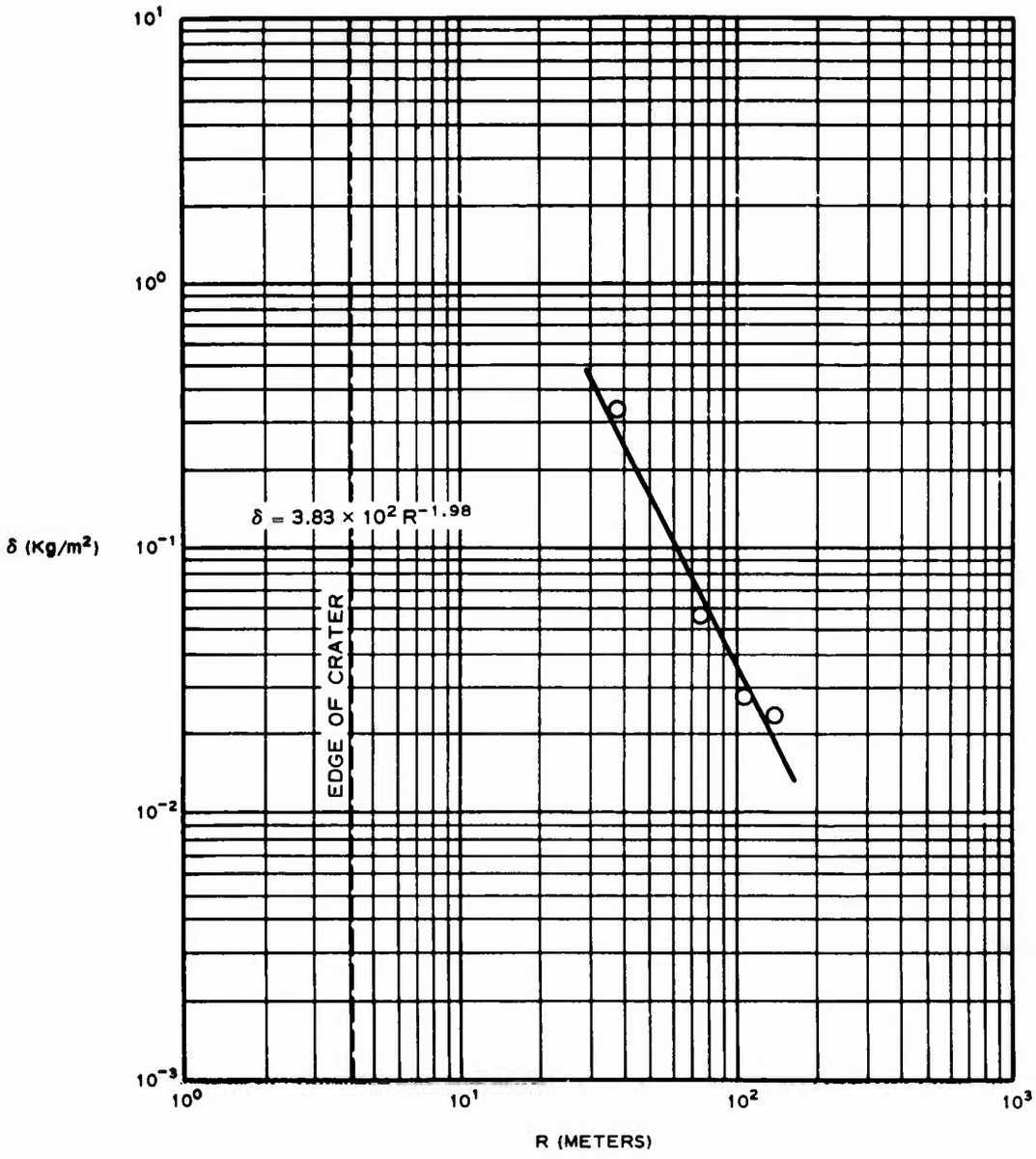

Figure A.9 Mass distribution (δ) versus radial distance from GZ (R) for ERA Round 110.

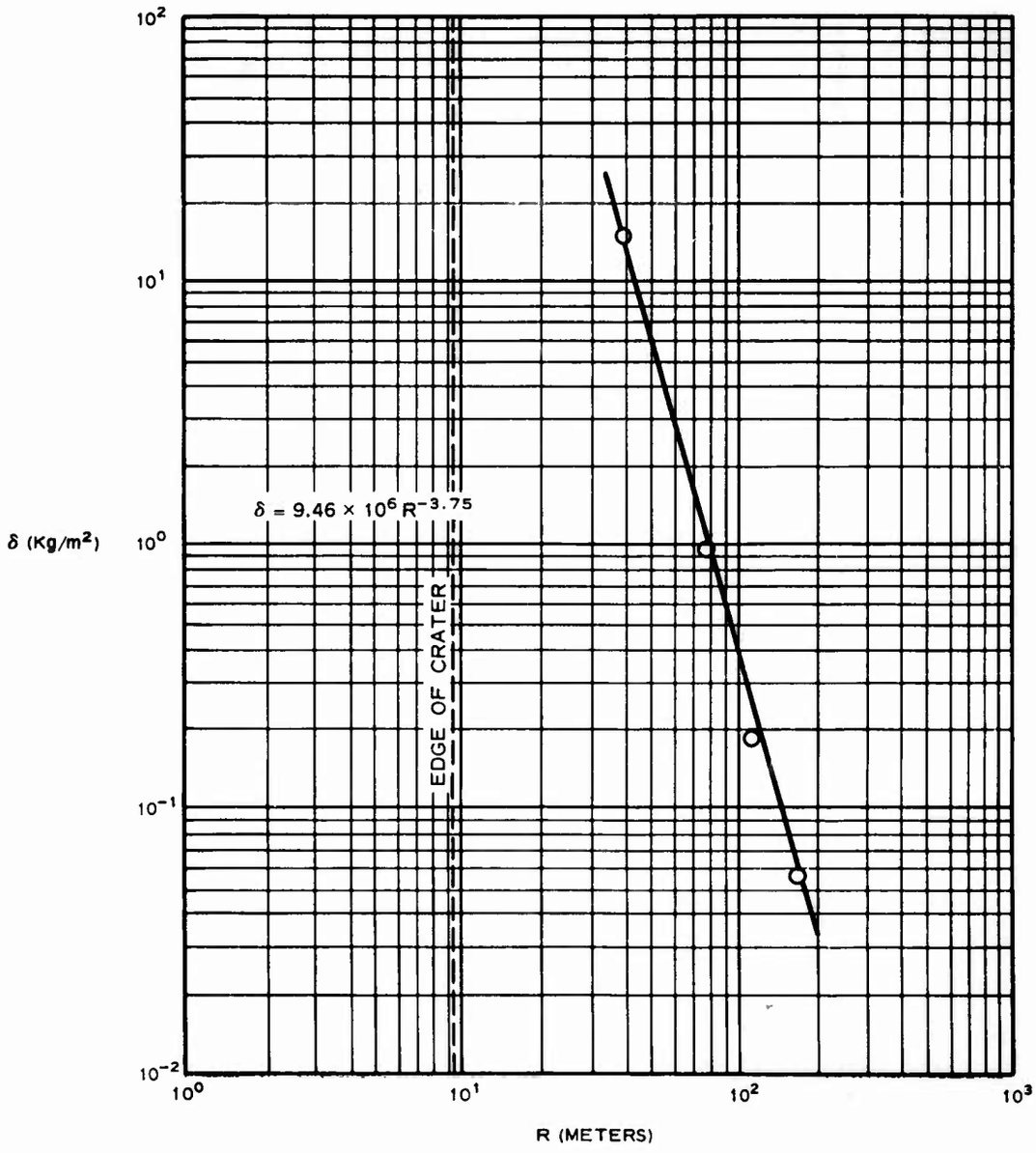

Figure A.10 Mass distribution (δ) versus radial distance from GZ (R) for ERA Round 112.

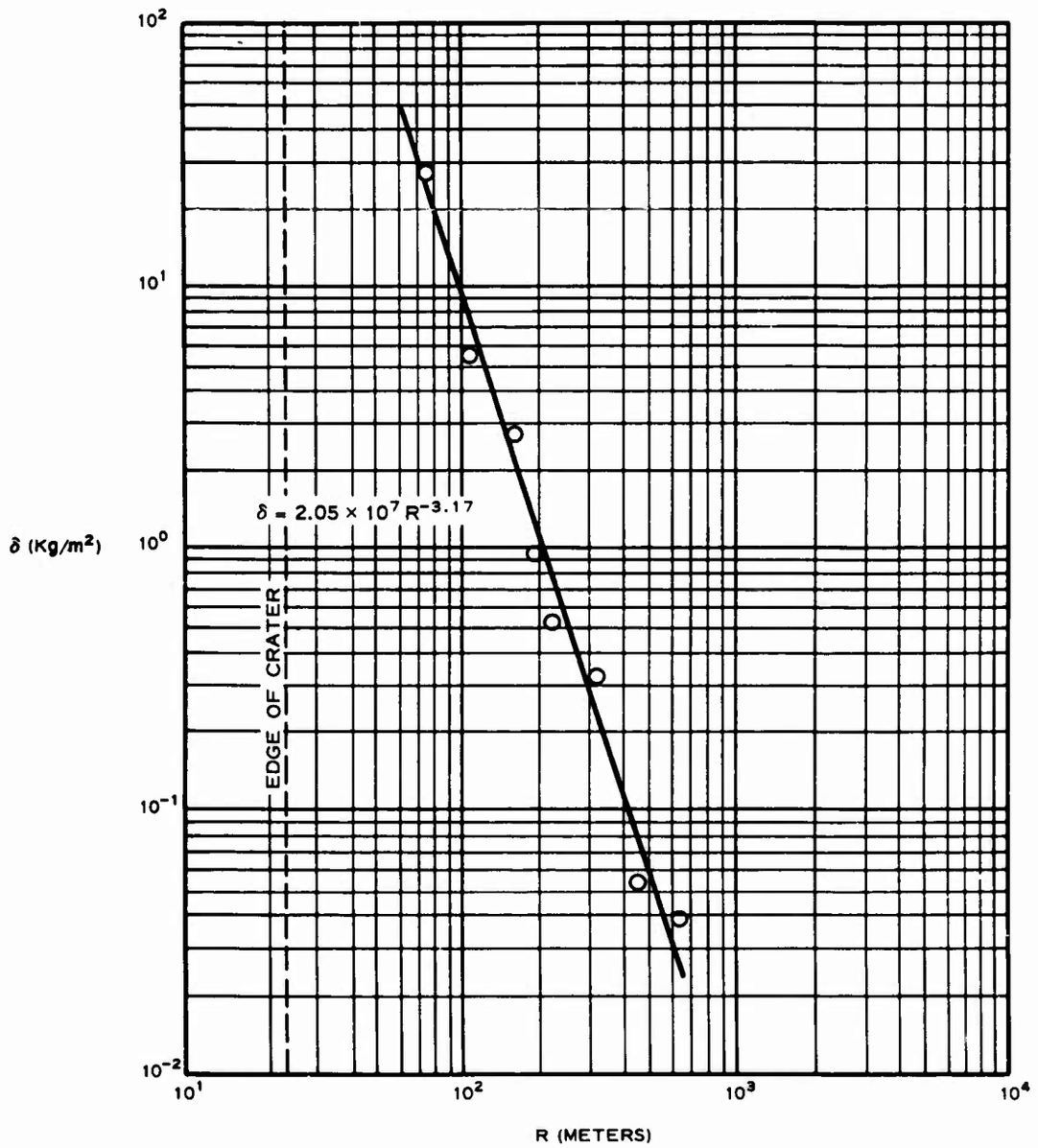

Figure A.11 Mass distribution (δ) versus radial distance from GZ (R) for ERA Round 115.

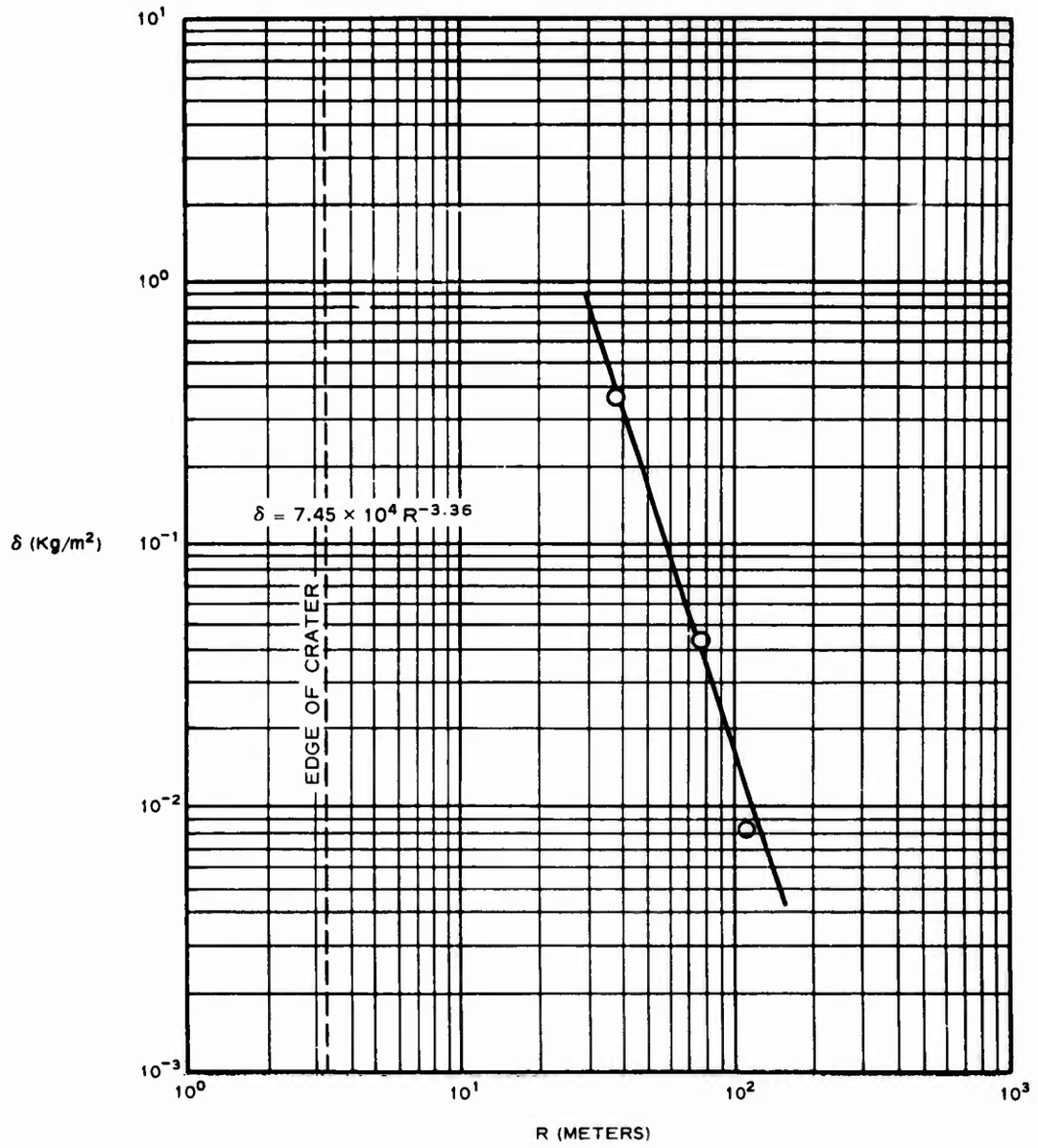

Figure A.12 Mass distribution (δ) versus radial distance from GZ (R) for ERA Round 304.

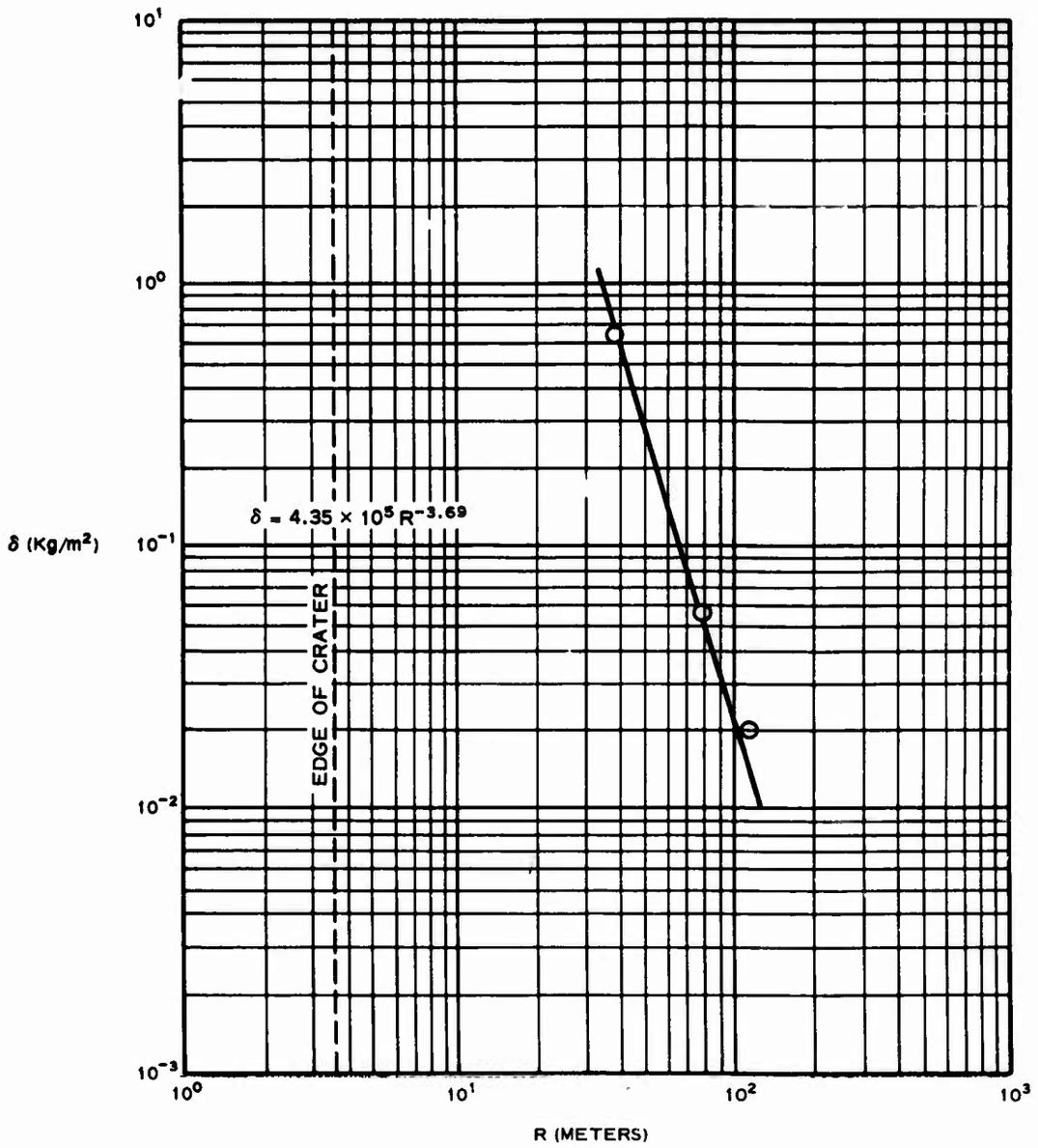

Figure A.13 Mass distribution (δ) versus radial distance from GZ (R) for ERA Round 305.

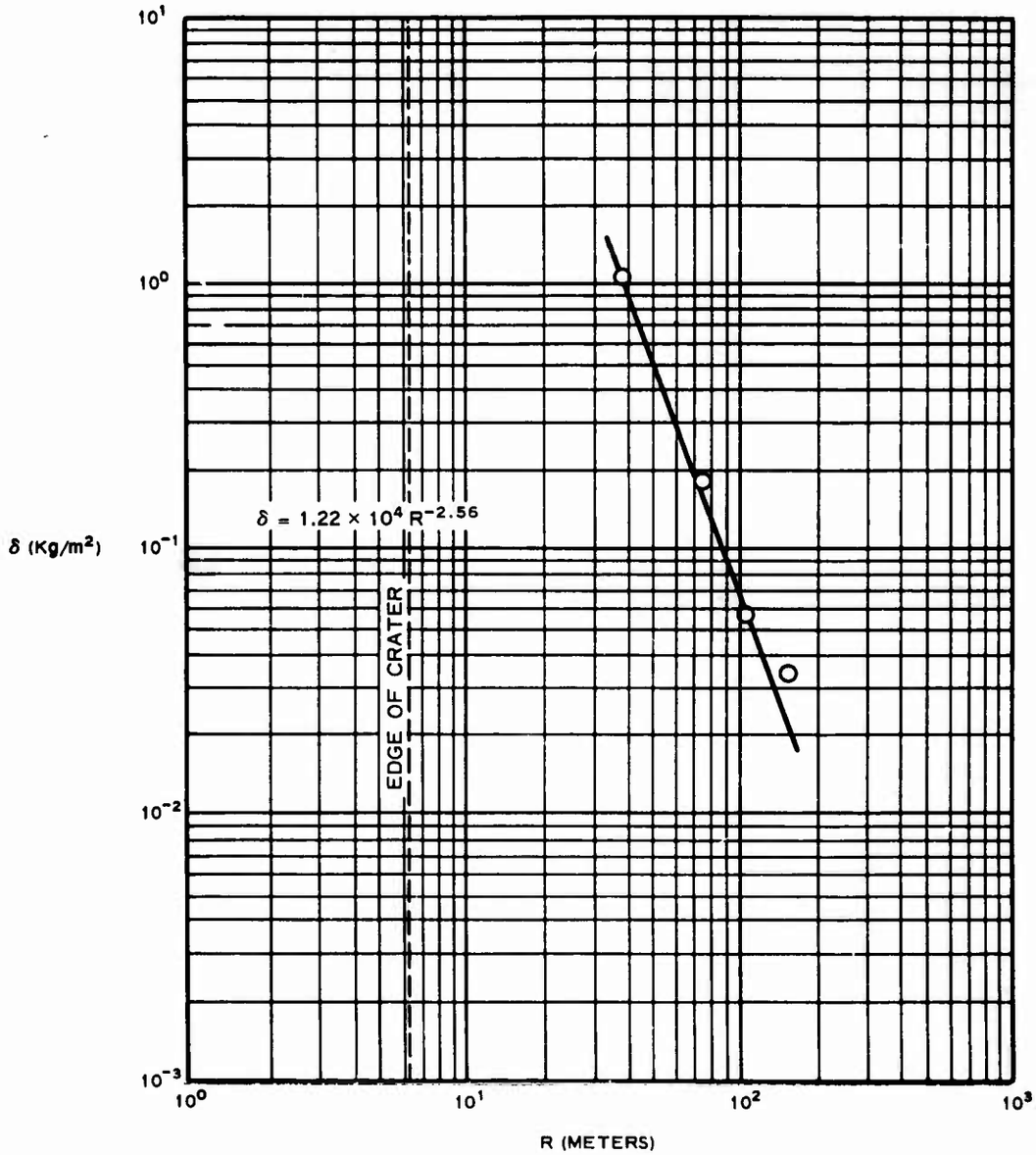

Figure A.14 Mass distribution (δ) versus radial distance from GZ (R) for ERA Round 308.

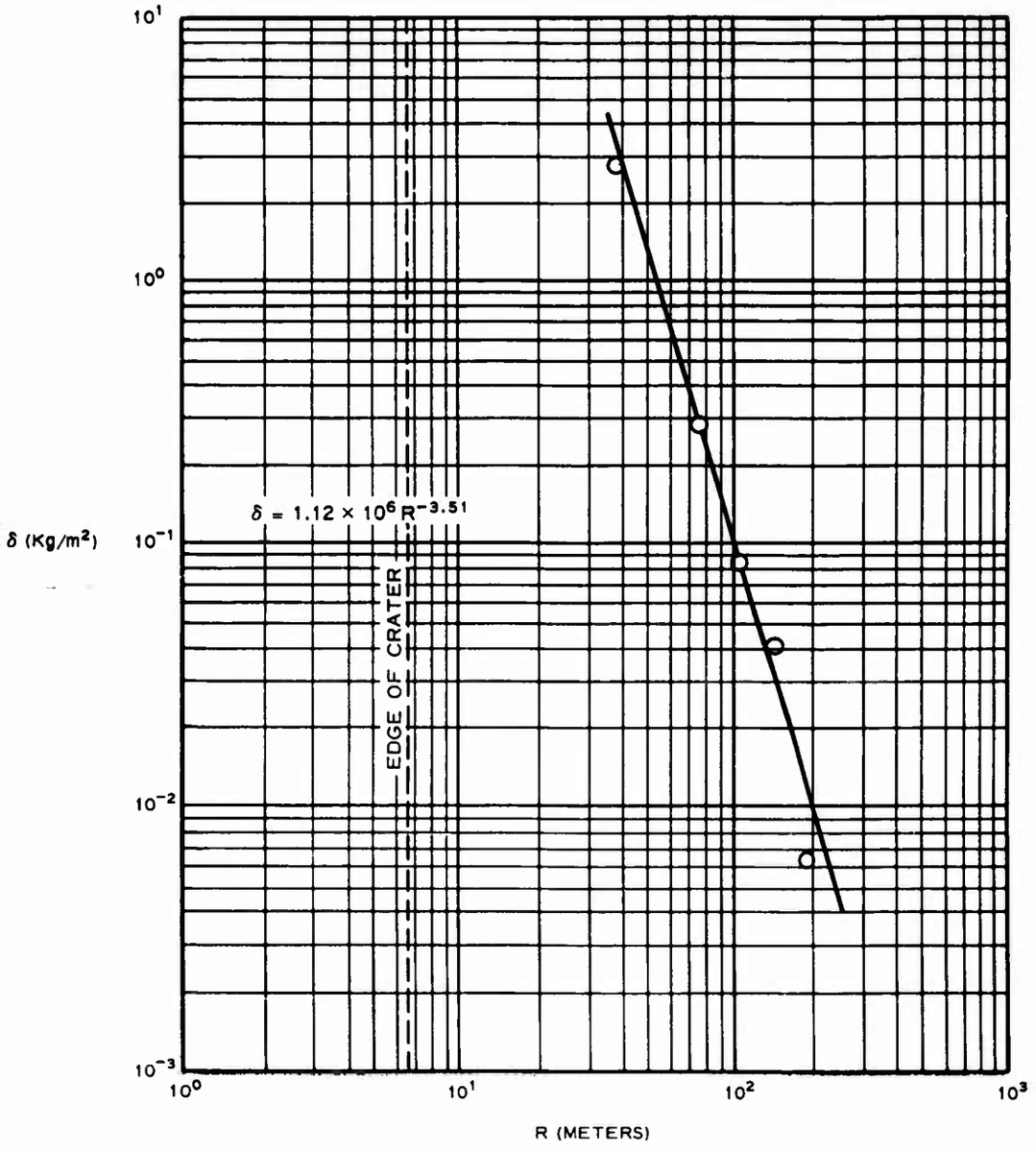

Figure A.15 Mass distribution (δ) versus radial distance from GZ (R) for ERA Round 309.

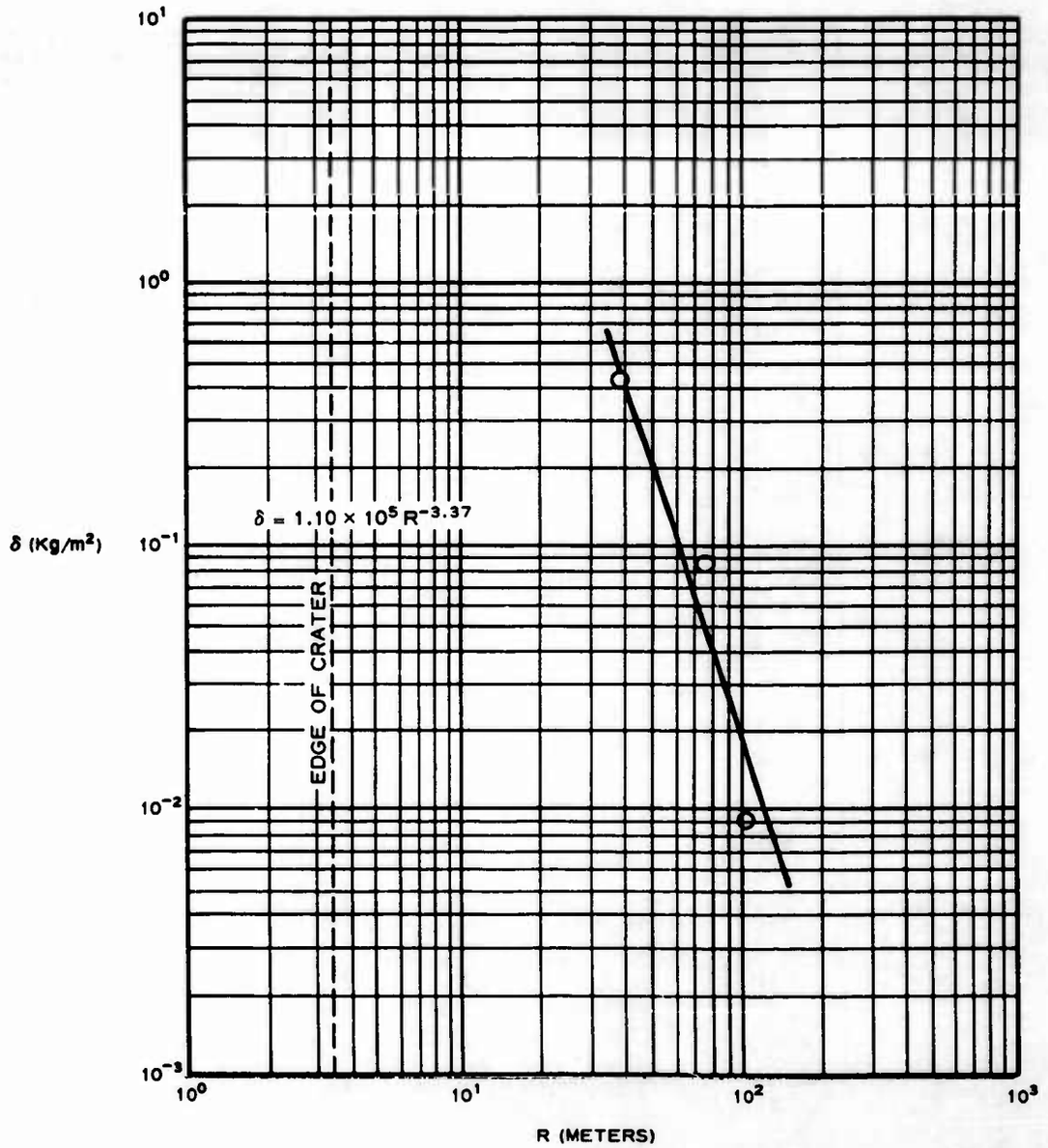

Figure A.16 Mass distribution (δ) versus radial distance from GZ (R) for ERA Round 310.

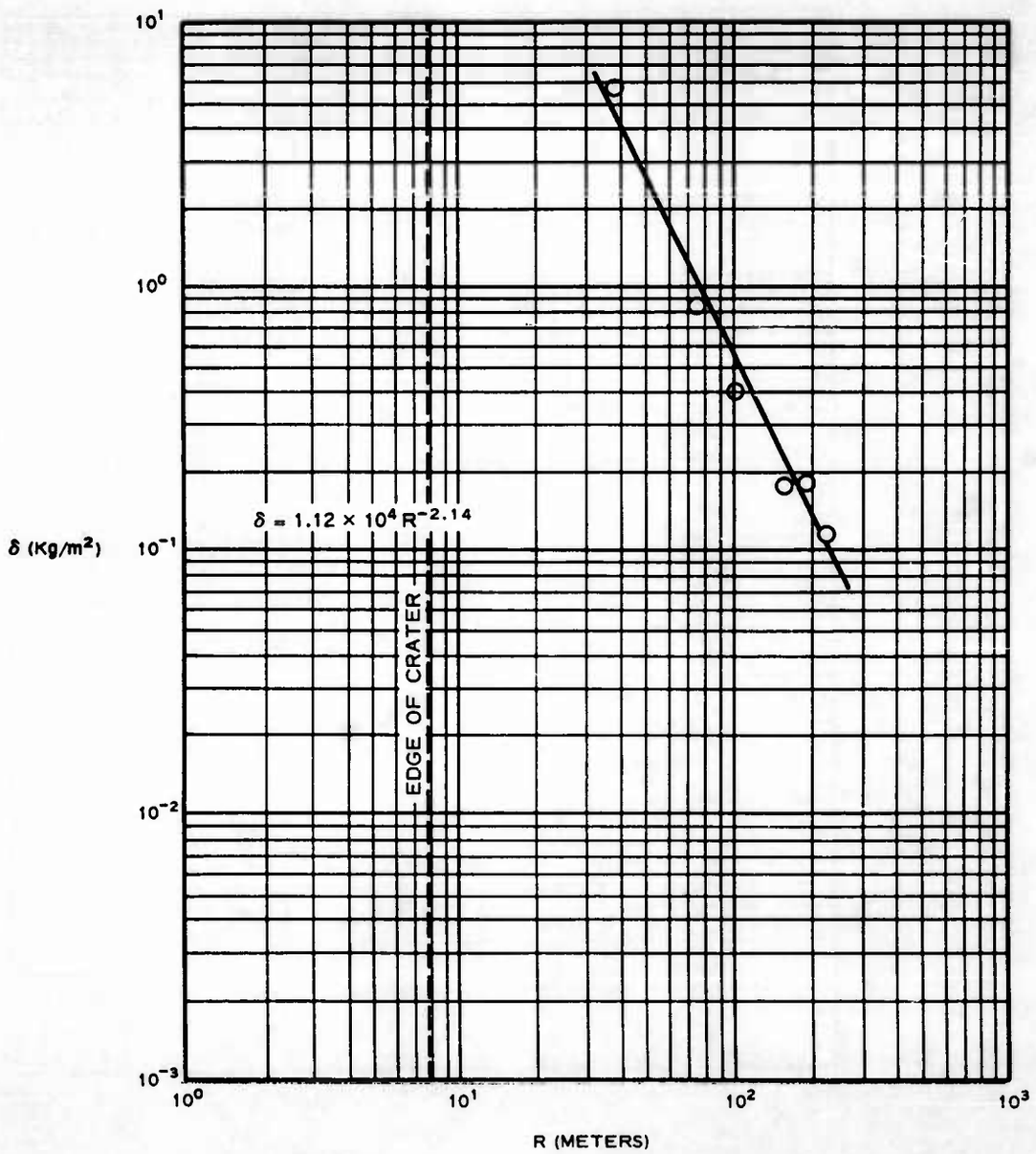

Figure A.17 Mass distribution (δ) versus radial distance from GZ (R) for ERA Round 312.

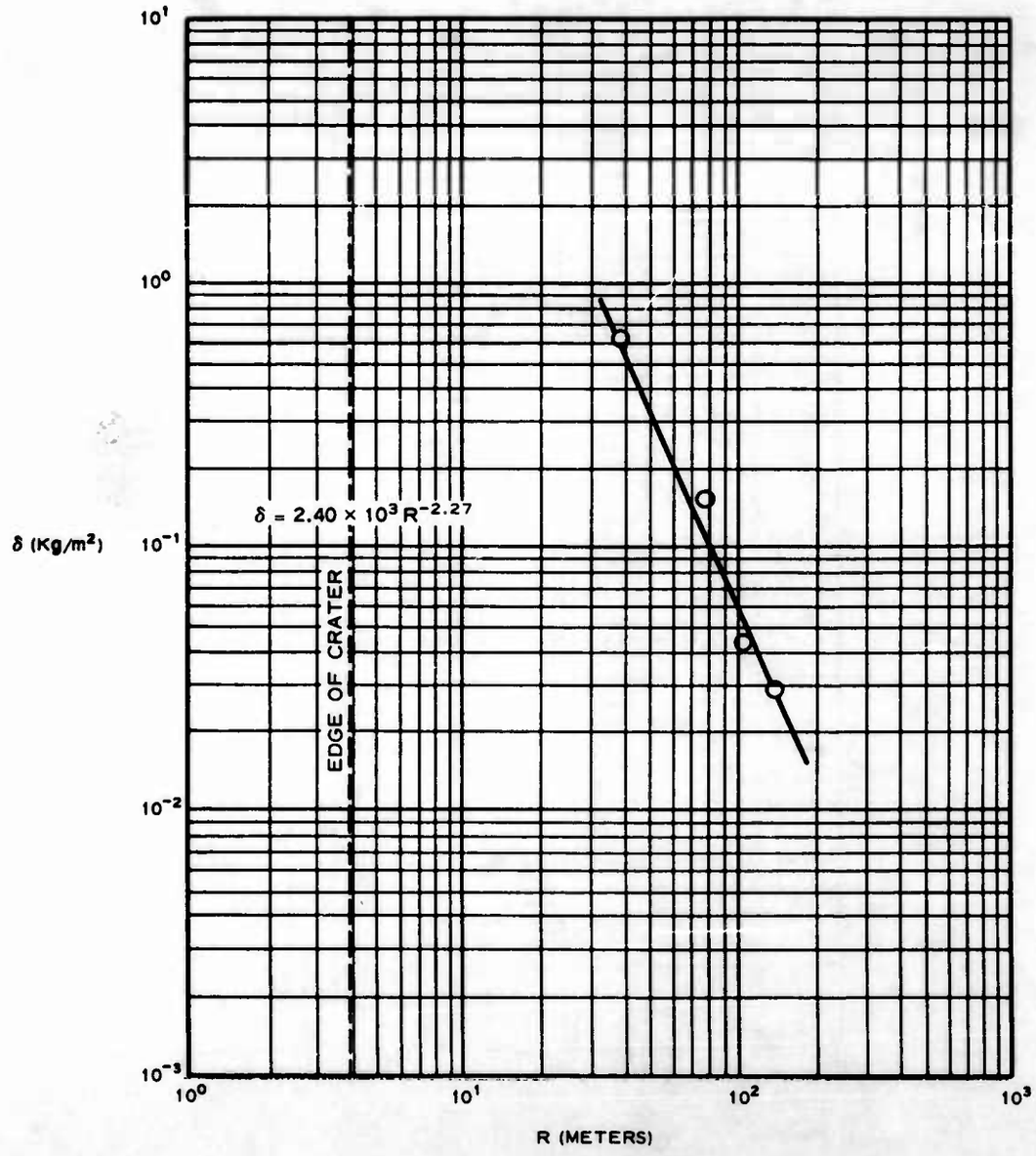

Figure A.18 Mass distribution (δ) versus radial distance from GZ (R) for ERA Round 313.

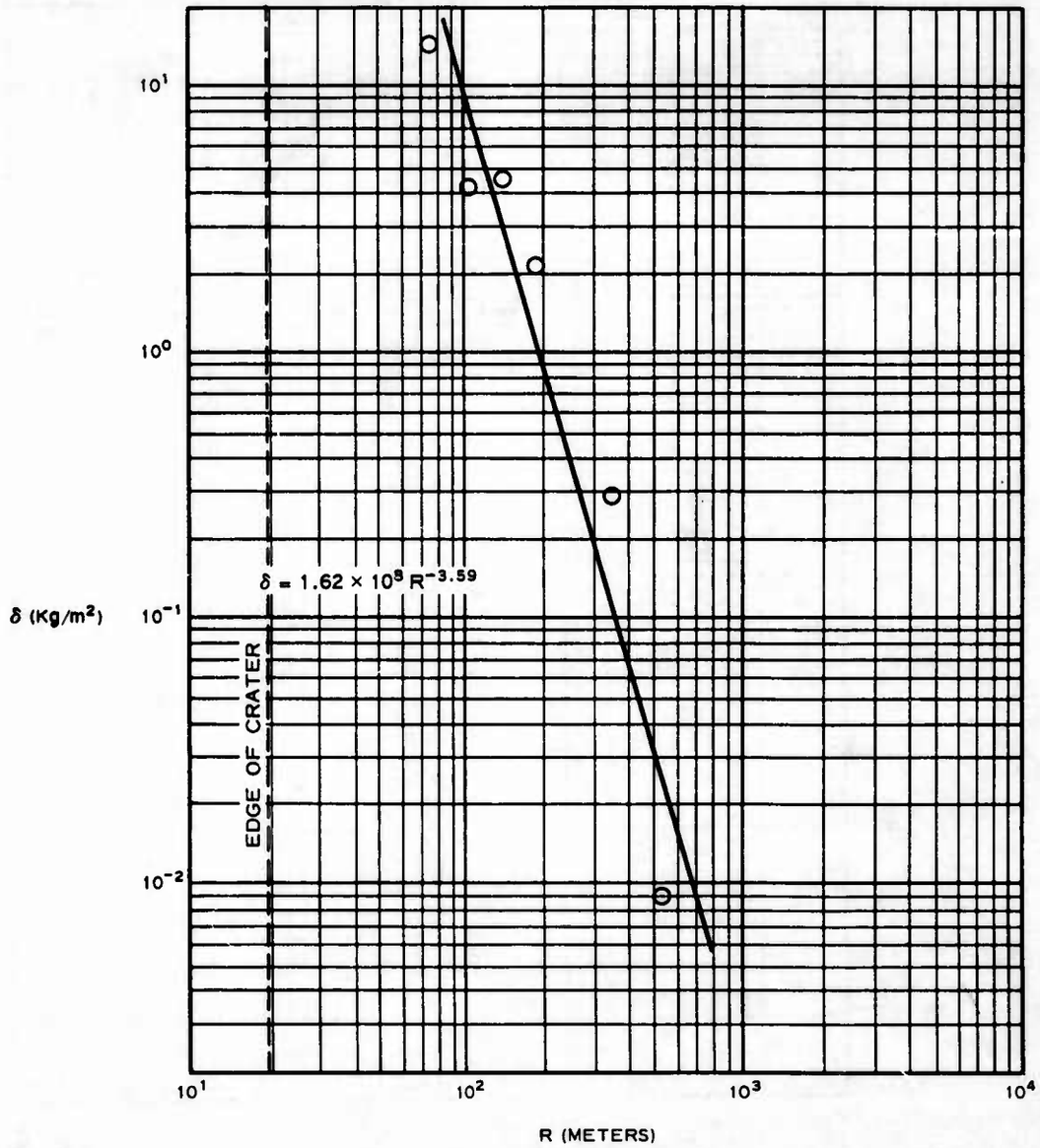

Figure A.19 Mass distribution (δ) versus radial distance from GZ (R) for ERA Round 315.

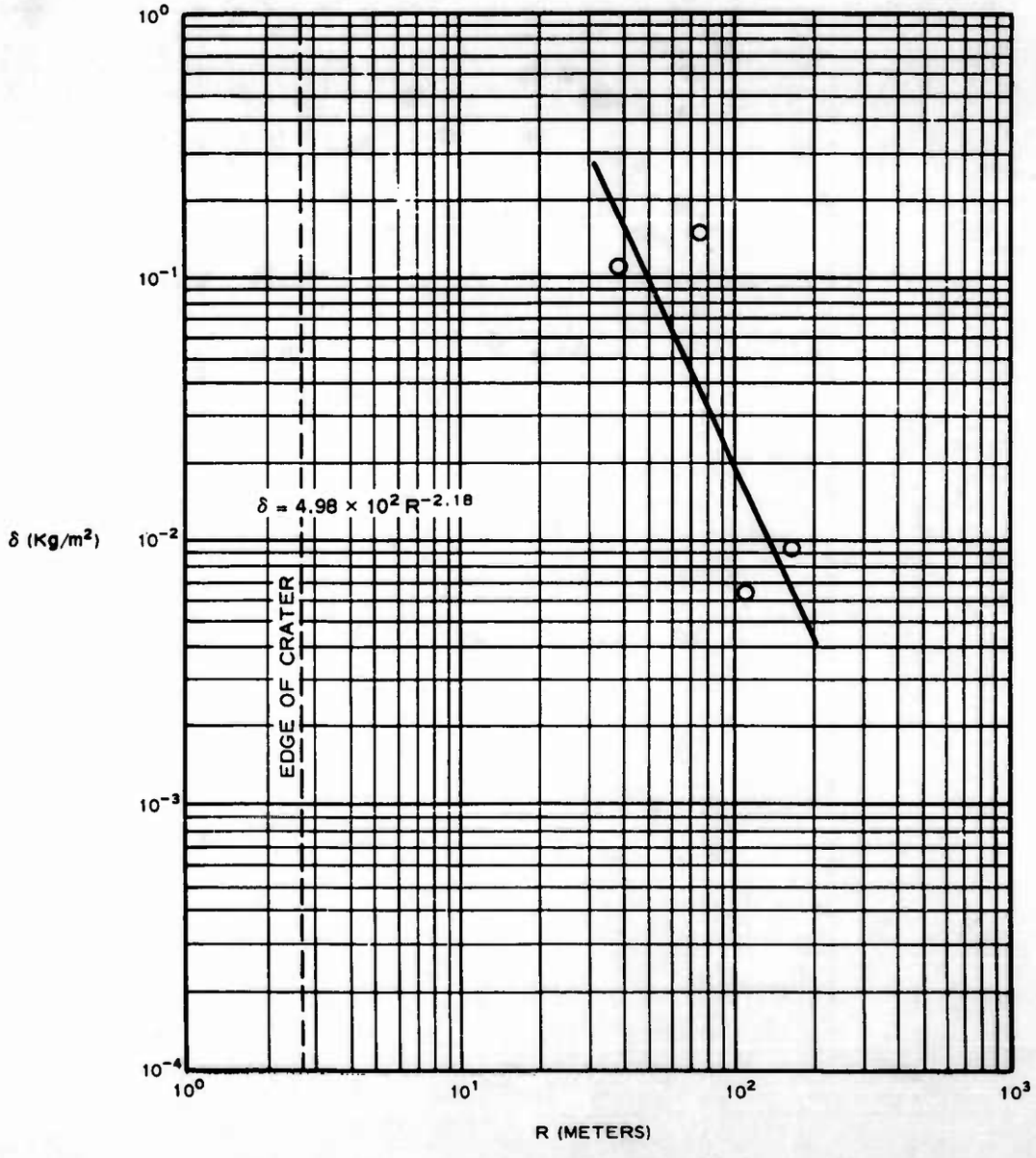

Figure A.20 Mass distribution (δ) versus radial distance from GZ (R) for ERA Round 316.

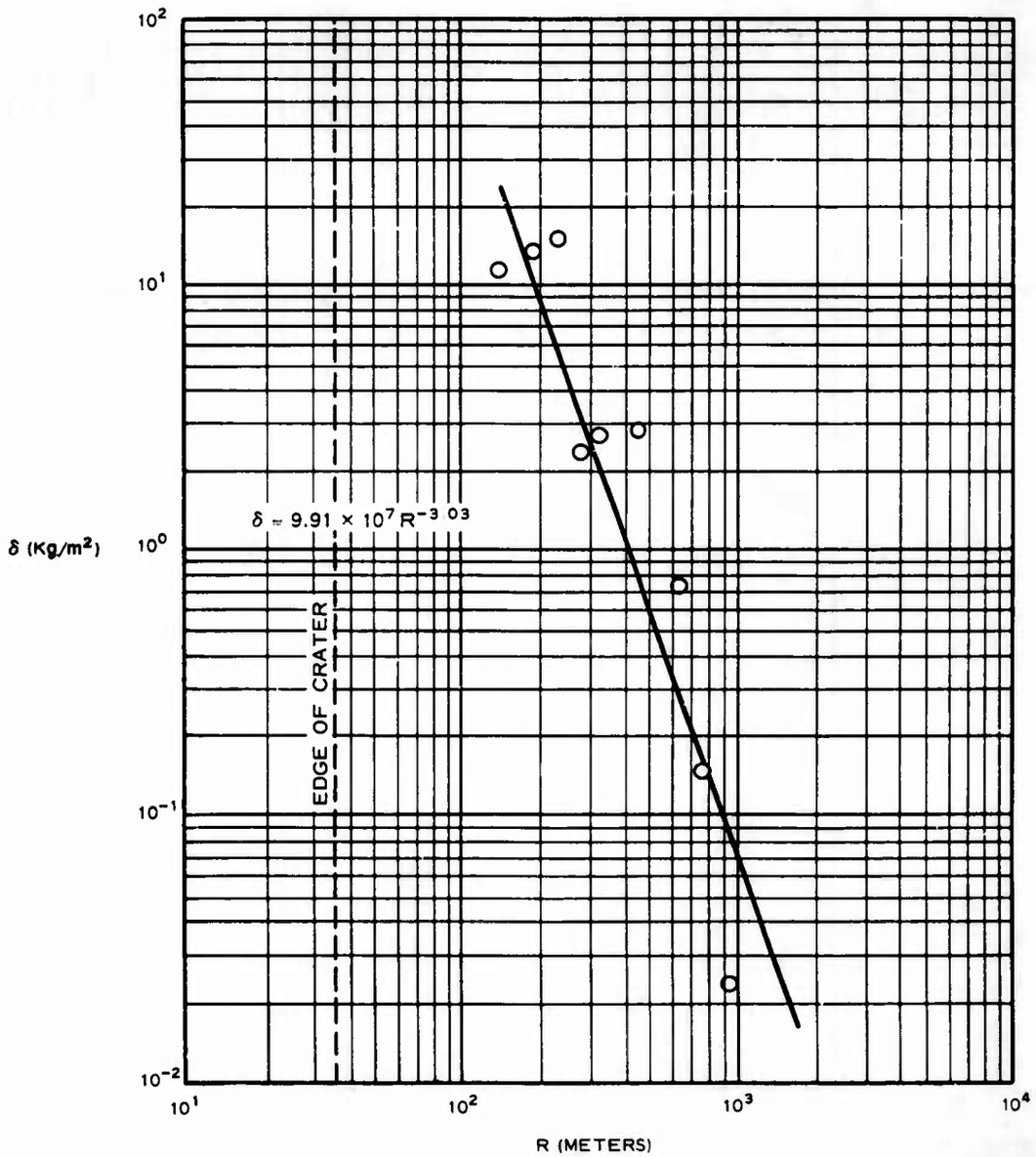

Figure A.21 Mass distribution (δ) versus radial distance from GZ (R) for ERA Round 318.

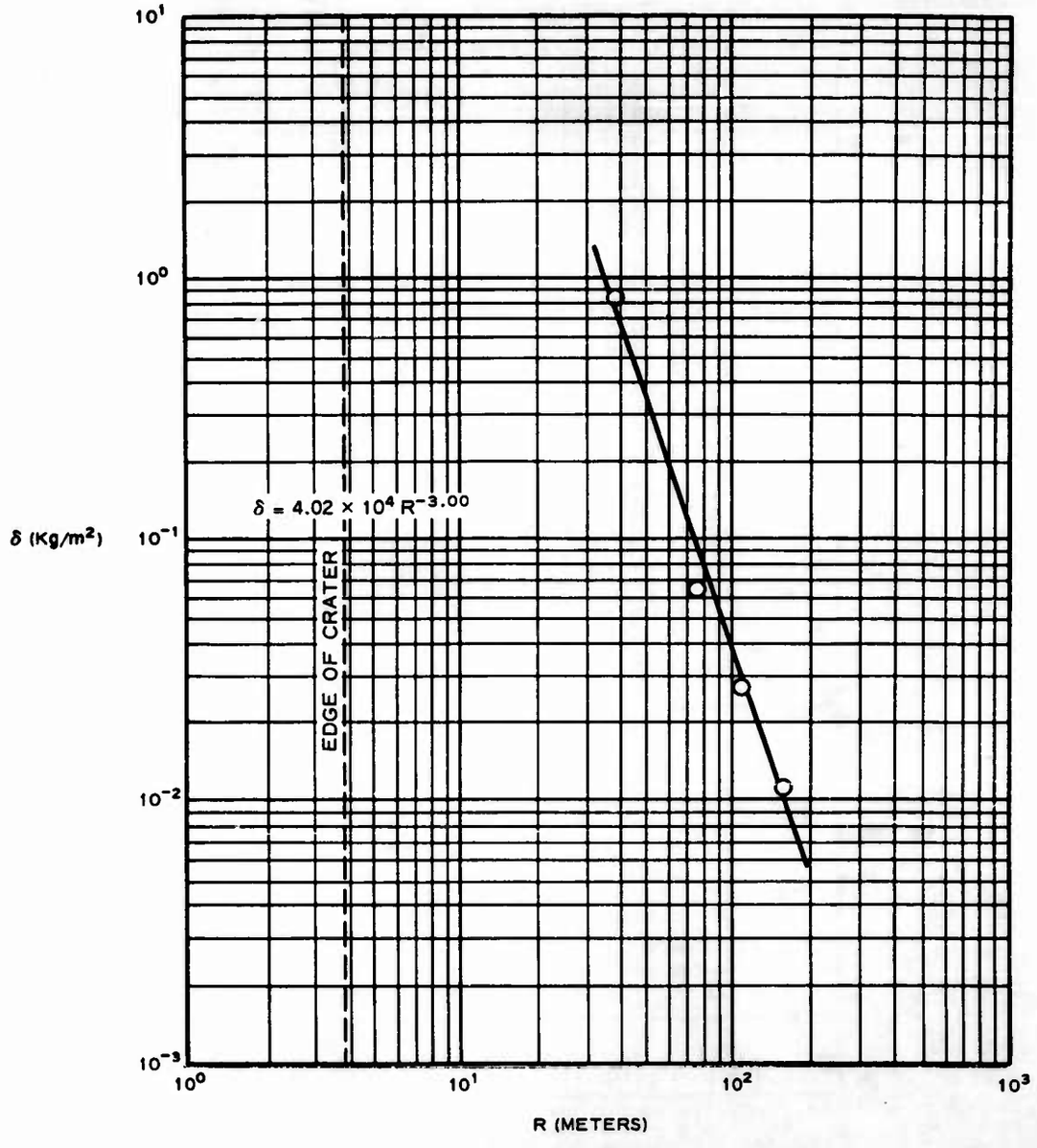

Figure A.22 Mass distribution (δ) versus radial distance from GZ (R) for ERA Symmetry Round.

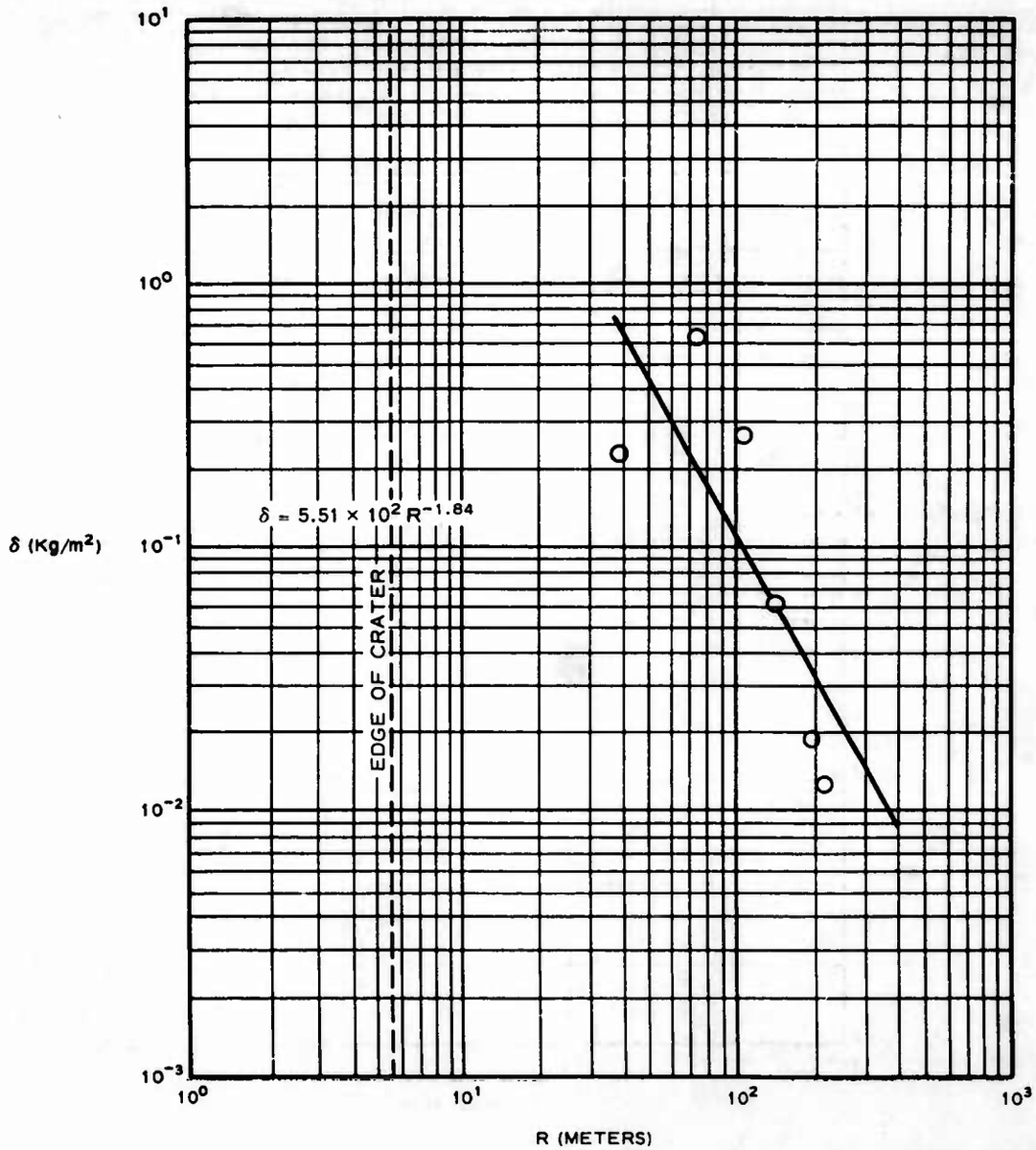

Figure A.23 Mass distribution (δ) versus radial distance from GZ (R) for ERA Round 402.

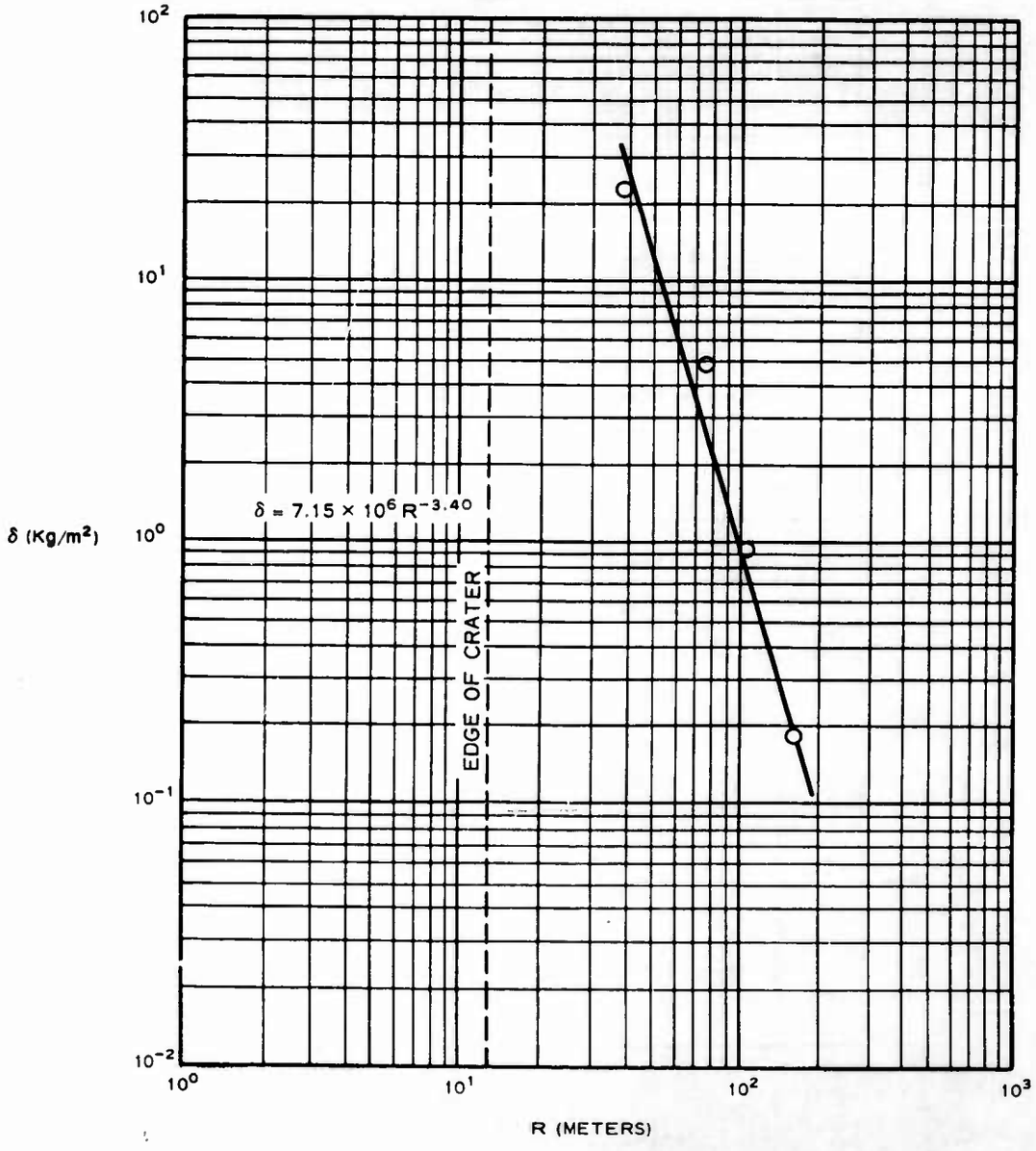

Figure A.24 Mass distribution (δ) versus radial distance from GZ (R) for ERA Round 403.

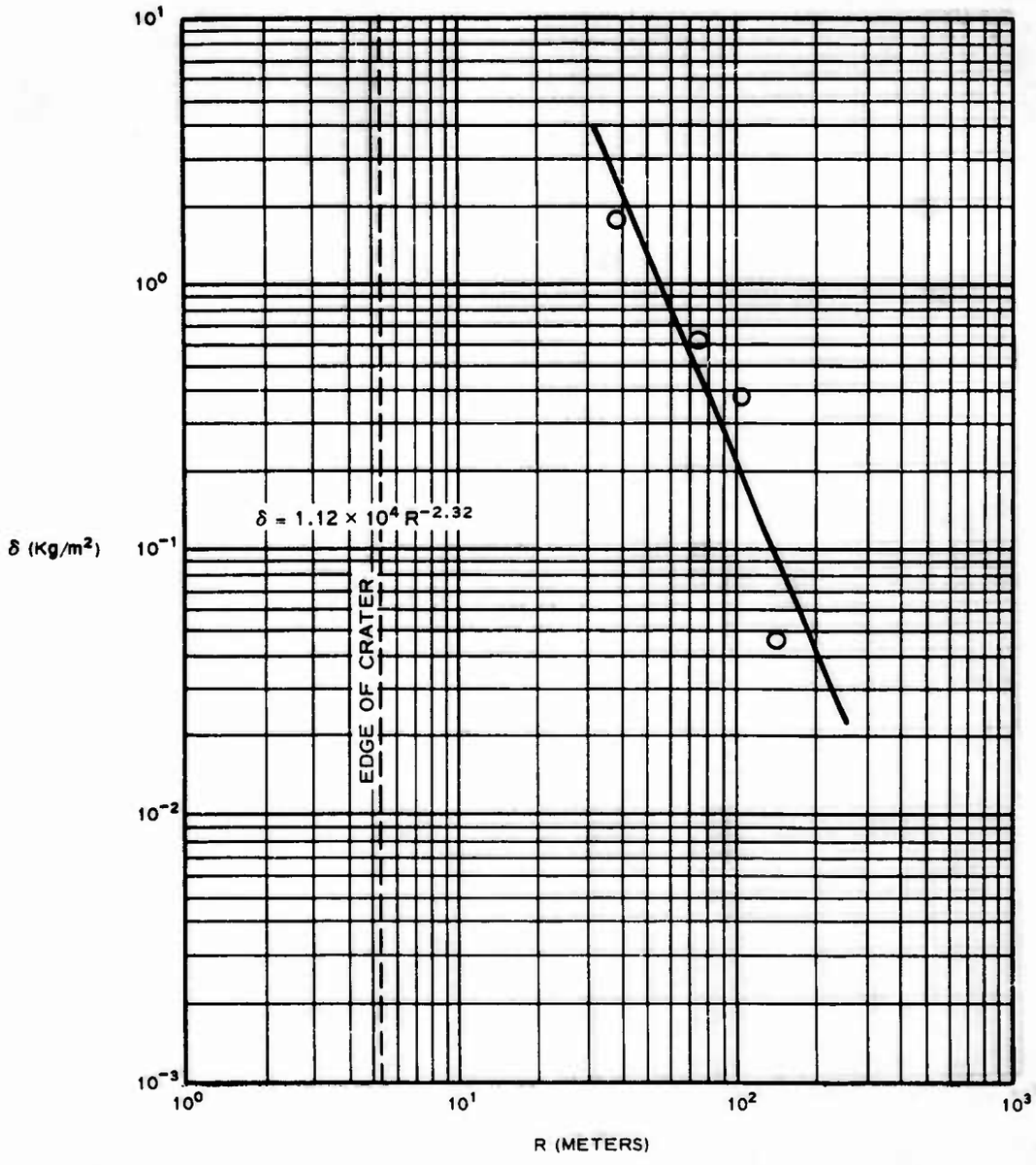

Figure A.25 Mass distribution (δ) versus radial distance from GZ (R) for ERA Round 404.

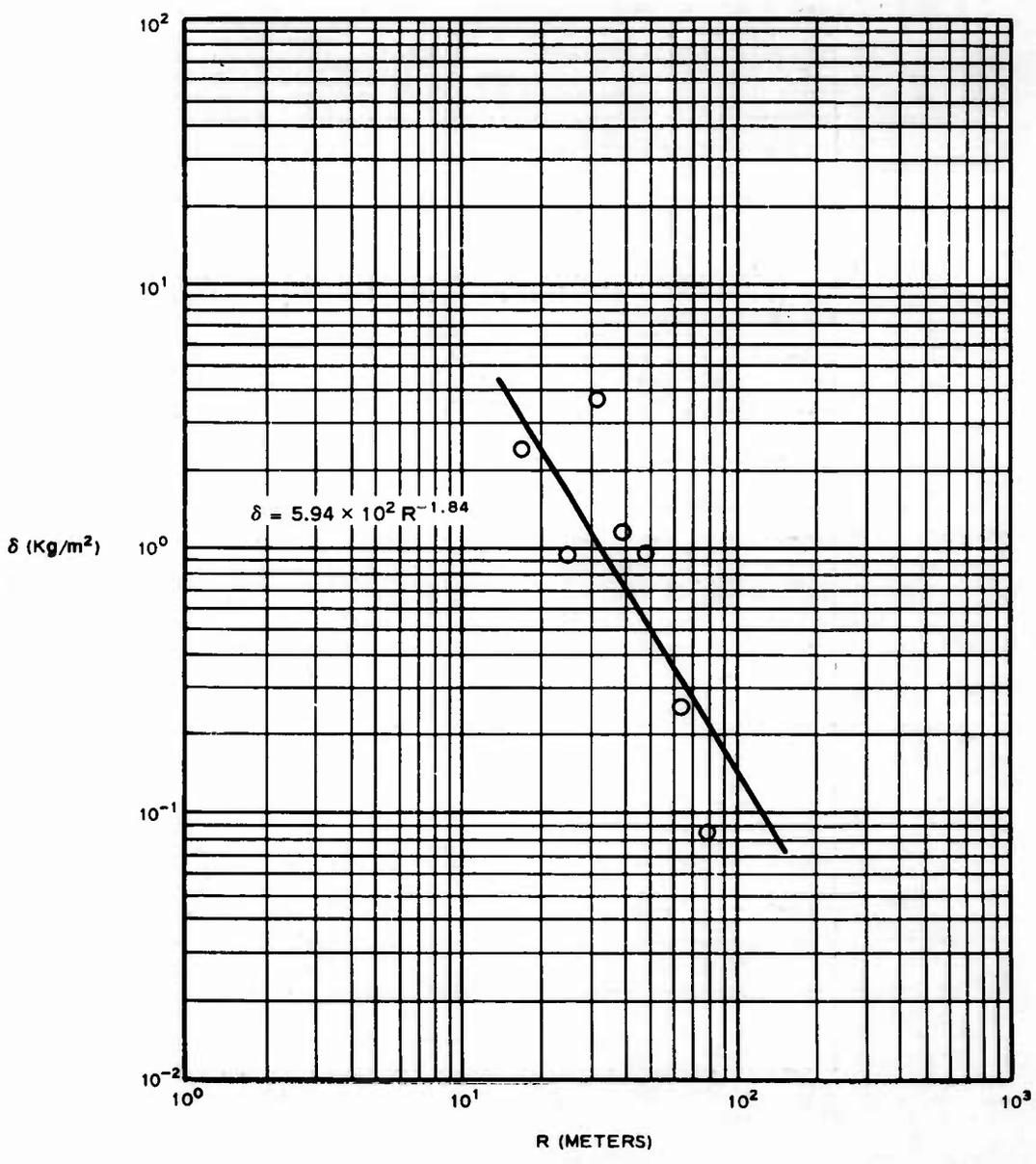

Figure A.26 Mass distribution (δ) versus radial distance from GZ (R) for ERA Round 501.

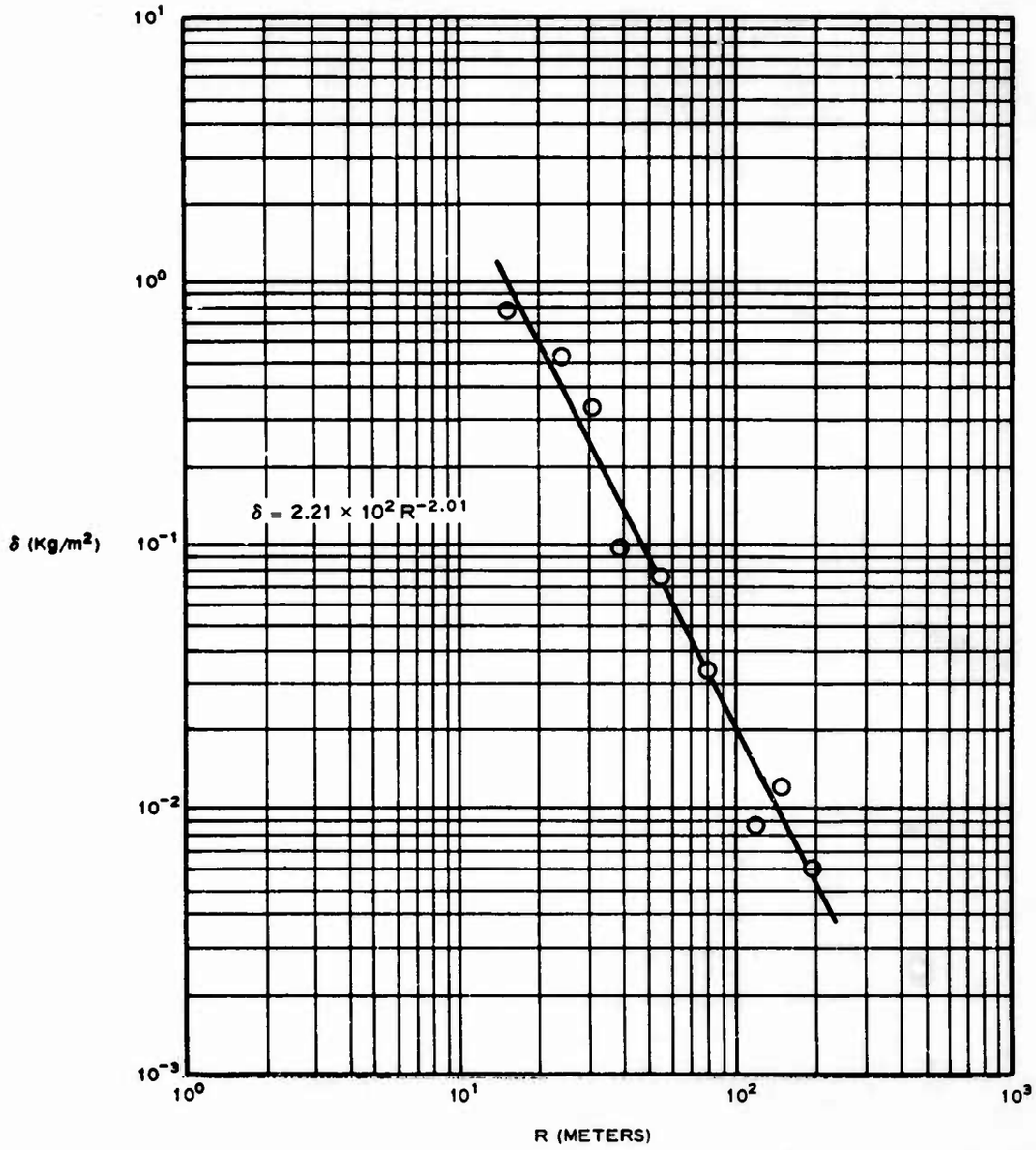

Figure A.27 Mass distribution (δ) versus radial distance from GZ (R) for ERA Round 803.

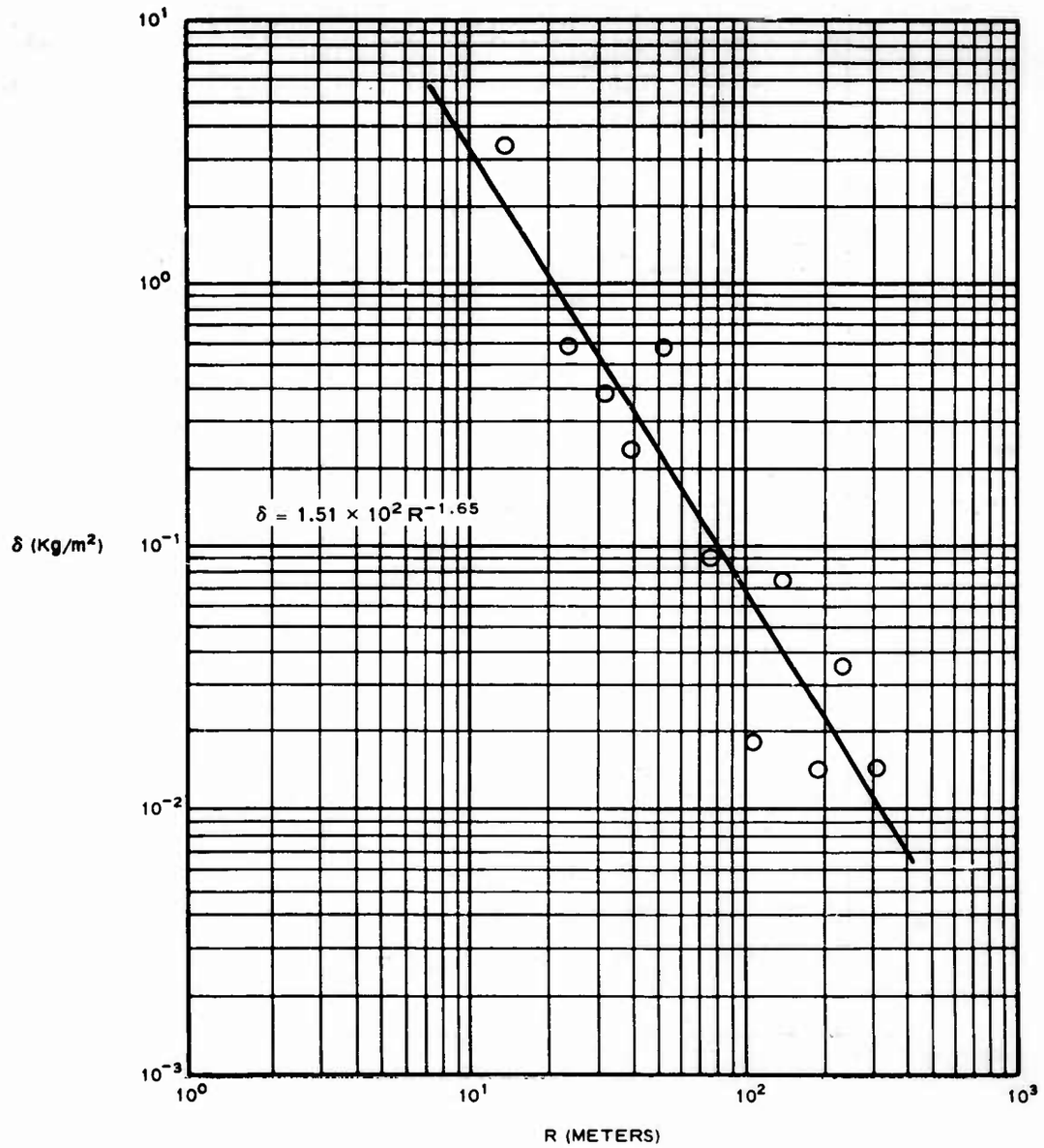

Figure A.28 Mass distribution (δ) versus radial distance from GZ (R) for ERA Round 804.

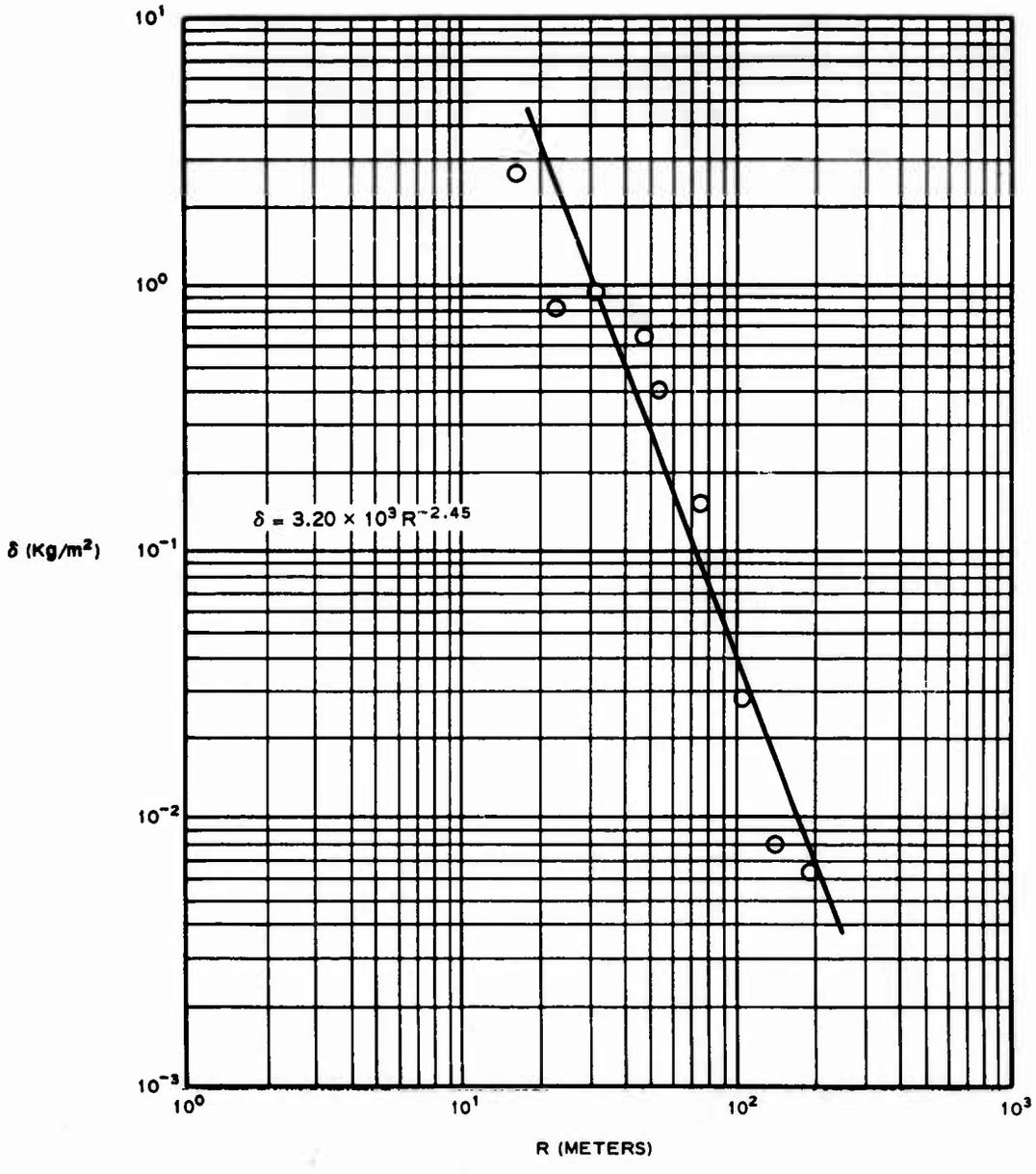

Figure A.29 Mass distribution (δ) versus radial distance from GZ (R) for ERA Round 805.

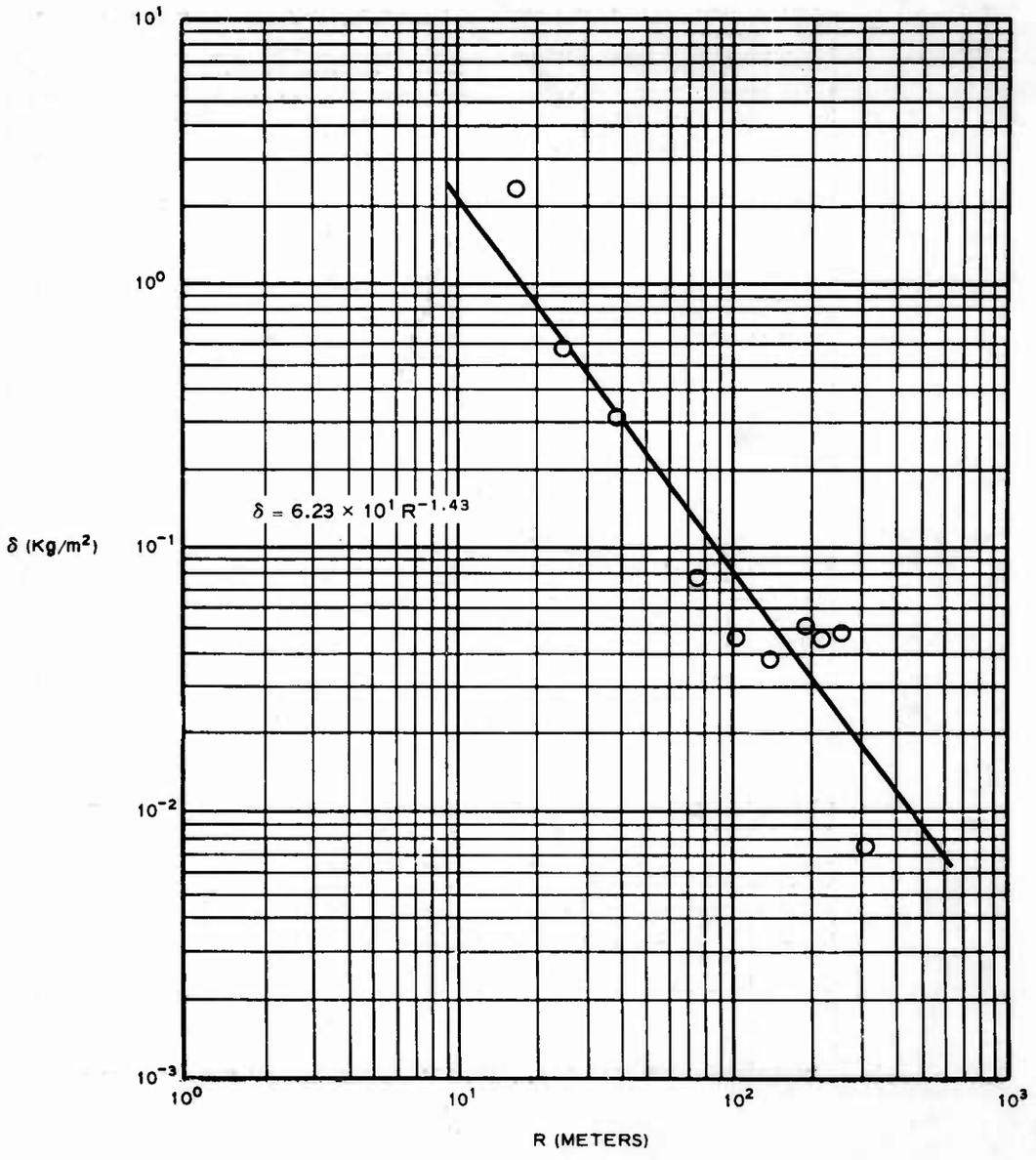

Figure A.30 Mass distribution (δ) versus radial distance from GZ (R) for ERA Round 807.

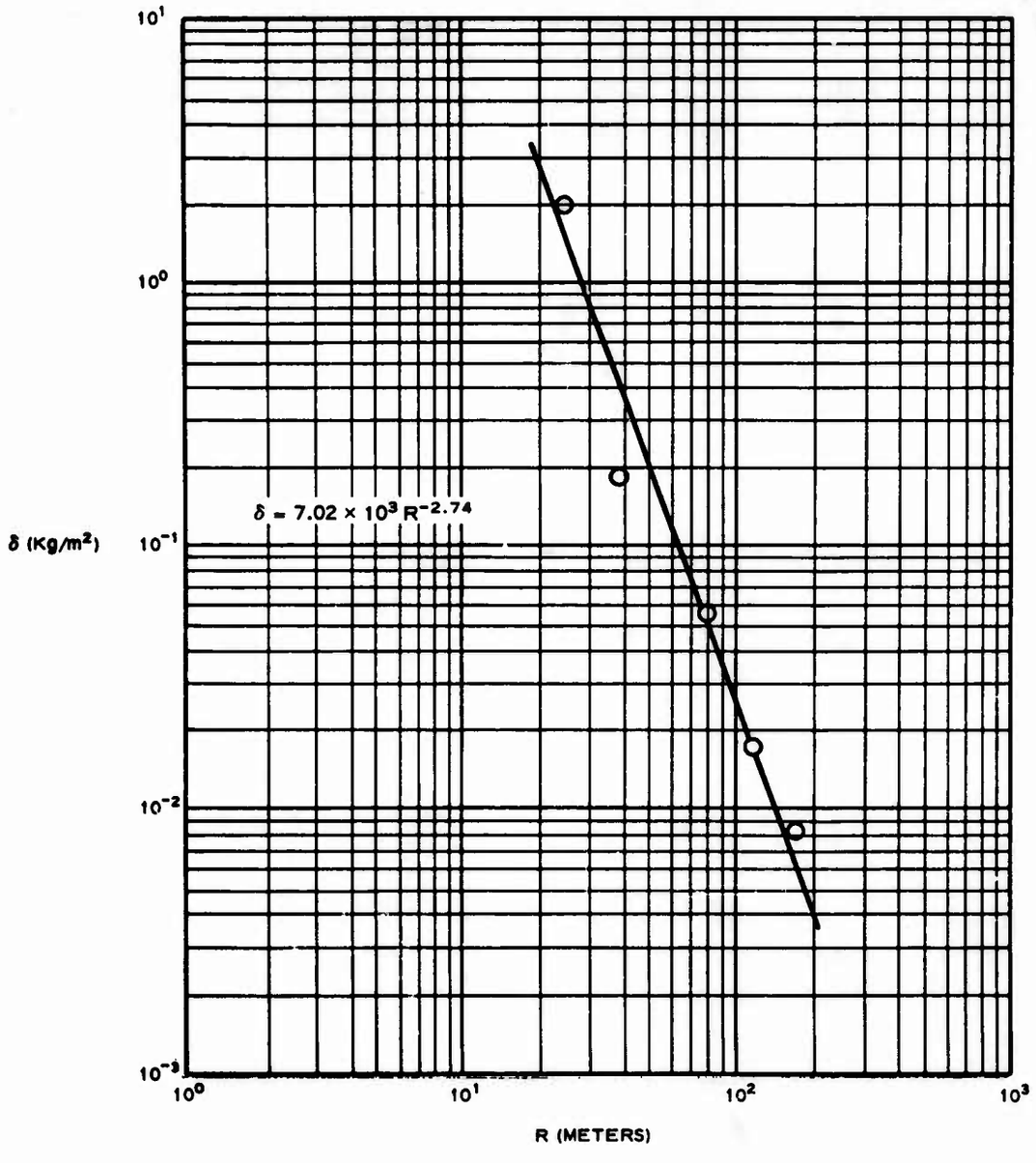

Figure A.31 Mass distribution (δ) versus radial distance from GZ (R) for ERA Round 808.

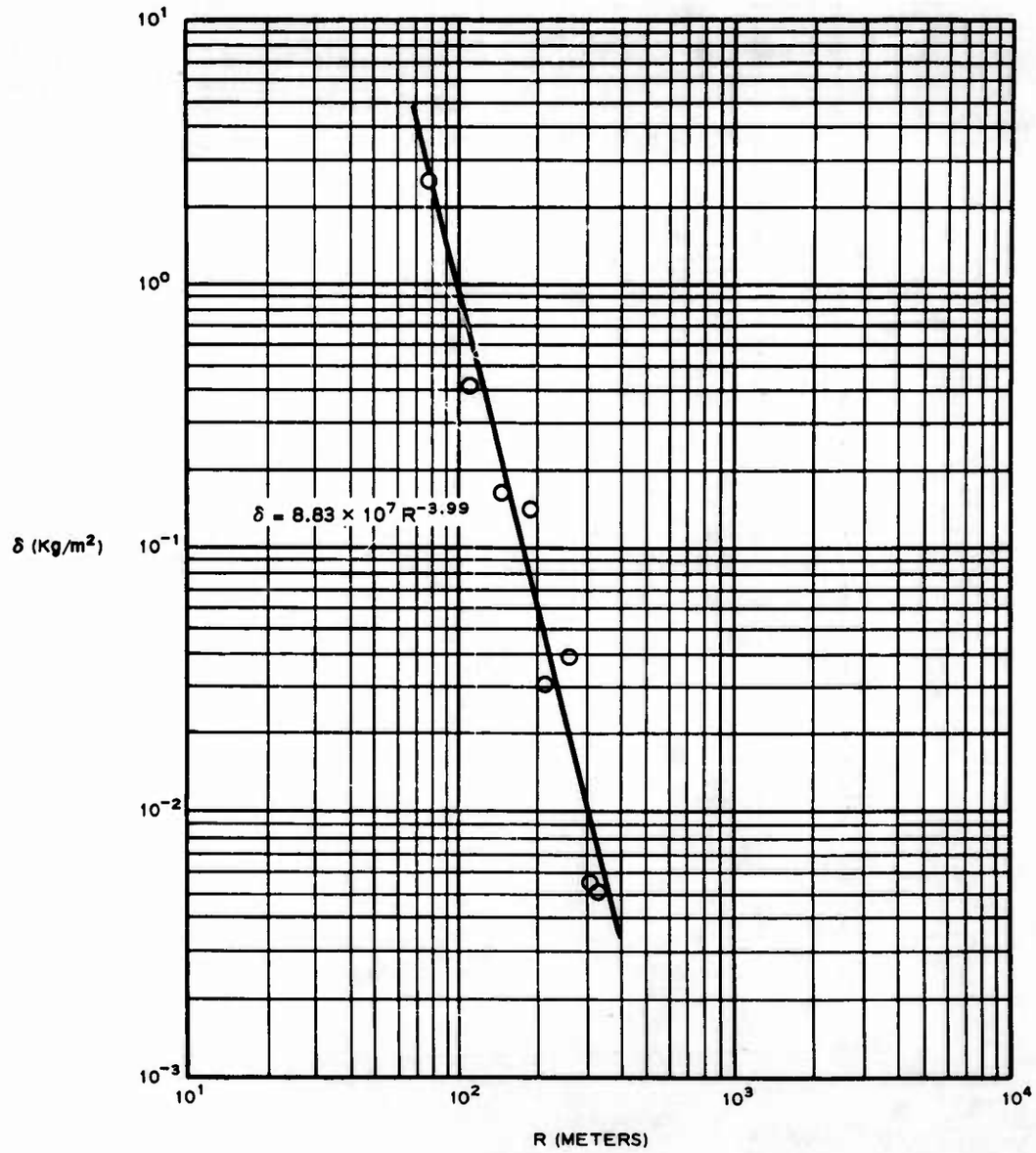

Figure A.32 Mass distribution (δ) versus radial distance from GZ (R) for ERA Round 810.

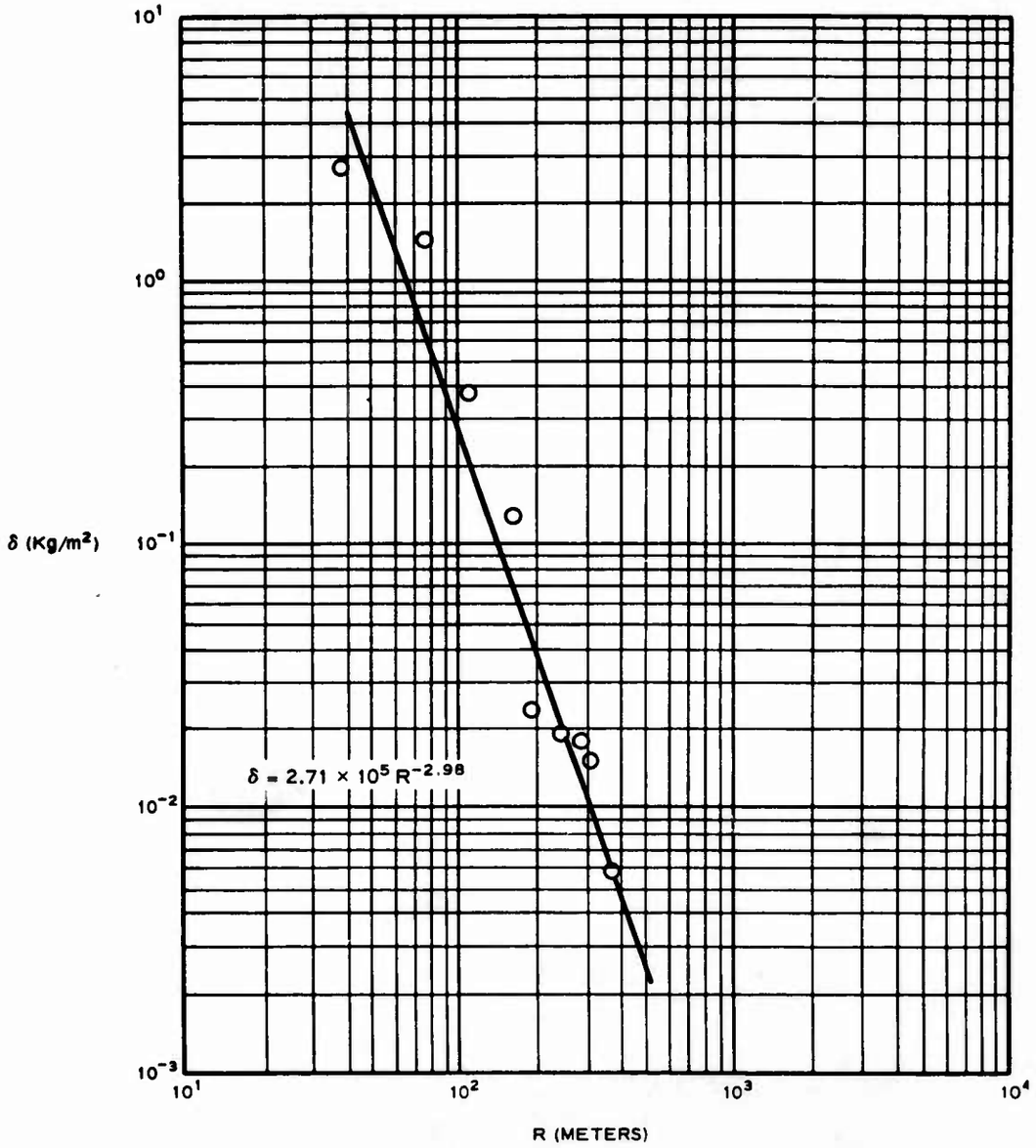

Figure A.33 Mass distribution (δ) versus radial distance from GZ (R) for ERA Round 811.

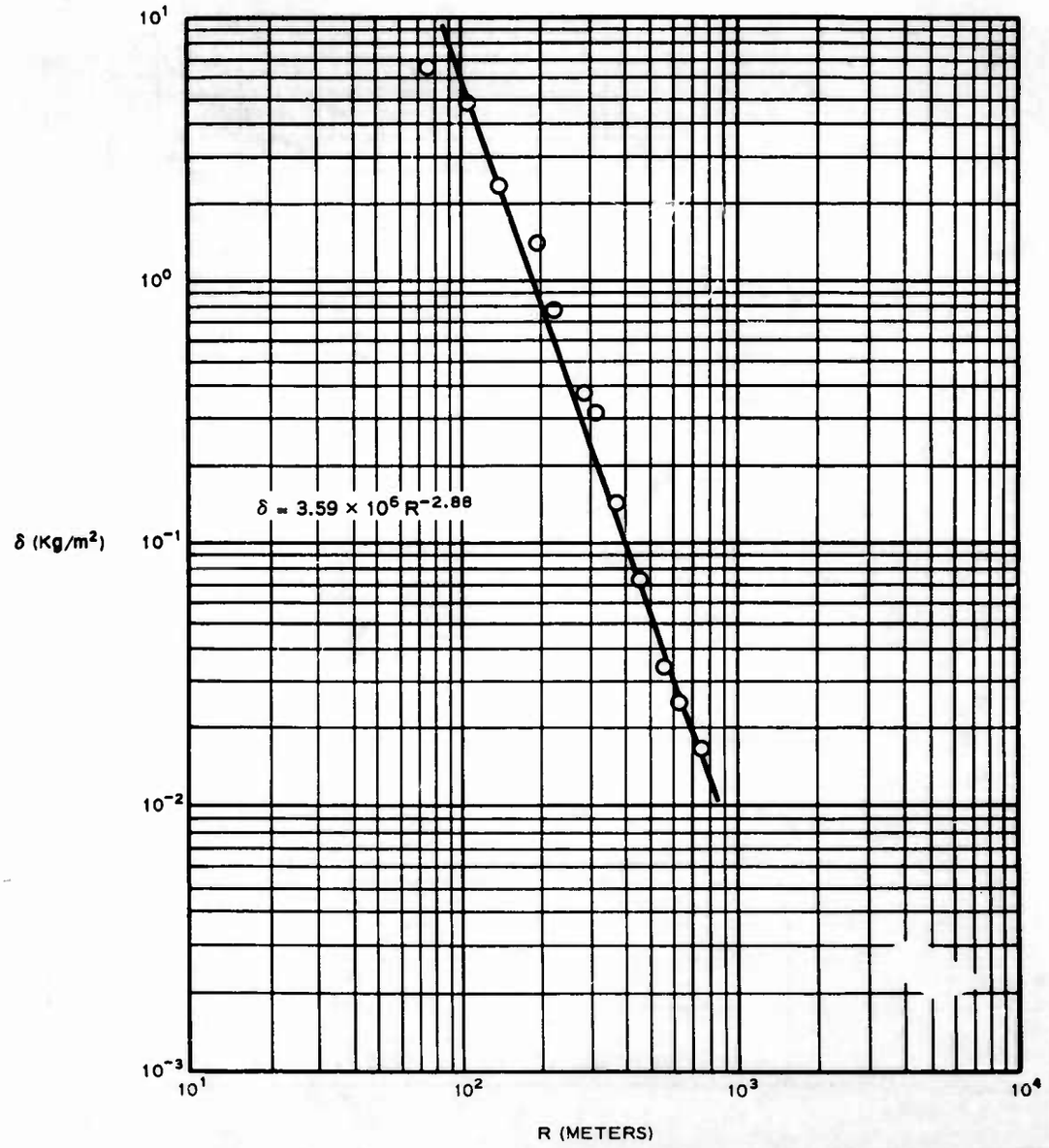

Figure A.34 Mass distribution (δ) versus radial distance from GZ (R) for ERA Round 814.

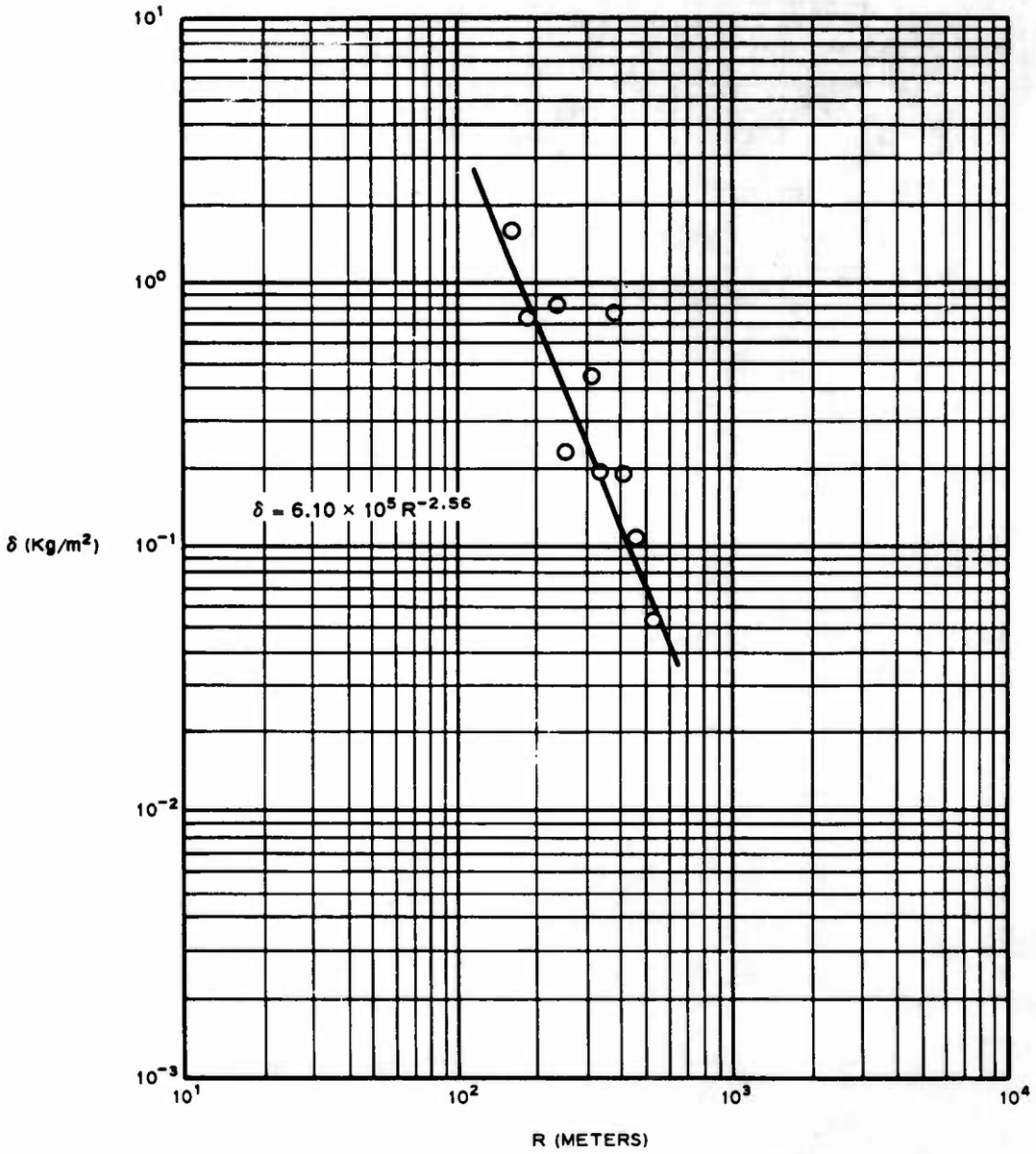

Figure A.35 Mass distribution (δ) versus radial distance from GZ (R) for ERA Round 815.

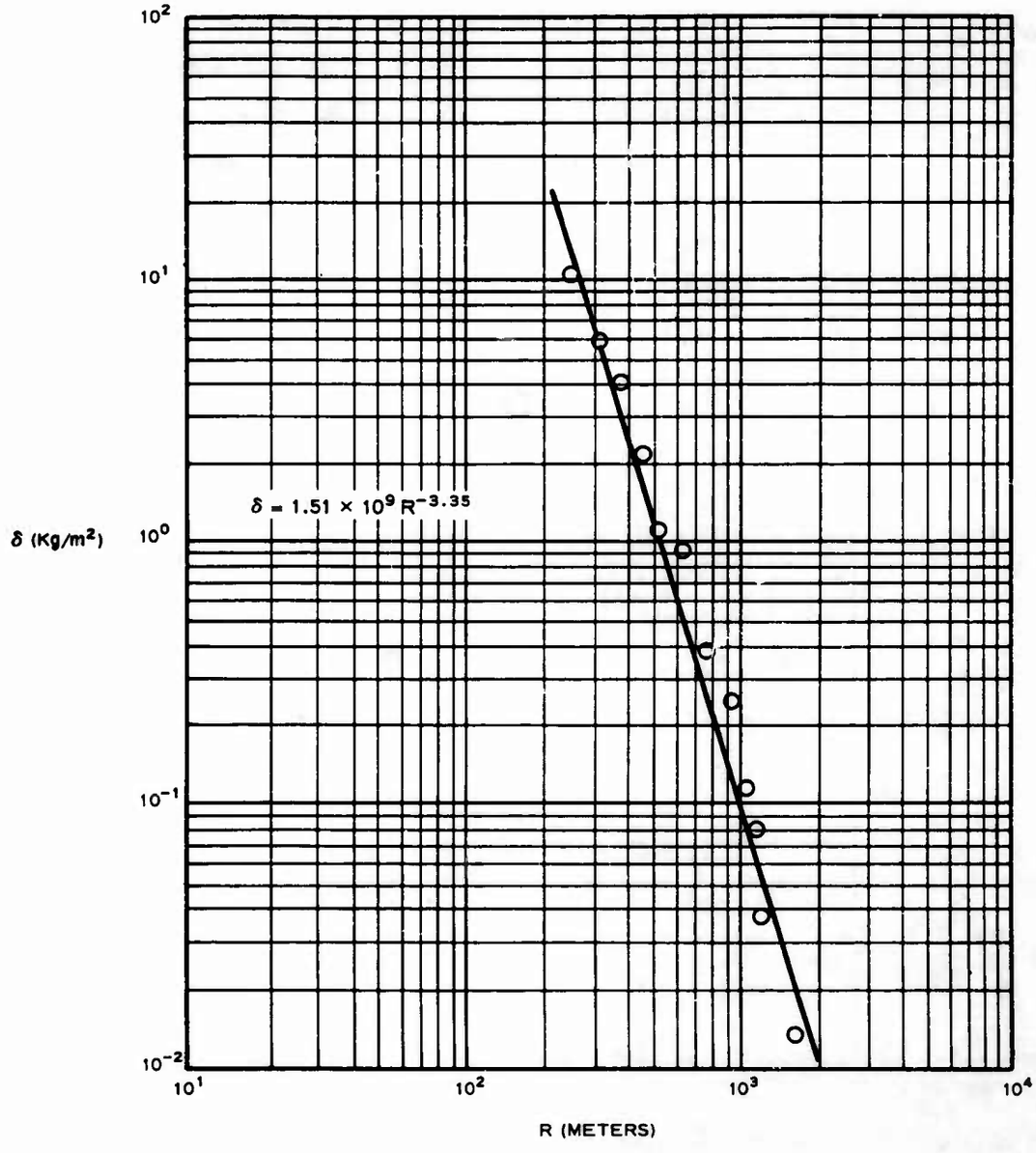

Figure A.36 Mass distribution (δ) versus radial distance from GZ (R) for ERA Round 817.

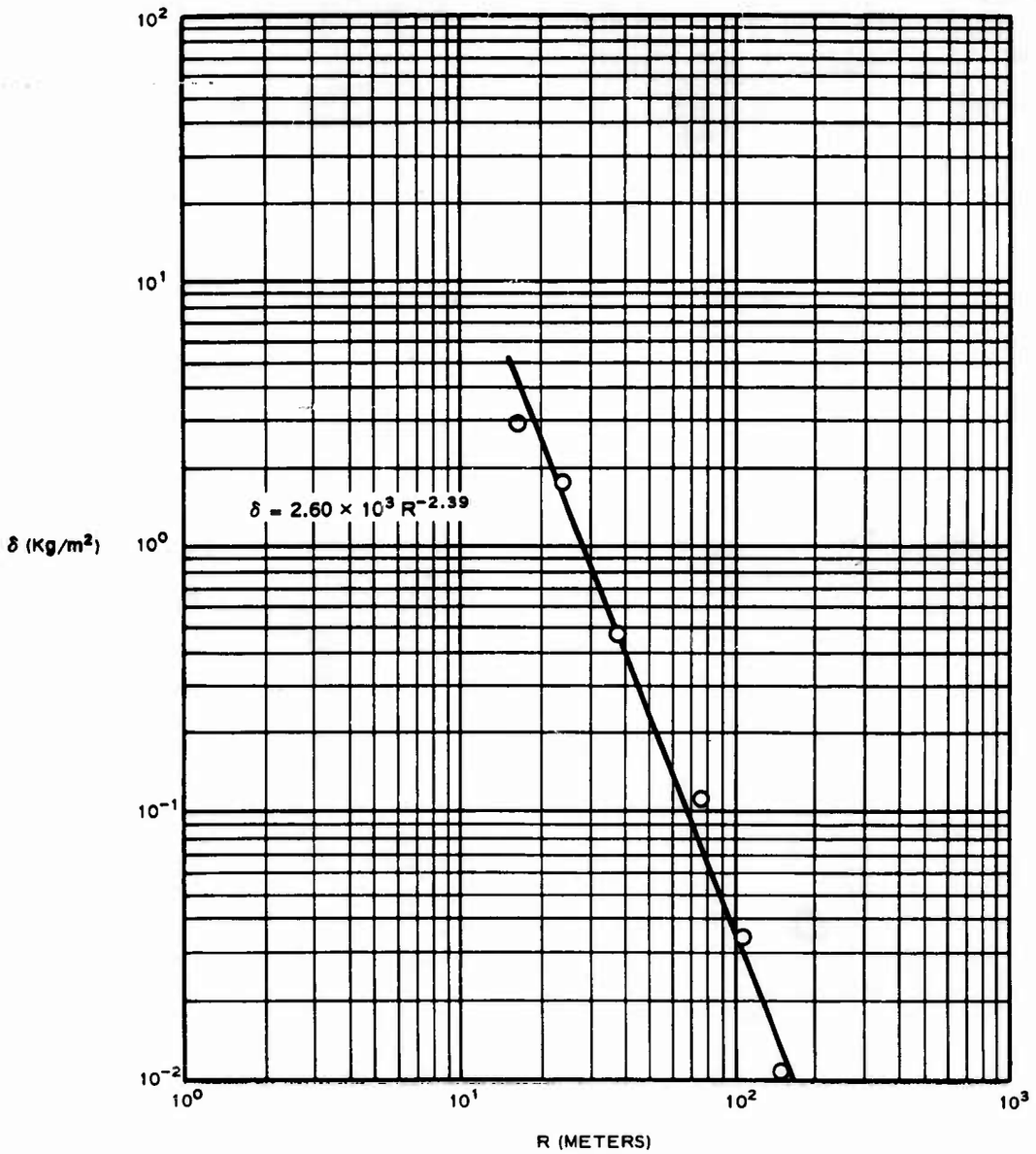

Figure A.37 Mass distribution (δ) versus radial distance from GZ (R) for ERA Round 819.

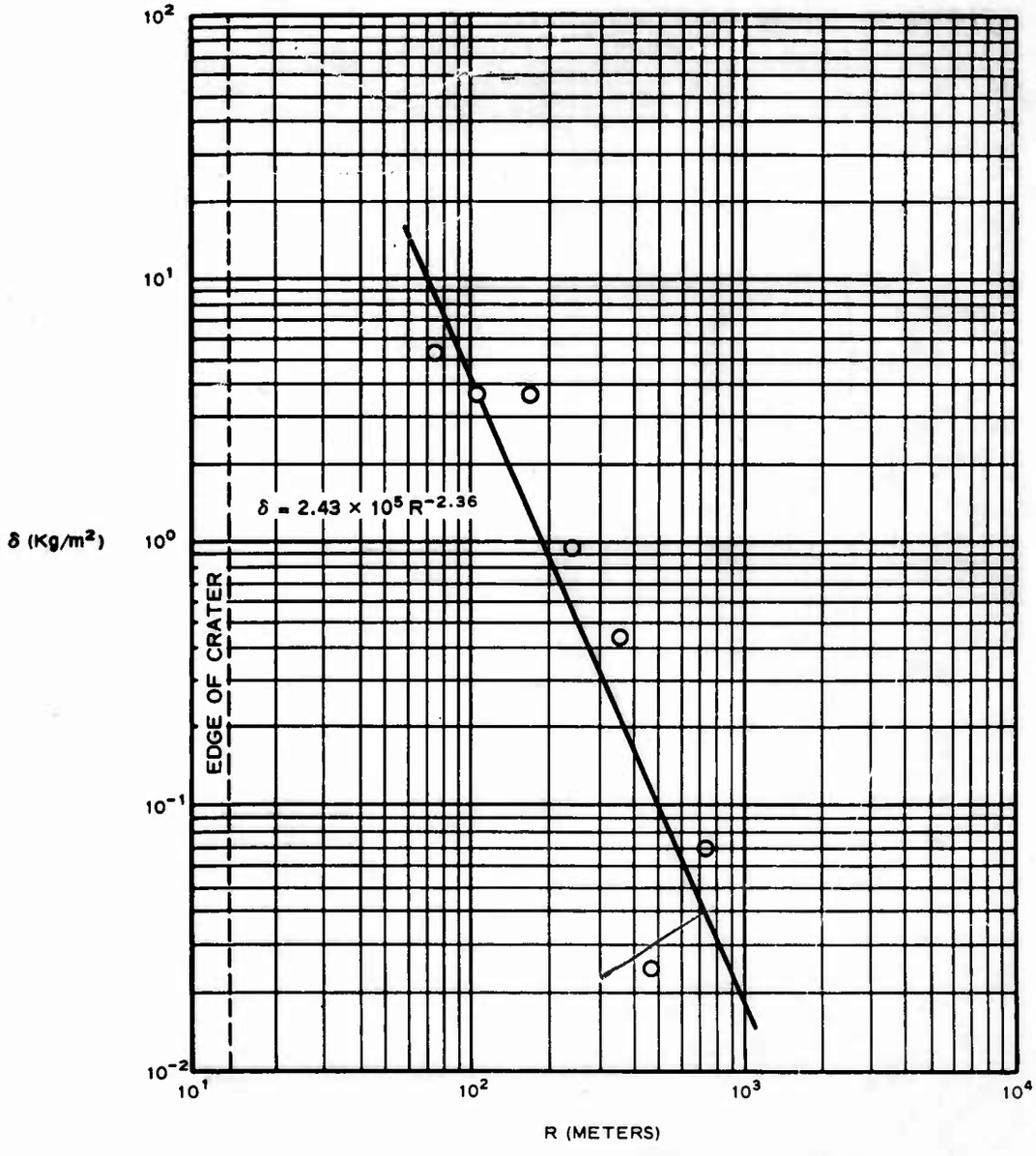

Figure A.38 Mass distribution (δ) versus radial distance from GZ (R) for Buckboard Shot 11.

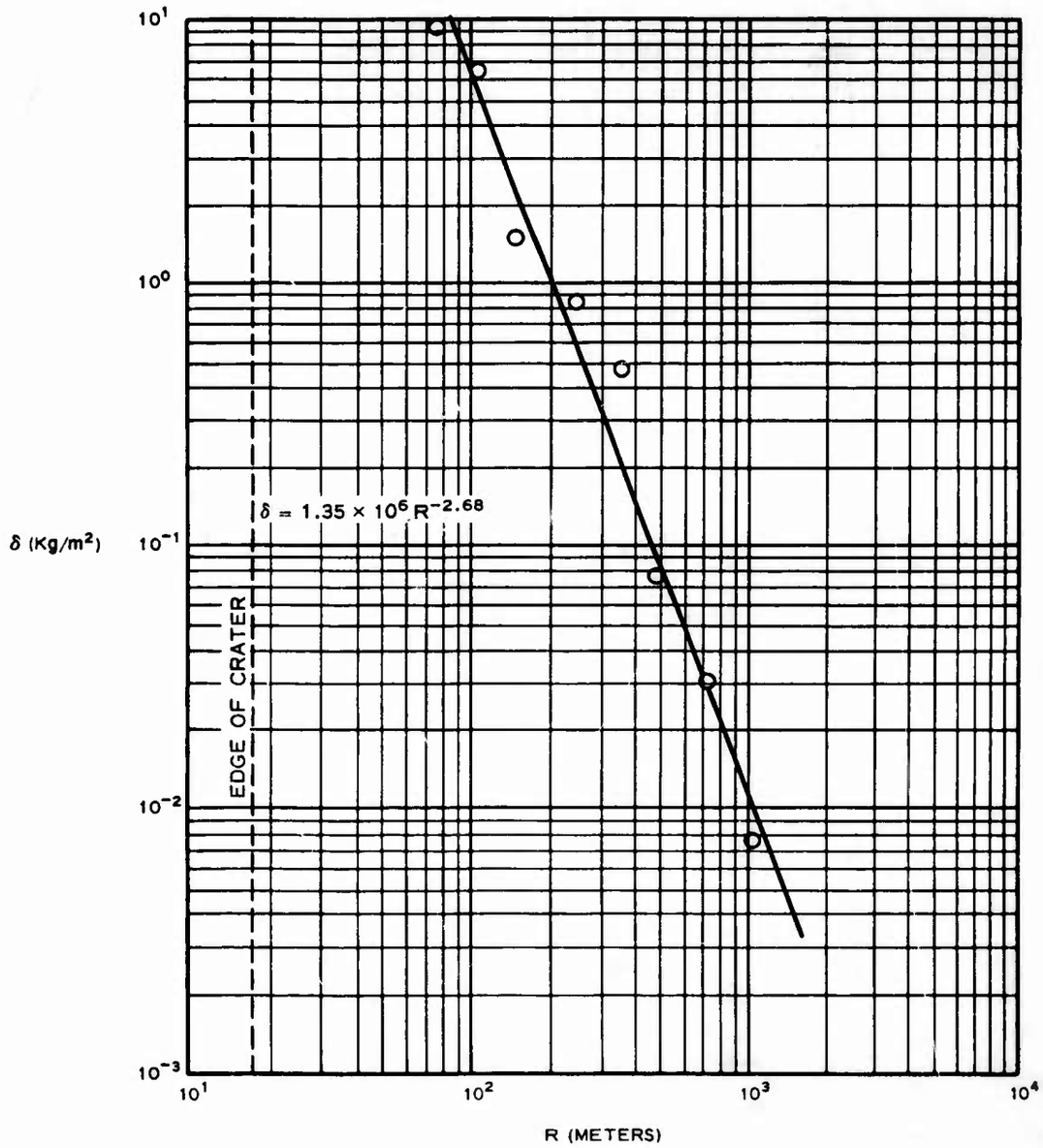

Figure A.39 Mass distribution (δ) versus radial distance from GZ (R) for Buckboard Shot 12.

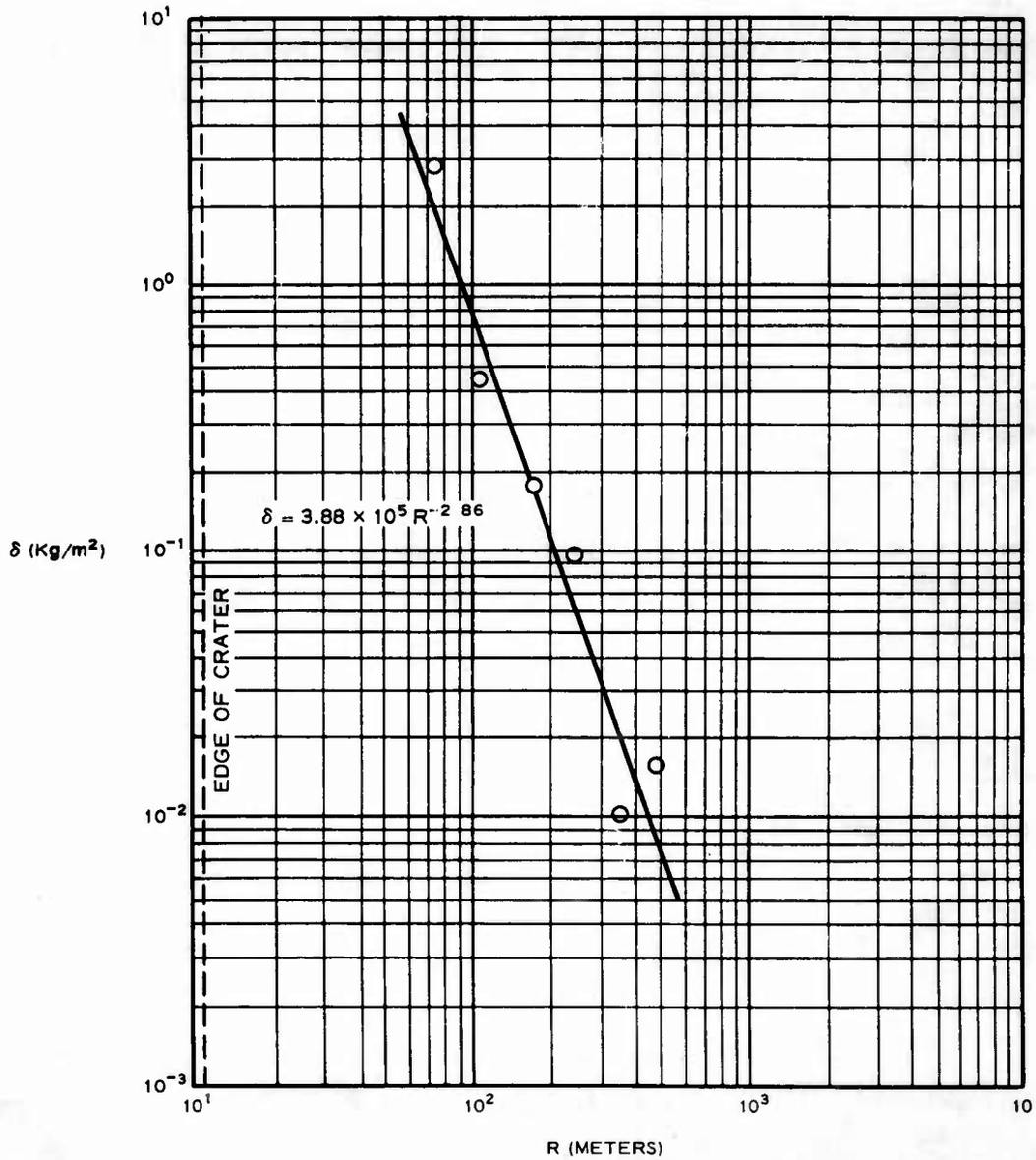

Figure A.40 Mass distribution (δ) versus radial distance from GZ (R) for Buckboard Shot 13.

REFERENCES

1. Engineering Research Associates, Inc.; "Underground Explosion Test Program"; Technical Report Nos. 4 and 5, Volume I (30 August 1952 and 15 February 1953), and Final Report Volumes I and II (30 August 1952 and 30 April 1953); 1902 West Minnehaha Ave., St. Paul W4, Minn., or 507 18th St. South, Arlington, Va.; North Central Publishing Co., St. Paul, Minn.; Unclassified.

2. R. H. Carlson and W. A. Roberts; unpublished paper "Distribution of Ejecta from Cratering Explosions"; April 1963; Boeing Airplane Co., Seattle 24, Wash.; Unclassified.

3. D. J. Kempster; unofficial draft "Surface Burst of a 100 Ton TNT Hemispherical Charge (1961), Crater and Ejecta Deposit Measurements"; Suffield Technical Note No. 85; 9 April 1962; Suffield Experimental Station, Ralston, Alberta, Canada; Unclassified.

4. R. H. Carlson and W. A. Roberts; "Ejecta Study of 100-Ton Suffield Explosive Cratering Shot"; August 1962; Boeing Airplane Co., Seattle 24, Wash.; Unclassified.

5. R. H. Carlson; "Local Distribution of Material Ejected by Surface Explosions: White Tribe Interim Report"; August 1961; Boeing Airplane Co., Seattle 24, Wash.; Unclassified.

6. W. A. Roberts; "Distribution of Debris Ejected by the Stagecoach Series of High Explosive Cratering Bursts"; October 1961; Boeing Airplane Co., Seattle 24, Wash.; Unclassified.

7. R. H. Carlson and W. A. Roberts; "Ejecta Studies--Sedan Event"; December 1962; Boeing Airplane Co., Seattle 24, Wash.; Unclassified.

8. A. J. Chabai and R. H. Bishop; "Project Stagecoach: 20-Ton HE Cratering Experiments in Desert Alluvium; Final Report"; May 1962; Chapter 4 (Particulate Distribution) and Chapter 7 (Missile Hazard from Partly Contained Explosions); Sandia Corp., Sandia Base, Albuquerque, N. M.; Unclassified.

9. A. J. Chabai; "Project Buckboard: 20-Ton and 1/2-Ton High Explosive Cratering Experiments in Basalt Rock; Final Report"; August 1962; Chapter 4 (Fine Particulate Distribution); Sandia Corp., Sandia Base, Albuquerque, N. M.; Unclassified.

10. H. G. Snay; "The Scaling of Underwater Explosion Phenomena"; 30 June 1961; U. S. Naval Ordnance Laboratory, White Oak, Md.; Unclassified.

11. M. D. Nordyke; Memorandum to J. Philip dated 2 January 1962; Lawrence Radiation Laboratory, Livermore, Calif.; Unclassified.

12. J. Allen; Memorandum, Subject: Miscellaneous Matters in Connection with Project Danny Boy Reports, dated 15 January 1963; Lawrence Radiation Laboratory, Livermore, Calif.; Unclassified.

13. J. N. Strange, C. W. Denzel, and T. I. McLane III; "Cratering from High Explosive Charges: Analysis of Crater Data"; Technical Report No. 2-547, Report 2; June 1961; U. S. Army Engineer Waterways Experiment Station, Vicksburg, Miss.; Unclassified.

14. M. D. Nordyke; "On Cratering. A Brief History, Analysis and Theory of Cratering"; 22 August 1961; Lawrence Radiation Laboratory, Livermore, Calif.; Unclassified.

15. G. Murphy; "Similitude in Engineering"; 1950; Ronald Press Co., New York, N. Y.; Unclassified.

16. R. H. Carlson, Boeing Airplane Co.; telephone conversation with L. K. Davis, 27 May 1963; Unclassified.

17. A. J. Chabai, Sandia Corp.; telephone conversation with L. K. Davis, 29 May 1963; Unclassified.

ABBREVIATIONS FOR TECHNICAL AGENCIES

ARA	Allied Research Associates Inc., Boston
ARF	Armour Research Foundation, Illinois Institute of Technology, Chicago 16
BOEING	The Boeing Company, Aero-Space Division, Seattle Attn: R. H. Carlson
EG&G	Edgerton, Germeshausen, and Grier, Inc., Boston, Las Vegas, and Santa Barbara
ERDL	U. S. Army Engineer Research & Development Laboratory, Fort Belvoir
LRL	Lawrence Radiation Laboratory, Livermore
NDL	U. S. Army Chemical Corps., Nuclear Defense Laboratory, Maryland
REECo	Reynolds Electrical and Engineering Co., Las Vegas
SC	Sandia Corporation, Albuquerque
SRI	Stanford Research Institute, Menlo Park
UCLA	University of California, Los Angeles
USC&GS	Coast and Geodetic Survey, Washington, D. C. and Las Vegas
USPHS	U. S. Public Health Service, Las Vegas
USWB	U. S. Weather Bureau, Las Vegas
WES	USA C of E Waterways Experiment Station, Vicksburg

UNCLASSIFIED